REVISED MODELS FOR BIPOLAR INTEGRATED CIRCUIT SIMULATION

By

BEING SONG WU

A DISSERTATION PRESENTED TO THE GRADUATE SCHOOL
OF THE UNIVERSITY OF FLORIDA IN
PARTIAL FULFILLMENT OF THE REQUIREMENTS
FOR THE DEGREE OF DOCTOR OF PHILOSOPHY

UNIVERSITY OF FLORIDA

1989

ACKNOWLEDGMENTS

I would like to express my sincere appreciation to the chairman of my supervisory committee, Professor Fredrik A. Lindholm, for his guidance and encouragement during the course of this work. I also thank Professors Chih T. Sah, Armand Neugroschel, Sheng S. Li and Chen C. Hsu for their participation on my supervisory committee.

I am grateful to my colleagues, Mr. Ju-Sung Park for his help in experiments, Mr. Chetan Parikh for his thorough review of this work and Dr. Tae-Won Jung for supply of devices. Thanks are extended to my other colleagues and friends, Dr. Jong Shik Park, Dr. Juin-Jei Liou, Dr. Jeremiah R. Lowney, Dr. Konstantinos Misiakos, Dr. Shuy Young Yung, Mr. Meng-Kei Chen for helpful discussions.

I am indebted to my fiancee, Shwu, and my family for their love and support during all the years of this work.

The financial support of the Semiconductor Research Corporation and the Defense Advanced Research Projects Agency is gratefully acknowledged.

TABLE OF CONTENTS

		Page
ACKNOWLEDGMENTS		ii
LIST OF SYMBOLS		vi
ABSTRACT		viii
CHAPTER		
ONE	INTRODUCTION	1
TWO	ONE-DIMENSIONAL NON-QUASI-STATIC MODELS FOR ARBITRARILY AND HEAVILY DOPED QUASI NEUTRAL LAYERS IN BIPOLAR TRANSISTORS	5
2.1	Introduction	5
2.2	Systematic Derivation of the Models	6
2.2.1	Overview of the Derivation	6
2.2.2	Derivation for the Base Layer	10
2.2.3	Corresponding Equivalent Circuits for the Base Layer	14
2.2.4	Models for Emitter Layer	23
2.3	Comparisons and Assessments	25
2.3.1	Review of Previous Models	25
2.3.2	Large-Signal Models	25
2.3.3	Small-Signal Models	29
2.4	Summary	39
THREE	ONE-DIMENSIONAL ALL-INJECTION NON QUASI STATIC MODELS FOR ARBITRARILY DOPED QUASI NEUTRAL LAYERS IN BIPOLAR JUNCTION TRANSISTORS INCLUDING PLASMA INDUCED ENERGY-GAP NARROWING	43
3.1	Introduction	43
3.2	Derivation of the Models	45
3.2.1	Method of Derivation	47
3.2.2	Inclusion of Plasma-Induced Energy Gap Narrowing	60
3.2.3	Inclusion of Significant Majority Hole Current (Low Current Gain)	62
3.3	Assessments	65
3.3.1	Large-Signal Models	65
3.3.2	Small-Signal Models	68
3.4	Conclusions	77

FOUR HIGH INJECTION NON-QUASI-STATIC COMPACT MODELS FOR BIPOLAR JUNCTION TRANSISTORS HAVING LIGHTLY DOPED COLLECTORS 83

4 1 Introduction 83
4 2 Models For Base Layers 85
4 2 1 Governing Equations for Model Derivation 85
4 2 2 Models for High and Low Injection 90
4 2 3 Models for All-Level Injection 94
4 2 4 Remarks 96
4 3 Models for Collector Layers 98
4 3 1 Overview 98
4 3 2 Model derivation 101
4 4 Results 108
4 5 Conclusions 112

FIVE NON QUASI-STATIC MODELS INCLUDING ALL INJECTION LEVELS AND DC AC AND TRANSIENT EMITTER CROWDING IN TRANSISTORS 114

5 1 Introduction 114
5 2 Derivation of the Models 117
5 2 1 Basic Equations and Main Assumptions 117
5 2 2 Low Injection 120
5 2 3 High Injection 126
5 2 4 Onset of Emitter Crowding 131
5 2 5 ALL-Injection Models 133
5 3 Assessments 136
5 3 1 DC Crowding 136
5 3 2 AC Crowding 146
5 3 3 Transient Crowding 150
5 4 Modifications and Extensions 152
5 4 1 Modifications 152
5 4 2 Extensions 153
5 5 Conclusions 154

SIX CONCLUSIONS AND EXTENSIONS 155

6 1 Conclusions 155
6 2 Extensions 158
6 2 1 Avalanche Breakdown 156
6 2 2 Collector and Base Current Spreading 156
6 2 3 Current Crowding in the Emitter Layer and Contact 157
6 2 4 Models for Heterojunction Bipolar Transistors(HBT) 157

APPENDICES

A PROOF OF RECIPROCITY IN THE QUASI-NEUTRAL BASE LAYER 160

B LIST OF THE PARAMETERS FOR THE MODELS DERIVED IN CHAPTER TWO 161

C LIST OF THE PARAMETERS FOR THE MODELS DERIVED IN CHAPTER THREE 163

D LIST OF THE PARAMETERS FOR THE MODELS DERIVED IN CHAPTER FOUR 165

E LIST OF THE PARAMETERS FOR THE MODELS DERIVED IN CHAPTER FIVE 167

REFERENCES 169

BIOGRAPHICAL SKETCH 178

LIST OF SYMBOLS

$D_{n,p}$	Electron, hole diffusivity
$\mu_{n,p}$	Electron, hole mobility
$\tau_{n,p}$	Electron, hole lifetime
$L_{n,p}$	Electron, hole diffusion length $[=(D_{n,p}\tau_{n,p})^{1/2}]$
$J_{N,P}$	Electron, hole current density
J_{Nx}, J_{Px}	X component of the electron, hole current density
J_{Ny}, J_{Py}	Y component of the electron, hole current density
$I_{Se,Sc}$	Saturation current in the base/emitter, base/collector junctions
n_{ie} = n_i	Position independent intrinsic carrier concentration
n_{ie}	Effective intrinsic carrier concentration
n, p	Electron, hole concentration
$\Delta n, \Delta p$	Excess electron, hole concentration
p_0, n_0	Hole, electron concentration in thermal equilibrium
E_{no}, E_{po}	Hole, electron electric field in thermal equilibrium
$E_{n,p}$	Hole, electron electric field
E_{nx}, E_{px}	X component of hole, electron electric field
E_{ny}, E_{py}	Y component of hole, electron electric field
E_c, E_v	Conduction, valence band edge
$v_{N,P}$	Electron, hole quasi-Fermi potential
v_{QF}	Separation of quasi Fermi potential (= $v_P - v_N$)
$N_{Deff}(x)$	Effective electron doping concentration

$N_{Aeff}(x)$	Effective hole doping concentration
N_A N_D N_e	Base, emitter, collector doping concentrations
K	Doping ratio
L	One half of the emitter width
Z	Emitter length
$W_{e,b,c}$	Emitter, base, collector thicknees
A, A_c	Emitter, collector ares (A = 2L Z)
q	Magnitude of electronic charge
k	Boltzmann constant
T	Absolute temperature
S_{pe} S_{pc}	Surface recombination velocity for holes at the emitter, collector contacts
ΔE_g	Apparent energy-gap narrowing
τ_f τ_r	Forward, reverse base transit time
τ_{et} τ_{tc}	Emitter collector transit time
$\tau_{d,ed,cd}$	Base, emitter, collector delay time
τ_{tx} τ_{ty}	Base transit time in x y direction
τ_{dx} τ_{dy}	Base delay time in x y direction
f_T	Cut-off frequency
β	current gain
$\mathcal{L}$	Integral operator corresponding to Laplace transformation
s	Variable of Laplace transformation

Abstract of Dissertation Presented to the Graduate School of the University of Florida in Partial Fulfillment of the Requirements for the Degree of Doctor of Philosophy

REVISED MODELS FOR BIPOLAR INTEGRATED CIRCUIT SIMULATION

By

Being Song Wu

August 1989

Chairman: Fredrik A. Lindholm
Major Department: Electrical Engineering

One-dimensional and two-dimensional non-quasi-static circuit models for the quasi-neutral layers of bipolar transistors are systematically derived from the hole and electron current and continuity equations. They can be combined with models now available for the p/n junction space charge layer to yield a network representation for the entire transistor that describes dc, small signal and large signal (nonlinear) transient responses. The models consist of less than two lumped circuit elements, yet their functional dependencies on physical makeup and terminal currents and voltages yield greater accuracy than that provided by previously available models. The new models apply for all doping profiles and injection levels, and they include hole or electron propagation delay and dc, ac and transient emitter crowding at a higher level of accuracy than was formerly attainable. They include a previously ignored energy-gap shrinkage arising at high current densities and injection levels from

carrier-carrier interaction as well as the more commonly treated position-dependent energy-gap narrowing, diffusivity, and recombination lifetime that occure at low injection levels from high shallow level impurity concentrations. Traditional high level injection mechanisms, such as the Webster and Kirk effects, are included. To address aspects of modeling peculiar to heterojunction bipolar transistors, the models can accommodate quasi fields resulting from composition variations and the associated space-dependent energy gaps.

Assessment by experiments and by computer simulation shows that the new models have advantages over their predecessors in simulating high speed or high frequency or high power bipolar integrated circuits. Despite the complicated mechanisms included, the models are compact enough for use in circuit simulators such as SPICE. In such simulations, accuracy may be traded for model complexity, which enables a tradeoff between central-processing unit (CPU) time and accuracy. This enhances the utility of the models in computer-aided-design applications.

CHAPTER ONE
INTRODUCTION

In the development or analysis of the contemporary bipolar integrated circuits, an accurate and comprehensive computer-aided-design tool which includes process, device and circuit simulators is essential to informed design. The utility of circuit simulators depends strongly on the adequacy of the circuit models used. Therefore complete and accurate circuit models are required for designing integrated circuits.

Most existing models for circuit simulation, such as the Gummel-Poon model [1], rely on the quasi static approximation. This approximation misses the detail of the transient response associated with the time required for carriers to propagate in any direction within the quasi-neutral layers. Thus, in the time domain (digital circuits), propagation delay is incompletely described by such models, and in the frequency domain (analog circuits), the models fail to describe adequately the frequency dependencies of the port impedances and the magnitudes and phase angles of the transfer functions [2]-[17]. These discrepancies are particularly significant in circuit simulation when the intrinsic layers dominate transistor performance. Thus they are important for 1) transistors with thick base layers (power transistors), 2) transistors with small input resistances (emitter-coupled logic circuit), 3) transistors in the common base configuration

and 4) heterojunction transistors because the intrinsic layers dominate the transistor performance in these cases

The purpose of this study is to improve the existing quasi-static models, such as the Gummel-Poon model in SPICE2 [18] for transient and frequency circuit simulation. As will be seen in Chapter Two, the use of a systematic method for the model derivation accomplishes the improvements and yields so-called non-quasi-static models. The method utilizes an integration scheme to deal with the time- and position dependent coefficients of the continuity and current equations and results in analytical expressions for current and carrier densities in low and high injection. Truncating the resulting current expressions with respect to time variables leads to non-quasi-static lumped circuit models for low and high injection. Applying a fitting scheme between the models for low and high injection will then extend the model to moderate injection. A hierarchy of the models can result either from various orders of truncation with respect to time variables or from various ways of partitioning with respect to positional variables in the quasi-neutral layers. This study focuses on quasi-neutral layers. Appending models for the junction space charge layers and the extrinsic resistances and capacitances then produces a model for the overall transistor.

In bipolar transistor modeling for circuit simulation it has been traditional to employ the quasi-static approximation, thus neglecting the effects of carrier propagation delay. The prominent exception to this statement has been in small signal models for frequency response in which an excess phase factor has been inserted to improve the phase

versus frequency representation of various two-port parameters such as current gain α or β. This approach, however, does nothing to improve the magnitude versus frequency representation. In this study all models, large-signal and small-signal, developed in each chapter are non quasi static and accurately include carrier propagation delay.

It has also been traditional in transistor modeling for circuit simulation to assume idealized doping profiles. Most of the modeling details of transistor physics in this study accommodate arbitrary doping profiles and include various physical mechanisms in accordance with the following chapter outline:

Chapter Two—arbitrarily and heavily doped quasi neutral base and emitter layers operating in low injection (including position-dependent diffusivity, lifetime and energy gap narrowing due to dopant-carrier interaction).

Chapter Three—arbitrarily doped quasi-neutral base layers operating at all injection levels (including the Webster effect [19] and energy gap narrowing from carrier-carrier interaction [20]-[23]).

Chapter Four—arbitrarily and heavily doped quasi-neutral base layers and lowly doped quasi neutral collector layers operating at all injection levels (including the Webster effect, the Kirk effect [24]-Fermi-Dirac statistics, position dependent diffusivity, lifetime and energy gap narrowing due to dopant-carrier as well as carrier-carrier interactions).

Chapter Five—exponentially doped quasi-neutral base layers operating at all injection levels (including dc, ac and transient emitter crowding [25]-[37])

Chapter Six sketches possible extensions of the models developed in Chapters Two through Five and concludes this work

The models have nearly a traditional equivalent circuit form They consist of connections of passive circuit elements and controlled sources, consistent with the exact model for the continuity and current equations put forth by Sah [38] The models are not exactly traditional transistor equivalent circuits because they contain inductances and negative capacitances in the network representation for the intrinsic transistor These additional elements serve to include non quasi-static effects while restraining the overall model complexity We incorporate these additional circuit elements into SPICE2 by using "user-defined controlled sources " which are FORTRAN subroutines accessed by SLICE [39] Because the models are compatible with the Gummel-Poon model, we may also implement the models into SPICE2 by directly modifying the source codes

In the simulation of transient or frequency responses, the models developed provide better accuracy than does the conventional Gummel Poon model We assess the improvements by comparing against experiment and computer simulations using SLICE and PISCES [40] for dc, ac and transient simulations The experiments employ the HP 4145A Semiconductor Parameter Analyzer for dc and s-parameter and the HP 4194A Impedance/Gain-Phase Analyzer for ac simulations

The analytical solutions obtained during the model derivation enable us to study how device makeup and excitation affect the transistor performance They also provide information for parameter extraction

CHAPTER TWO
ONE DIMENSIONAL NON-QUASI-STATIC MODELS FOR ARBITRARILY AND HEAVILY DOPED QUASI NEUTRAL LAYERS IN BIPOLAR TRANSISTORS

2.1 Introduction

The most widely used one dimensional model for circuit simulation of bipolar transistor circuits is the integral charge-control model by Gummel and Poon [1], which Kroemer [41] extended to characterize heterojunction bipolar transistors having an arbitrary doping profile and an arbitrary space dependence of the energy gap in the quasi neutral base layer. To account for time-varying large-signal and small-signal excitations [42] [43] it is traditional to use the quasi static approximation, which assumes that carriers injected across a junction proceed with infinite velocity during transients so that the steady-state form of the space distribution of excess carriers is maintained at each instant of time [44]

In this chapter, we avoid the inaccuracies of the quasi-static approximation while restraining model complexity, yet still accommodate arbitrary doping and energy-gap profiles, in both the emitter and the base quasi-neutral layers. Thus the models developed apply for silicon and for compound semiconductor heterojunction bipolar transistors in particular, we treat the case of a heavily doped base layer in silicon transistors, which is relevant because the small size of individual devices in an integrated circuit requires net doping levels above $10^{18} cm^{-3}$ improvement beyond the quasi-static approximation has

practical importance for several reasons one being that some applications require accuracy in transfer functions for frequencies a decade or more above the unity-gain frequency [45]

From the viewpoint of analysis, the problem of developing small-signal and large signal non quasi static models that accommodate arbitrary doping and arbitrary energy-gap profiles is challenging Even for the quasineutral base layer, the partial differential equations encountered have time and space dependent coefficients and are nonlinear if moderate or high-level injection occurs Moderate-level injection in which $p > 10^{18}$ cm^{-3} occurs in transistor base layers subjected to high current densities [46] In this chapter, we eliminate the time dependence of the coefficients and the nonlinearity by restricting attention to the case of low-level injection and one dimensional current flow In subsequent chapters, which will build on the foundation laid here we expand our analysis to include moderate and high level injection as well as transient emitter crowding

In Section 2 2 we sketch a systematic method for deriving non-quasi-static models for arbitrarily and heavily doped base and emitter layers Section 2 3 compares the dc and transient responses of the resulting models to those of computer and laboratory experiments The advantages of the models developed are summarized in the Section 2 4

2 2 Systematic Derivation of the Models

2 2 1 Overview of the Derivation

We will indicate here how we include the non-quasi static effects of propagation delay directly from the continuity equations and

associated physics for the p-type quasi-neutral base and n-type quasi-neutral emitter layers, as noted, we assume low injection. The derivation follows the scheme illustrated in the flow charts of Figs. 2.1(a) and 2.1(b). As indicated in Fig. 2.1(a), the continuity equations and the current equations (which are partial differential equations, denoted by p. d. e.) are reduced to ordinary differential equations by Laplace transformation with respect to time. For p-type quasi-neutral layers, these ordinary differential equations are

$$[s + 1/\tau_n(x)]\,\mathcal{L}\{\Delta n(x,t)\} = (1/q)d\mathcal{L}\{j_N(x,t)\}/dx \qquad (2.1)$$

$$\mathcal{L}\{j_N(x,t)\} = q\mu_n(x)\mathcal{L}\{\Delta n(x,t)E_n(x,t)\} + qD_n(x)d\,\mathcal{L}\{\Delta n(x,t)\}/dx \qquad (2.2)$$

where $\mathcal{L}$ is the integral operator corresponding to Laplace transformation.

For low injection, the electric field acting on the minority carriers is approximately time-independent, $E_n(x,t) = E_{no}(x)$. Thus (2.1) and (2.2) become linear ordinary differential equations with nonconstant coefficients. The time-dependent electric fields present in space charge layers are represented by capacitances in equivalent-circuit models [47].

As will be shown in Section 2.2.2, analytical solutions of these equations are obtained by integration and iteration. Once the analytical solutions emerge, they form the basis for the development of the models. Straightforward reformulation of the solutions into a two-port network form produces the matrix description indicated in Fig. 2.1(b). The matrix elements are infinite series in s, reflecting the distributed nature of the quasi-neutral layers embodied in the partial

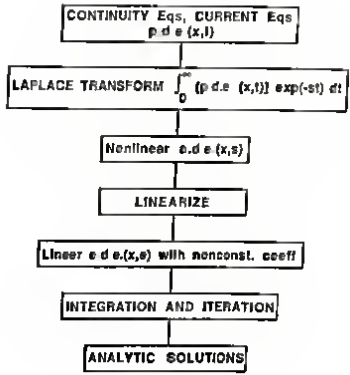

Fig 2.1 The flow chart of systematic derivation of the heavily doped non quasi static (HDNQS) equivalent circuit model (a) Analytic solutions including the effects of carrier propagation delay derived directly from the continuity equation (b) Circuit realization of the two port equation formed by analytic solutions

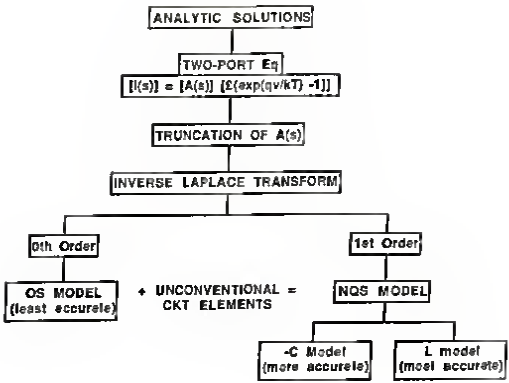

(b)

Fig 2.1—continued

differential equations that describe them To obtain an equivalent-circuit model which corresponds to ordinary differential equations in the independent variable t, one must truncate the matrix elements with respect to s and take the inverse Laplace transform Various truncations are possible Particular truncations produce quasi-static models, such as the Gummel-Poon model Other truncations produce non-quasi static models which include unconventional circuit elements, such as inductors or negative capacitors These truncations form the basis of the improved models developed here

2 2 2 Derivation for the Base Layer

For high-speed or high-frequency bipolar junction transistors the submicron base layer has a peak doping concentration greater than 10^{18} cm^{-3} to prevent punchthrough [48]-[50] According to Swirhun et al [51], the electron lifetime, electron mobility and energy gap in the p-type base layer significantly vary with $N_A(x)$ for $N_A > 10^{17}$ cm^{-3} Thus the coefficients in (2 1) and (2 2) depend on x which makes it difficult to directly obtain analytical solutions

By assuming low injection and nondegeneracy for the minority carriers we obtain the electric field, $E_n = d(E_c/q)/dx$ acting on the conduction-band electrons

$$E_n(x,t) = E_n(x) = E_{nc}(x) = (kT/q)d(\ln N_{Aeff})/dx \qquad (2\ 3)$$

where E_c is the conduction-band edge and

$$N_{Aeff} = N_A \exp(\Delta E_g/kT)$$

where ΔE_g is the apparent energy-gap narrowing defined in [51] which includes the effect of Fermi statistics.

Substituting (2.3) into (2.2) yields

$$\mathcal{L}\{j_N(x,t)\} = qD_n(x)[\mathcal{L}\{\Delta n(x,t)\}d(\ln N_{Aeff})/dx + d\mathcal{L}\{\Delta n(x,t)\}/dx] \qquad (2.4)$$

The boundary conditions at $x=0$ and $x=W_b$ are

$$\mathcal{L}\{\Delta n(0,t)\} = [n_{ie}^2/N_{Aeff}(0)]\mathcal{L}\{\exp(qV_{BE}/kT) - 1\} \qquad (2.5)$$

$$\mathcal{L}\{\Delta n(W_b,t)\} = [n_{ie}^2/N_{Aeff}(W_b)]\mathcal{L}\{\exp(qV_{BC}/kT) - 1\} \qquad (2.6)$$

We substitute (2.5) into (2.1) and (2.4) and integrate (2.1) and (2.4) from the emitter edge ($x = 0$) of the quasi-neutral base to an arbitrary position x in the base. This gives

$$\mathcal{L}\{n'(x,t)\} = n_e(x)[1 + (1/\eta)\int_0^x \mathcal{L}\{j'(x',t)\}dx'/D_n(x')n_e(x')] \qquad (2.7)$$

$$\mathcal{L}\{j'(x,t)\} = \mathcal{L}\{j'(0,t)\} + q\int_0^x \lambda^2(x'-s)D_n(x')\mathcal{L}\{n'(x',t)\}dx' \qquad (2.8)$$

where

$$n_e(x) = n_{ie}^2/N_{Aeff}(x)$$

$$\mathcal{L}\{n'(x,t)\} = \mathcal{L}\{\Delta n(x,t)\}/\mathcal{L}\{\exp(qV_{BE}/kT) - 1\}$$

$$\mathcal{L}\{j'(x,t)\} = \mathcal{L}\{j_N(x,t)\}/\mathcal{L}\{\exp(qV_{BE}/kT) - 1\}$$

$$\lambda^2(x-s) = (1 + s\tau_n(x))/L_n^2(x).$$

Equation (2.7) is of the form $A = a + f_1(B)$, and (2.8) is of the form $B = b + f_2(A)$. Thus $A = a + f_1\{b + f_2[a + f_1(B)]\}$, into which B

in (2.8) can be substituted. This procedure yields the iterative analytical expressions

$$\mathcal{L}\{n'(x,t)\} = n_o(x)\ [1 + \mathcal{L}\{j'(0,t)\}\sum_{i=1}^{\infty} A_{2i-1}(x,s)/q + \sum_{i=1}^{\infty} B_{2i}(x,s)] \tag{2.9}$$

where

$$A_{2i-1}(x,s) = \int_0^x dx_1/D_n(x_1)n_o(x_1) \int_0^{x_1} \lambda^2(x_2,s)D_n(x_2)n_o(x_2)dx_2$$

$$\int_0^{x_{2i-2}} dx_{2i-1}/D_n(x_{2i-1})n_o(x_{2i-1})$$

$$B_{2i}(x,s) = \int_0^x dx_1/D_n(x_1)n_o(x_1) \int_0^{x_1} \lambda^2(x_2,s)D_n(x_2)n_o(x_2)dx_2$$

$$\int_0^{x_{2i-1}} \lambda^2(x_{2i},s)D_n(x_{2i})n_o(x_{2i})dx_{2i}$$

From (2.9) we obtain the injected minority current

$$\mathcal{L}\{j_N(0,t)\} = -q\,\frac{1}{\sum_{i=1}^{\infty} A_{2i-1}(W_b,s)}[(1 + \sum_{i=1}^{\infty} B_{2i}(W_b,s))\,\mathcal{L}\{\exp(qv_{BE}/kT)-1\}$$

$$\mathcal{L}\{\exp(qv_{BC}/kT)\ 1\}] \tag{2.10}$$

If we integrate (2.1) and (2.2) from x to W_b instead of from 0 to x, we can obtain $\mathcal{L}\{j_N(W_b,t)\}$ by following the same procedure. By defining $\mathcal{L}\{j_N(0,t)\} = -i_1(s) = i_{EB}$, $\mathcal{L}\{j_N(W_b,t)\} = i_2 = i_{CB}$, $v_1 = v_{BE}$ and $v_2 = v_{BC}$, we obtain a two-port equation

$$\begin{bmatrix} i_1 \\ i_2 \end{bmatrix} = i_o \begin{bmatrix} A_{11}(s) & A_{12}(s) \\ A_{21}(s) & A_{22}(s) \end{bmatrix} \begin{bmatrix} \mathcal{L}\{\exp(qv_1/kT) - 1\} \\ \mathcal{L}\{\exp(qv_2/kT) - 1\} \end{bmatrix} \tag{2.11}$$

Truncating the matrix elements A_{ij} to the first order of s and neglecting the recombination, we obtain

$$A_{11} = 1 + sr_{11} \tag{2 12}$$

$$A_{12} = -1/(1 + sr_{12}) \tag{2 13}$$

$$A_{22} = 1 + sr_{22} \tag{2 14}$$

$$A_{21} = -1/(1 + sr_{21}) \tag{2 15}$$

where

$$l_s = (kT/q)\ A/\int_0^{W_b} \frac{1}{q\,\mu_n n_o}\,dx \tag{2 16}$$

$$r_{11} = \int_0^{W_b} \frac{1}{D_n n_o} \int_0^x n_o\,dx_1 dx - r_{12} \tag{2 17}$$

$$r_{12} = \int_0^{W_b} \frac{1}{D_n n_o} \int_0^x n_s \int_0^{x_1} \frac{1}{D_n n_o}\,dx_2 dx_1 dx \Big/ \int_0^{W_b} \frac{1}{D_n n_o}\,dx \tag{2 18}$$

$$r_{21} = \int_0^{W_b} \frac{1}{D_n n_s} \int_x^{W_b} n_o \int_{x_1}^{W_b} \frac{1}{D_n n_o}\,dx_2 dx_1 dx \Big/ \int_0^{W_b} \frac{1}{D_n n_o}\,dx \tag{2 19}$$

$$r_{22} = \int_0^{W_b} \frac{1}{D_n n_s} \int_x^{W_b} n_o\,dx_1 dx - r_{21} \tag{2 20}$$

The results (2 12)-(2 20) of this truncation have the following properties. First $A_{12} = A_{21}$ as is proved in Appendix A, which confirms the prediction [52]-[54] of reciprocity for bipolar transistors during transients. Second, the base delay time τ_d defined by Elmore [55] and Ashar [56] is $\tau_{21} = \tau_{12}$. Third, we have Kroemer's results for material having a nonuniform energy gap derived using the electron current equation with charge control [41]. His expression for I_e, the base saturation current, is equivalent to (2 15), his

expression for the forward and reverse transit times obey the relations $\tau_{tf} = \tau_{11} + \tau_{21}$ and $\tau_{tr} = \tau_{22} + \tau_{21}$

2 2 3 Corresponding Equivalent Circuits for the Base Layer

The network representation for (2 11)-(2 20) shown in Fig 2 2 results from redrawing the network implied by (2 11) using Kirchhoff's current law The element values in Fig 2 2 follow from this procedure, more systematically, from employing the nonlinear indefinite admittance matrix [57] These element values are

$$\begin{aligned} I_{jj}(s) &= I_o[A_{jj}(s) + A_{12}(s)]\mathcal{L}\{\exp(qv_j/kT) \quad 1\} \\ &= I_o[s(\tau_{jj} + \tau_{12})/(1 + s\tau_{12})]\mathcal{L}\{\exp(qv_j/kT) - 1\} \quad j = 1, 2 \end{aligned} \tag{2 21}$$

$$\begin{aligned} I_{12}(s) &= I_o[-A_{12}(s)]\ \mathcal{L}\{\exp(qv_1/kT) \quad \exp(qv_2/kT)\} \\ &= I_o(1 + s\tau_{12})^{-1}\ \mathcal{L}\{\exp(qv_1/kT) - \exp(qv_2/kT)\} \end{aligned} \tag{2 22}$$

By taking inverse Laplace transformation of (2 21) and (2 22), we obtain the large signal circuit models shown in Fig 2 3(a) and 2 3(b), where

$$R_{jj}\, i_{jj} + (1/C_{jj}) \int_0^t i_{jj}\, dt = v_j \qquad j = 1, 2 \tag{2 21a}$$

where

$$C_{jj} = I_o(\tau_{jj} + \tau_{12})[\exp(qv_j/kT) - 1]/v_j = R_{jj} = \tau_{21}/C_{jj} \qquad j = 1, 2 \tag{2 21b}$$

$$Ri_{12}(t) + L\, di_{12}(t)/dt = v_1 - v_2 \tag{2 22a}$$

where

$$R = (v_1 - v_2)/I_o[\exp(qv_1/kT) - \exp(qv_2/kT)]$$

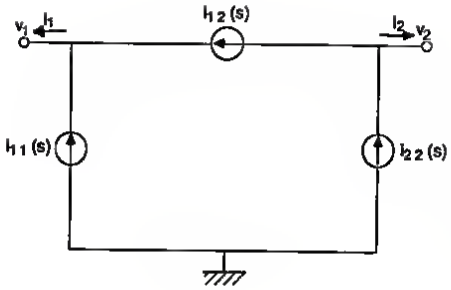

Fig. 2.2 A network representation of the two-port equation.

$$= (v_1 \quad v_2)/i_{QS} \,, \qquad L/R = \tau_{21} \tag{2 22b}$$

From now on we will refer to this model as the HDNQS (heavily doped non quasi-static) model.

In addition to the quasi neutral base, Fig. 2.3 also includs the effects of the quasi-neutral emitter a model for which will be derived in Section 2.2.4. We now compare the HDNQS model in Fig. 2.3(a) with the intrinsic Gummel-Poon model. The time constant $R_{jj}C_{jj}$ in Fig. 2.3(e) represents delay associated with the base storage current an effect that is absent in the Gummel-Poon model because no R_{jj} is present as a result of the quasi-static approximation. In Fig. 2.3(e), the time constant L/R represents the Elmore or Asher delay of the base conduction current, a delay not included in the Gummel-Poon model which therefore has no inductance. The C_{jj} in (2.21b) times R in (2.22b) will give the transit time $\tau_{jj} + \tau_{12}$. From a physical viewpoint $R_{jj}C_{jj}$ is the time constant for the excess majority hole distribution to reach steady state and L/R is the time constant for the excess minority electron distribution to reach steady state in the quasi-neutral base layer. Since the excess hole concentration must equal the excess electron concentration at each position and time to maintain quasi-neutrality $R_{jj}C_{jj} = L/R$. This is consistant with (2.21b) and (2.22b).

To prove the equivalence of Figs. 2-3(a) and 2-3(b), we consider forward active operation and focus on the quasi neutral p-type base layer. In Fig. 2-3(a), the voltage across C_{11} is defined as

$$v_{C11} = (1/C_{11}) \int_0^t i_{11} dt \tag{2 25}$$

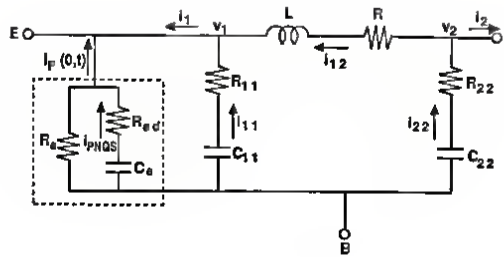

Fig. 2.3 The large-signal heavily doped non quasi-static (HDNQS) circuit models.
(a) The inductance model for the quasi neutral base layer and the quasi neutral emitter layer (the portion in the box).
(b) An alternate form of (a) for circuit application

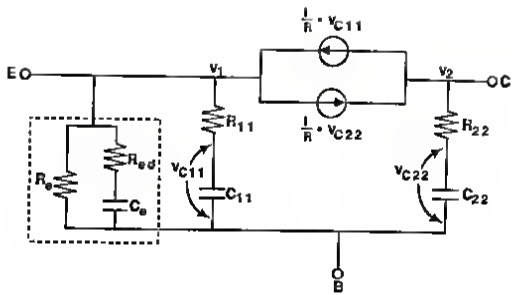

(b)

Fig. 2 3--continued

Dividing both sides of (2 26) by R and taking the Laplace transform gives

$$\mathcal{L}\left\{ \frac{v_{C11}}{R} \right\} = \left(\frac{1}{sRC_{11}} \right) \mathcal{L}\left\{ i_{11} \right\} = \frac{i_{11}(s)}{s\tau_{tf}} \tag{2 27}$$

Recall that $RC_{11} = \tau_{tf}$ From (2 21) and (2 22), we note that

$$i_{11}(s) = i_{12}(s)\, s(\tau_{11} + \tau_{12}) = i_{12}(s)\, s\tau_{tf} \tag{2 28}$$

Substituting (2 28) into (2 27) yields

$$\mathcal{L}\left\{ \frac{v_{C11}}{R} \right\} = i_{12}(s) \tag{2 29}$$

By taking the inverse Laplace transformation of (2 29) we obtain

$$\frac{v_{C11}(t)}{R(t)} = i_{12}(t) \tag{2 30}$$

Equation (2 30) shows that the HDNQS model in Fig 2 3(a) is equal to that in Fig 2 3(b) in the forward-active mode We can prove the equivalence of these two models in the reverse-active and saturation modes by following the same procedure The model of Fig 2 3(a) reveals the physical insight regarding delay explicitly it is more easily compared with the Gummel Poon model and the Seh model [38] than is the model of Fig 2 3(b) However, Fig 2 3(b) provides advantages in circuit implementation and in transformation from common base to common emitter or common collector configurations

The circuit elements of the model developed above are determined by device makeup (geometry, doping profile etc) their accuracy depends on the physical models used for energy-gap narrowing, mobility

and lifetime. Compared with the Gummel-Poon model, there are fewer parameters of this model that require extraction by terminal measurements because it contains more of the relevant physics. In Appendix B, we solve (2.21a) and (2.22a) and obtain a neo-quasi-static large-signal model with three voltage controlled current sources $i_{11}(t)$, $i_{22}(t)$ and $i_{12}(t)$ that is easily implemented in circuit simulators, such as SPICE.

For the small-signal case, by assuming $\delta v_j \ll kT/q$, we have

$$\exp(qV_j/kT) = \exp[q(V_j + \delta v_j)/kT] = \exp(qV_j/kT) \quad (1 + q\delta v_j/kT) \tag{2.31}$$

Substituting (2.31) into (2.21) and (2.22), we obtain the small signal HDNQS model shown in Fig. 2.4(a), in which

$$e_{jj} = qI_o(r_{jj} + r_{12}\{\exp(qV_j/kT)-1\}/kT \ , \ r_{jj} = r_{21}/e_{jj} \quad j = 1, 2 \tag{2.32}$$

$$r = (kT/q)/[I_o\exp(qV_2/kT)], \ L_{ee} = r_{21}r \tag{2.33}$$

$$g_m = I_o[\exp(qV_1/kT) - \exp(qV_2/kT)]/(kT/q) \tag{2.34}$$

where the subscript (ee) indicates small-signal excitation. Again, an alternate form of the small-signal model is shown in Fig. 2.4(b). Since the small-signal circuit model is linear, it is straightforward to prove that Fig. 2.4(a) and Fig. 2.4(b) are equal by employing Laplace transformation.

If we approximate $-A_{12}(s)$ in (2.22) by $1 - sr_{12}$, we obtain an alternate HDNQS model, in which the series combination of inductance and resistance in Fig. 2.3(a) and Fig. 2.4(a) is replaced by a negative capacitance in parallel with a conductance, where

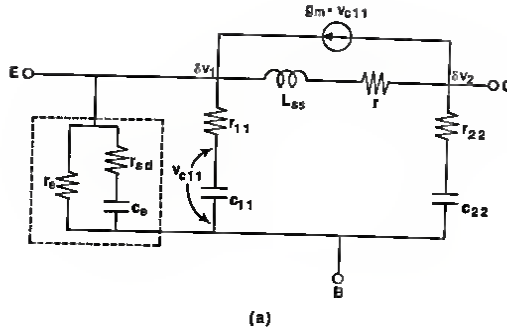

Fig 2 4 The small signal heavily doped near quasi-static (HDNQS) circuit model
(a) The inductance model for the quasi-neutral base layer and the quasi-neutral emitter layer (the portion in the box), Note that exchanging node E and node C gives another inductance model; (b) An alternate form of (a) for circuit application

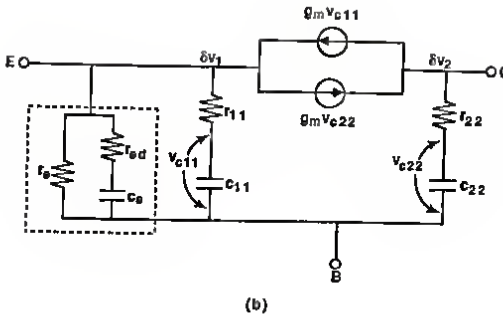

Fig. 2.4- continued

$$G = 1/R \quad -C = \tau_{12} G \quad g \quad = 1/t \quad t \quad = \tau_{12} g \tag{2.35}$$

The additional approximation, $(1 + s\tau_{12})^{-1} = 1 - s\tau_{12}$ used for this model, makes it less accurate in simulating the transconductance (y_{21}) for high frequencies at transients. Thus the non-quasi-static model developed by Klose and Wladet [7], which is equivalent to the negative capacitance model, is less accurate than the inductance model [11].

2.2.4 Models for Emitter Layer

Defining x=0 as the boundary between the quasi-neutral emitter and junction space-charge layers and $x=W_e$ as the emitter contact gives the boundary conditions

$$\mathcal{L}\{p(0,t)\} = [n_{ie}^2 / N_{Deff}(0)]\mathcal{L}\{\exp(qv_{BE}/kT) - 1\} \tag{2.36}$$

$$\mathcal{L}\{j_p(W_e, t)\} \approx qS_{pe}\mathcal{L}\{p(W_e, t)\} \tag{2.37}$$

Based on these boundary conditions, we obtain the injected minority hole current in the emitter layer by following the method described in Section 2.2.1

$$\mathcal{L}\{i_p(0,t) = I_{Be}[1 + s\tau_{et} /(1 + s\tau_{ed})]\ \mathcal{L}\{\exp(qv_{BE}/kT) - 1\} \tag{2.38}$$

Since the Auger lifetime could be comparable to the transit time in the emitter layer, we include recombination in deriving (2.38). Taking the inverse Laplace transformation of (2.38) yields the large-signal model for the emitter layer in Fig. 2.3, in which

$$i_p(0,t) = v_{BE}/R_e + i_{PNQS} \qquad (2\ 39)$$

where

$$R_e = v_{BE}/[I_{Eo}\exp(qv_{BE}/kT)]$$

and i_{PNQS} which represents the non quasi static emitter storage current satisfies the following equation

$$R_{ed}\, i_{PNQS} + (1/C_e)\int_0^t i_{PNQS}\, dt = v_{BE} \qquad (2\ 40)$$

where

$$C_e = \tau_{et}/R_e \quad , \quad R_{ed} = \tau_{ed}/C_e$$

In Appendix B we solve (2.40) and get i_{PNQS} in a form suitable for circuit simulation. By applying (2.31) to (2.38) we obtain the small signal model for emitter layer shown in Fig. 2.4, where

$$r_e = (kT/q)/[I_{Eo}\exp(qV_{BE}/kT)] \quad , \quad c_e = \tau_{et}/r_e \quad , \quad r_{ed} = \tau_{ed}/c_e \qquad (2\ 41)$$

In Appendix B, we list the expressions for the emitter saturation current I_{Eo}, the emitter delay time τ_{ed} and the emitter transit time τ_{et}. By substituting I_{Eo} and τ_{et} into (2.39) and (2.40), we find that R_e and C_e in our model are equivalent to those in the second-order quasi-neutral quasi-equilibrium (QNQE) emitter model derived by Park et al. [58]. The additional resistor R_{ed} in series with C_e describes the non quasi-static storage current in the emitter layer.

Recently, Seitchik et al. [10] presented a modified Gummel-Poon model by utilizing truncations of expressions for $y_{11}(s)$, $y_{21}(s)$ and $\beta(s)$, that neglect delay associated with hole storage in the emitter layer. Comparing the delay times in the base and emitter layers

however, shows that the emitter delay time could be ten times larger than the base delay time for polysilicon contact emitters. Thus our inclusion of the emitter delay improves accuracy. We shall show indirect justification of this statement in Figs. 2.10(a) and 2.10(b).

2.3 Comparisons and Assumptions

2.3.1 Review of Previous Models

Recent work has sought to improve the accuracy of the one-dimensional Gummel-Poon model by including non-quasi-static effects. In one such effort, Pemaun and Veeraraghavan limited their attention to space independent base doping profiles in low injection [6]. Klose and Wieder [7] treated arbitrary base doping profiles, using approximations that yielded an accuracy, for exponential doping profiles in the base, equivalent to that of the negative capacitance model of Chen et al. [11]. Chen et al. also provided greater accuracy in what they called an inductance model for an exponentially doped profile. From now on we will refer to this as the EDPL model (exponential doping profile inductance model). Seitchik et al. [10] developed a modified Gummel-Poon model for exponentially doped profiles by using truncations of expansions for $y_{11}(s)$, $y_{21}(s)$ and $\beta(s)$.

2.3.2 Large Signal Models

To illustrate the improvements of the large signal HDNQS (heavily doped non-quasi static) models over the original Gummel-Poon model [1] we compare the transient collector current predicted by the models with the exact solution in Fig. 2.5. The exact solution is the solution of

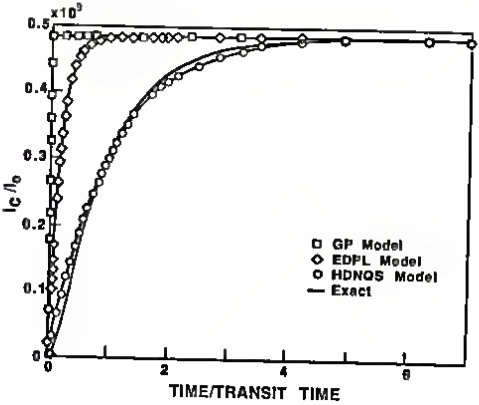

Fig 2 5 The collector current response to a large-signal step input voltage derived via the Gummel-Poon (GP) model, via the exponentially doping profile inductance (EDPL) model and via the heavily doped non-quasi-static (HDNQS) model , compared with the exact solution A Gaussian profile is used in this simulation

(2 11) without truncating $A_{21}(e)$. In comparison, we consider a p type base layer having a Gaussian profile in which the peak doping exceeds $10^{18}cm^{-3}$ (heavy doping). We focus on the forward active mode, assume a nearly step input voltage and, for the present, no base resistance.

In Fig. 2.5, we also show the prediction of the EDPL model, which uses space-independent diffusivity, mobility, and energy gap to get compact analytic solutions. If base resistance is negligible, the delay exhibited in Fig. 2.5 is entirely contributed by the intrinsic carrier propagation delay. For an exact step-function voltage, the Gummel-Poon model would show no delay because it assumes infinite minority carrier velocity. The EDPL model, with delay included, underestimates the delay time by about 70%. The HDHQS model, incorporating a Gaussian profile having doping effects modeled after Swirhun [51], and delay gives a response within 5% of the exact solution.

For simplicity, we have normalized the collector current by saturation current I_0 and have assumed the same I_0 for each model. If we had included changes in I_0 due to the heavy doping effects and the varying doping profile, the predictions of the EDPL model and the Gummel-Poon model would have shown even larger deviation from the exact solution than those illustrated in Fig. 2.5. Figure 2.6 illustrates the Asher delay time [56] versus the variance σ^2 of the Gaussian profile for the three different models shown in Fig. 2.6. The Gummel-Poon (GP) model shows no delay; for the EDPL model the delay is substantially underestimated.

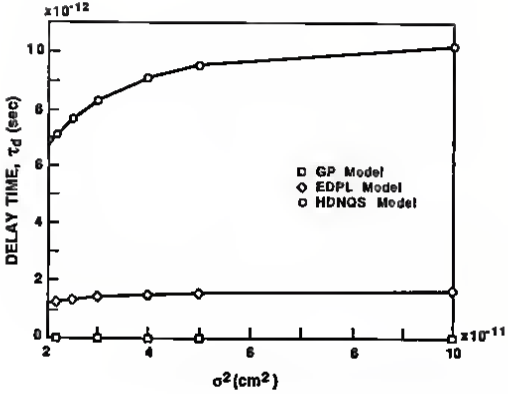

Fig 2 6 Comparison of the intrinsic propagation delay time predicted by the Gummel-Poon (GP) model, by the exponentially doping profile inductance (EDPL) model and by the heavily doped non-quasi-static (HDNQS) model versus the variance σ^2 of Gaussian profiles, $10^{18}\exp(-x^2/\sigma^2)$.

Usually the base delay time ($R_{11}\,C_{11}$) $\approx \beta^{-1}\tau_{tf}$. Hence for an ideal step current source input, the transient response of the non-quasi-static model will only slightly differ from that of the quasi-static model. However, an emitter-coupled logic (ECL) circuit uses an emitter follower as the input stage to reduce the base storage time and to enhance the driving capability [59]. Thus the input source resistance for an ECL circuit is small (10-100 ohms). Because the base resistance of advanced transistors is also small (about 10-100 ohms for the devices fabricated by MOSAIC III [60]), ECL circuits are voltage driven. Hence non-quasi-static models such as those developed here are needed in principle for accurate ECL transient simulations. The utility of such models is even more pronounced in power and power-electronic applications where thick base layers are used.

2.3.3 Small-Signal Models

2.3.3.1 h_{21} and y_{21}

To assess the validity of the small-signal model, we compare several model predictions of the phase of the current gain (h_{21}) and the phase of the transconductance (y_{21}) with laboratory experiment in Figs. 2.7(a) and 2.7(b). The experiment makes use of a large transistor for which non-quasi-static effects become important at low frequencies and multi-dimensional effects are insignificant in low injection. Figures 2.8(a) and 2.8(b) illustrate the structure and doping profile of the devices measured. We measured the transistors by standard s-parameter techniques. The DC operating point is defined by $I_C = 100\ \mu A$ and by $V_{BC} = -9.3$ volts. Because the doping profile is nearly

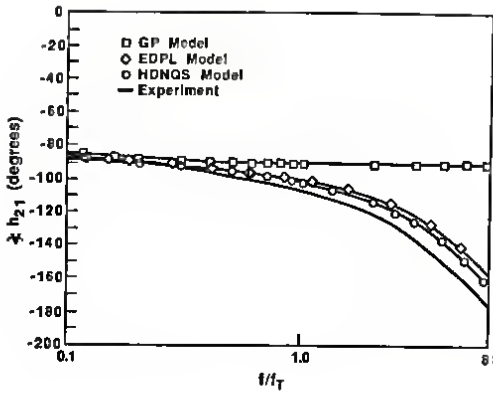

Fig. 2.7 Comparison of the relative phase predicted by the Gummel-Poon (GP) model, by the exponentially doping profile inductance (EDPL) model and by the heavily doped non-quasi-static (HDNQS) model with experimental data. (a) b_{21}; (b) y_{21}.

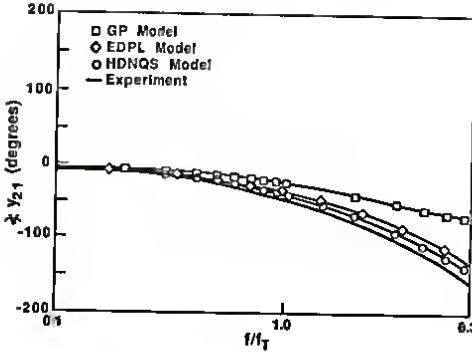

Fig. 2.7—continued

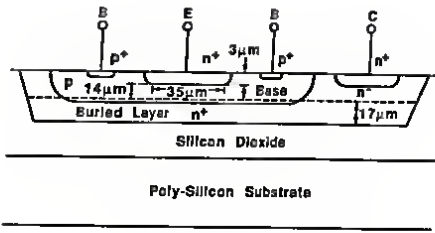

Fig. 2.8 The transistor measured (a) The structure, (b) The doping profile

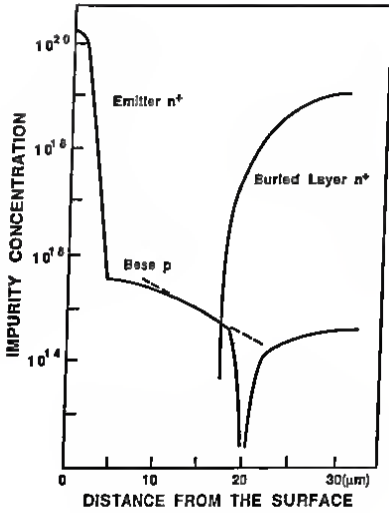

(b)

Fig 2.8 (continued

exponential and the peak doping density is less than 10^{17} cm ^{3}, the EDPL model and the HDNQS model produce comparable results in this simulation, and their improvements over the GP model are significant

To demonstrate the superiority of the HDNQS model for homojunction and heterojunction bipolar transistors, we take a uniform profile with a linearly varying gap as an example [41] and compare in Fig. 2.9 the phase of $y_{21}(\omega)$ predicted by various models with the exact solution. As shown in Fig. 2.9, the HDNQS model developed here agrees with the exact solution for frequencies beyond the cutoff frequency, whereas the EDPL model and the GP model fail to follow the exact solution even below this frequency. A multi-section EDPL model can perform comparably to the HDNQS model, but at the expense of additional CPU time.

2.3.3.2 y_{11} and h_{11}

In Figs. 2.10(a) and 2.10(b), we compare against exact solutions the magnitude and the phase of y_{11} predicted by the four different small signal models. The four different models are shown in Fig. 2.11. Figure 2.11(a) shows the small-signal GP model [42], which is based on the quasi-static approximation. Figure 2.11(b) demonstrates the Seitchik's model, which includes the non quasi-static effect in the base layer. Figure 2.11(c) describes the exponentially doping profile inductance (EDPL) model, which includes the base non quasi-static effect by adding the inductance into Fig. 2.11(a) [6]. Figure 2.11(d) exhibits the HDNQS model, which includes non quasi-static effects in both emitter and base layers. For simplicity, we simulate a uniformly doped (10^{17} cm^{-3}) base layer with 0.5 μm thickness and a uniformly

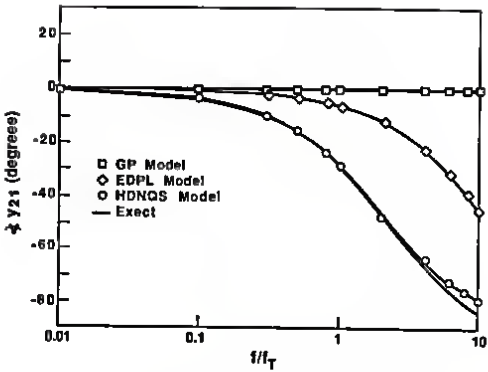

Fig. 2.9 Comparison of the relative phase of y_{21} predicted by the Gummel-Poon (GP) model by the exponentially doping profile inductance (EDPL) model and by the heavily doped non-quasi-static (HDNQS) model with the exact solution A uniformly doped base layer with linearly varying energy gap is assumed

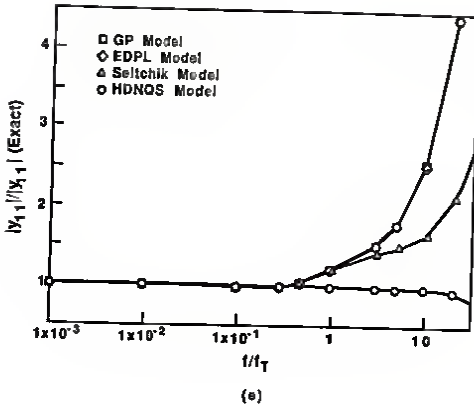

Fig. 2.10 Comparison of y_{11} predicted by four different models shown in Fig. 2.11 with the exact solution
(a) The magnitude, (b) The relative phase

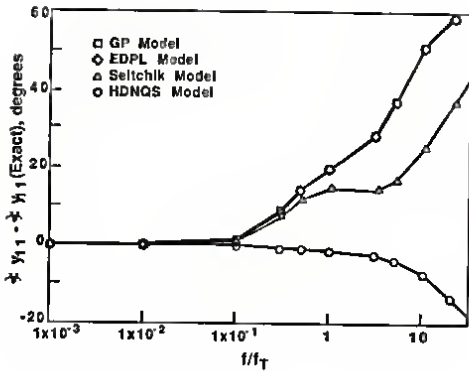

(b)

Fig 2.10 -continued

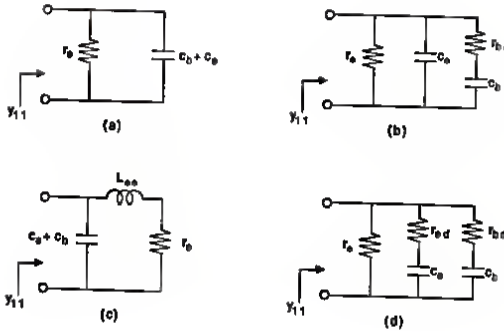

Fig 2 11 The input ports of four different small-signal models (a) The Gummel-Poon (GP) model (no base delay and emitter delay), (b) The Seitchik's model (base delay denoted by resistance in series with capacitance) (c) The exponentially doping profile inductance (EDPL) model (base delay denoted by resistance in series with inductance), (d) The heavily doped non-quasi-static (HDNQS) model which includes base delay and emitter delay

doped (10^{20} cm^{-3}) emitter layer with 1 5 μm thickness and with a polysilicon emitter contact The discrepancies between the model predictions and the exact solution shown in Figs 2 10(a) and 2 10(b) imply that non quasi-static effects are important in the emitter layer as well as in the base layer For most transistors operating in low injection the non-quasi-static model in Fig 2 11(b) provides accurate simulations of $y_{11}(\omega)$ up to the cutoff frequency f_T But for those transistors in which the emitter delay time τ_{ed} is comparable to $\beta\ \tau_d$ or to τ_{et} we need the non-quasi-static model in Fig 2 11(d) to simulate y_{11} adequately for $f \approx f_T$ Figure 2 12 compares the magnitude and the phase of h_{12} predicted by the GP model and the HDNQS model with experiment As shown in Figs 2 12(a) and 2 12(b), the prediction of the HDNQS model agrees with the experimental data for frequency up to ten times the cutoff frequency In contrast the GP model fails to predict the experimental data beyond cutoff frequency

2 4 Summary

A systematic method was developed to derive non-quasi-static large-signal and small-signal models for quasi neutral layers in homojunction and heterojunction bipolar transistors In this method we analytically solve the continuity equations and the current equations To obtain the solution we

use Laplace transformation with respect to time

integrate with respect to position,

apply boundary conditions

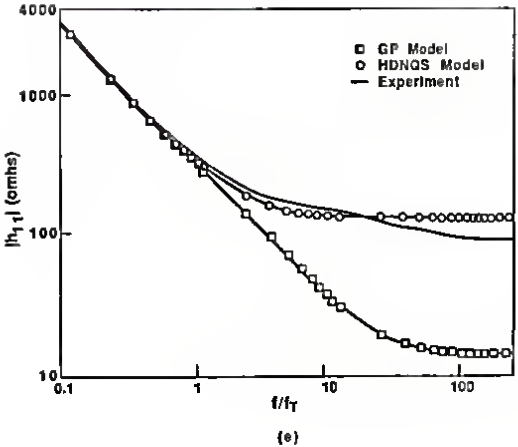

Fig. 2.12 Comparison of h_{11} predicted by the heavily doped non-quasi-static (HDNQS) model and the Gummel-Poon (GP) model with the experimental data.
(a) The magnitude, (b) The phase.

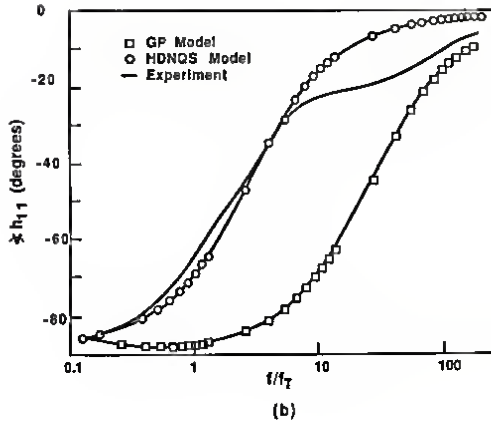

Fig. 2.12 (continued)

The resulting solutions of these equations are in the form of infinite series in e Truncation with respect to e at different orders yields various models with different complexities and accuracies The models accommodate arbitrarily and heavily doped profiles For the simulation of high speed or high frequency integrated circuits they are more accurate than the Gummel-Poon model The application of this method to include moderate and high level injection as well as for ac and transient emitter crowding will be discussed in next chapters

CHAPTER THREE
ONE-DIMENSIONAL ALL INJECTION NON QUASI-STATIC MODELS FOR ARBITRARILY DOPED QUASI NEUTRAL LAYERS IN BIPOLAR JUNCTION TRANSISTORS INCLUDING PLASMA-INDUCED ENERGY GAP NARROWING

3.1 Introduction

The purpose of this chapter is to develop non quasi static circuit models for quasi neutral layers in bipolar junction transistors that are general enough to include all injection levels and impurity profiles. These models, when coupled with existing models for the junction space-charge layers, improve the Gummel-Poon model [1], which is widely used for transient or frequency response simulations. The Gummel-Poon model is based on the quasi-static approximation, which assumes that carriers propagate with infinite velocity in the quasi-neutral layers. This assumption reduces the accuracy of transient and frequency response simulations.

Recently several non quasi static models [2]-[12] that avoid the inaccuracies of the quasi-static approximation have been presented. These models, however, are based on assumptions that limit their range of applicability because either a specific base doping profile or the condition of low injection was assumed in their derivation.

In this chapter, we derive new quasi-static models for quasi-neutral layers under low injection and high injection based on the Shockley equations and the systematic method discussed in Chapter Two and [14] and reviewed briefly here, a method that applies for all

doping profiles but is restricted to low injection. In developing models for all levels of injection, we use a fitting scheme related to that in [41] to include all levels of injection within quasi-neutral layers. We can use terminal measurements or results from device simulators to optimize the fitting parameters.

In treating high injection in the base, it is common to assume that the majority current density is negligible, which allows a simple calculation of the electric field. In this chapter, we analytically account for the presence of significant majority base current for any level of injection which includes the special case of low transistor beta.

We also quantitatively include the effects of the additional Coulomb shielding that results when the electron and hole concentration exceed about 10^{17} cm^{-3}, conditions that occur in digital bipolar integrated circuits [46]. The presence of a high density electron-hole plasma causes energy-gap shrinkage, the magnitude of which has been determined by experiment [20], by a Debye screening model [21], and by many body theory [22]. The engineering implications of a very high-injection plasma has received attention in [23].

The derivation in this chapter is based on the assumptions of a one-dimensional $n^+/p/n^+$ structure. In next two chapters, we will extend this method to derive non-quasi-static circuit models that include emitter crowding and base pushout and still accommodate any doping profile and all injection levels.

The models developed have nearly a traditional equivalent-circuit form. They consist of connections of passive circuit elements and

controlled sources, consistant with Sah's exact model [38] for the Shockley equations. The models are not exactly traditional transistor equivalent circuits because they contain negative capacitances or inductances in the network representation for the intrinsic transistor. These elements serve to include non quasi-static effects while restraining the overall model complexity. We incorporate these circuit elements into SPICE2 by using "user-defined controlled sources," which are FORTRAN subroutines accessed by SLICE [39].

3.2 Derivation of the Models

We follow the traditional practice of dividing the transistor into junction space charge and quasi-neutral layers. As the main example treated, we focus on a p-type base layer, although the treatment can be generalized to accommodate the emitter and collector layers.

One-dimensional carrier transport in the quasi-neutral layers of bipolar junction transistors is described by two current equations and two continuity equations

$$j_n(x,t) = q\mu_n(x)n(x,t)E_n(x,t) + qD_n(x)(\partial n(x,t)/\partial x) \tag{3.1}$$

$$j_p(x,t) = q\mu_p(x)p(x,t)E_p(x,t) - qD_p(x)(\partial p(x,t)/\partial x) \tag{3.2}$$

$$\partial n(x,t)/\partial t = (1/q)(\partial j_n(x,t)/\partial x) - n(x,t)/\tau_n(x) \tag{3.3}$$

$$\partial p(x,t)/\partial t = -(1/q)(\partial j_p(x,t)/\partial x) - p(x,t)/\tau_p(x) \tag{3.4}$$

where $E_{n,p}$ are the electric fields acting on electrons and holes respectively.

In the development that follows, we begin in Sec. 3.2.1 by treating fully the simplest case in which hole current and energy-gap

narrowing in the p-type base are both negligible This treatment suffices if (a) the hole current is much smaller than the electron current and (b) the doping level and the hole and electron densities are less than approximately 10^{17} cm^{-3} In Sec 3 2 2, we include the energy gap narrowing induced by large hole and electron densities We then indicate extensions in Sec 3 2 3 to accommodate the large hole current in the base layer.

From (3 2) and the assumption that the energy gap E_g is independent of x

$$E_p(x,t) = (j_p + qD_p \partial p/\partial x)/q\mu_p p \approx E_n(x,t) \tag{3 5}$$

Energy-gap narrowing for low injection is treated in the chapter two and [14] In Section 3 2 3 we include plasma induced energy gap narrowing

Substituting (3 5) into (3 1) yields the nondimensional relation

$$\frac{p\mu_p j_N(x,t)}{n\mu_n j_p(x,t)} \quad 1 = \frac{1}{j_p}\left(qD_p \frac{\partial p}{\partial x} + qD_n \frac{\partial n}{\partial x} \quad \frac{p\mu_p}{n\mu_n}\right) \tag{3 6}$$

Equation (3 6) holds for all levels of injection. We do the boundary conditions

$$\Delta n_j = (1/2)\{ [N_{Aj}^2 + 4n_i^2(\exp(v_{QFj}/V_T) 1)]^{1/2} - N_{Aj}\} \quad j=1\ 2\ \ldots, \tag{3 7}$$

obtained from the quasineutrality condition Here $v_{QFj} = v_{Fj} - v_{Nj}$ is the difference between the hole and electron quasi-Fermi potentials at $x = x_j$ In (3 7) Δn_j denotes the excess electron density at $x = x_j$ and N_{Aj} represents the doping concentration at $x = x_j$

For forward-active operation, the electron density at the base edge of the collector depletion layer and the electron current density are correlated as first explained by Middlebrook [62]. This interdependence is important particularly for the analysis of base pushout. Thus, for full generality, use of (3.6) and (3.7) for forward-active operation requires a simple iteration procedure employing such expressions for this interdependence as those found in the work of de Graaff [63].

3.2.1 Method of Derivation

3.2.1.1 Arbitrary doping profiles and low and high injection

Consider a p-type quasi-neutral intrinsic base layer. We approximate an arbitrary practical doping profile $N_A(x)$ plotted logarithmically versus x by a piecewise linear curve (Fig. 3.1). In Fig. 3.1, subscripts j and j+1 denote the edges (x_j and x_{j+1}) of the subregion of the base that defines any segment of the piecewise linear curve. In the subregion $\Delta x_j = x_{j+1} - x_j$,

$$N_A(x) = N_{Aj} \exp(qE_j x/kT) \quad \text{or} \quad \ln N_A(x) = qE_j x/kT + \ln N_{Aj} \tag{3.8}$$

In (3.8), E_j is the built-in electric field in an exponentially doped base subregion Δx_j for low-level injection

$$E_j = -(kT/q)\ln(K_j)/\Delta x_j \tag{3.9}$$

where $K_j = N_{Aj}/N_{A,j+1}$.

In this section, we assume a position-independent energy gap for electrons and holes and consider each Δx_j to be thin enough that D_n is constant through its thickness. To illustrate the method of derivation

in the simplest way, at this point we assume that $(p/n)(\mu_p/\mu_n)[j_N(x,t)/j_p(x,t)] \gg 1$ in eqn. (3.6). (This is consistent with the approach taken by many previous authors who assumed negligible majority hole current in the p-type base.) We will relax this assumption later, in Section 3.2.3.

Substituting (3.6) into (3.3) yields

$$\partial n/\partial t = D_n[n\,\partial^2(\ln p)/\partial x^2 + \partial n/\partial x\,\partial(\ln p)/\partial x + \partial^2 n/\partial x^2] - n/\tau_n(x) \tag{3.10}$$

Taking the Laplace transform of (3.10) for low-level injection ($n = \Delta n \ll p \approx N_A$) and high level injection ($p = \Delta p \approx \Delta n = n \gg N_A$) yields for each Δx_j:

$$d^2\Delta n/dx^2 - (1/\Delta x_j)\ln K_j\,(d\Delta n/dx) \quad (1 + s\tau)\Delta n/L^2 = 0 \tag{3.11}$$

where for low injection

$$\tau = \tau_n,\ L = L_n = (D_n\tau_n)^{1/2}$$

and for high injection

$$\tau = \tau_H,\ L = (D_H\tau_H)^{1/2} \text{ with } D_H = 2D_n,\ K_j = 1$$

In (3.11), s is the Laplace transformation variable, which equals d/dt.

Equation (3.11) is an ordinary differential equation with coefficients independent of x. Combining its solution at ports $j = 1$ and $j + 1 = 2$ with the expression for the injected electron current density in (3.1), we obtain analytic solutions in a two-port form

$$\begin{bmatrix} I_1(s) \\ I_2(s) \end{bmatrix} = \begin{bmatrix} A_{11}(s) & A_{12}(s) \\ A_{21}(s) & A_{22}(s) \end{bmatrix} \begin{bmatrix} \Delta n_1(s)\sqrt{K} \\ \Delta n_2(s)/\sqrt{K} \end{bmatrix} \tag{3.12}$$

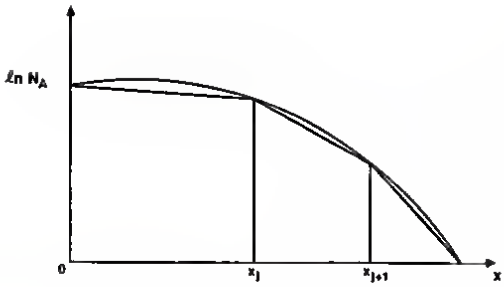

Fig 3.1 A piece-wise linear curve for fitting arbitrarily doped base layers in logarithmic scale

where

$$A_{11} = (AqD/\Delta x)[\lambda\coth(\lambda) + (\ln K/2)]/\sqrt{K}$$

$$A_{22} = (AqD/\Delta x)[\lambda\coth(\lambda) - (\ln K/2)]\sqrt{K}$$

$$A_{12} = -(AqD/\Delta x)\lambda\operatorname{csch}(\lambda)$$

$$A_{21} = -(AqD/\Delta x)\lambda\operatorname{csch}(\lambda)$$

$$\lambda^2 = (\ln K/2)^2 + \Delta x^2(s/D)$$

Excluding the effect of series resistance, $A_{12} = A_{21}$. The expressions for the matrix elements A_{ij} shown above are based on the approximation that the recombination lifetime is small compared with the base transit time, which holds in many transistors.

To obtain the non-quasi-static circuit realization of (3.12), we first truncate the matrix elements A_{ij} to the first order of s. This approach improves the truncation used in [65], in which some of the coefficients of s^0 and s^1 terms are also truncated. The two-port equations of (3.12) correspond to either a hybrid-π network representation or a π network representation [2]. Here, to be consistent with the form of conventional Gummel-Poon model, we adopt the π representation, which yields the large-signal circuit model shown in Fig. 2.2. In this figure,

$$i_{11}(s) = [A_{11}(s) + A_{12}(s)]\Delta v_1(s)\sqrt{K} \qquad (3.13)$$

$$= (AqD/\Delta x f_1)\,[sr_f/(1 + sr_d)]\,\Delta v_1(s)$$

$$i_{22}(s) = [A_{22}(s) + A_{21}(s)]\Delta v_2(s)/\sqrt{K} \qquad (3.14)$$

$$= (AqD/\Delta xf_1)\ [sr_r/(1 + sr_d)]\ \Delta n_2(s)/K$$

$$i_{12}(s) = [-A_{12}(s)]\ [\Delta n_1(s)\ \sqrt{K} - {}_2\Delta n\ (s)/\sqrt{K}] \qquad (3\ 15)$$

$$= (AqD/\Delta xf_1)\ (1 + sr_d)^{-1}\ [\Delta n_1(s) - \Delta n_2(s)/K]$$

Here r_f is the forward bass transit time, r_r is the reverse bess transit time, and r_d is the base delay time defined by Elmore [55] and Ashar [56]. Expressions for these time constants and for f_1, which relates the doping gradient to the saturation current, are listed in Appendix C.

By taking the inverse Laplace transform of (3.13), (3.14) and (3.15), we obtain the large-signal circuit model shown in Fig. 3.2 (a), in the figure,

$$R_{jj}\ i_{jj} + (1/C_{jj})\ \int_0^t i_{jj}dt = v_j \qquad j = 1,\ 2 \qquad (3\ 16)$$

where

$C_{11} = (AqD/\Delta xf_1)\ (r_f)[\Delta n_1(t)/v_1]$, $R_{11} = r_d/C_{11}$

$C_{22} = (AqD/\Delta xf_1K)\ (r_r)[\Delta n_2(t)/v_2]$ $R_{22} = r_d/C_{22}$

and

$$Rf_{12}(t) + L\ di_{12}(t)/dt = v_1 - v_2 \qquad (3\ 17)$$

where

$R = (v_1 + v_2)/(AqD/\Delta xf_1)\ [\Delta n_1 - \Delta n_2/K]$, $L = r_dR$.

The inductor L and the resistor R_{11} (R_{22}), which are not present in the Gummel-Poon model, represent the carrier propagation delay of the bass conduction current and of the base storage current respectively. In Fig. 3.2(b) we show an alternate form of the large signal model for

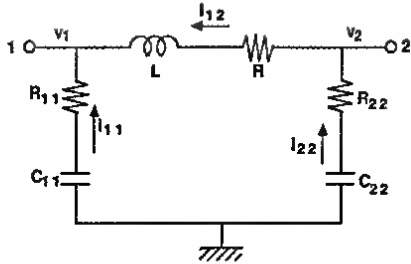

Fig. 3.2 The large signal equivalent circuit models for subregion A_{xj} (a) The inductance model for the quasi-neutral base layer (b) An alternate form of (a) for circuit application

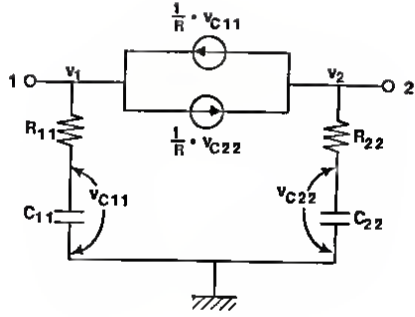

Fig 3 2 continued

circuit implementation. The equality of Figs. 3.2(a) and 3.2(b) is proved in Chapter Two and [14].

For the small-signal case, by assuming $\delta v_j \ll mkT/q$, we have

$$\exp(qv_j/mkT) = \exp[q(V_j + \delta v_j)/mkT] \approx \exp(qV_j/mkT)\,(1 + q\delta v_j/mkT) \tag{3.18}$$

where $m=1$ for low injection and $m=2$ for high injection. Substituting (3.18) into (3.13), (3.14) and (3.15), we obtain the small-signal model shown in Fig. 3.3(a), in which

$$c_{11} = (AqD_n/\Delta x f_1)\,(r_F)(q\Delta N_1/kT), \quad r_{11} = r_d/c_{11} \tag{3.19}$$

$$c_{22} = (AqD_n/\Delta x f_1 K)\,(r_x)(q\Delta N_2/kT), \quad r_{22} = r_d/c_{22} \tag{3.20}$$

$$r = (kT/q)/(AqD_n/\Delta x f_1)\,(\Delta N_2/K), \quad L_{ee} = r_d r \tag{3.21}$$

$$F_m = (q/kT)/(AqD_n/\Delta x f_1)[\Delta N_1 \quad \Delta N_2/K) \tag{3.22}$$

where ΔN_1 and ΔN_2 denote the excess carrier densities on dc bias and the subscript (ss) indicates small-signal excitation. An alternate form of the small-signal model appears in Fig. 3.3(b).

The models with the inductance (Figs. 3.2a and 3.3a) reveal delay explicitly. They are more easily compared with the Gummel-Poon model and the Sah model than are the models of Figs. 3.2(b) and 3.3(b). The models with the voltage-controlled current sources (Figs. 3.2b and 3.3b), however, provide advantages in circuit implementation.

Approximating $A_{12}(s)$ in (3.15) by $1 - sr_d$ gives the negative capacitance version of the non quasi-static model, in which the series combination of inductance and resistance in Fig. 3.2 and Fig. 3.3 is replaced with a negative capacitance in parallel with a conductance,

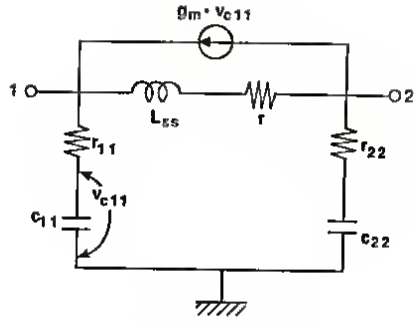

Fig 3 3 The small-signal equivalent circuit model for subregion Δx_j (a) The inductance model for the quasi-neutral base layer. Note that exchanging node E and node C gives another inductance model, (b) An alternate form of (a) for circuit application.

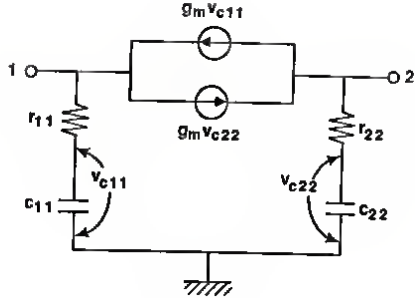

Fig. 3-3--continued

$$G = 1/R, \quad C = \tau_d G, \quad g = 1/r, \quad -c = -\tau_d g \tag{3 23}$$

The additional assumption, $(1 + e\tau_d)^{-1} \approx 1 - e\tau_d$ makes the negative capacitance model less accurate than the inductance model in simulating transconductance (y_{21}) at high frequencies and in representing the large-signal transient response [11]

3 2 1 2 Equivalent-Circuit Models for ALL Injection Levels

Since an analytic model for the base layer in moderate injection is difficult to get because the continuity equation is nonlinear, we fit parameters (such as τ_E, τ_R and τ_d and the forward and reverse collector currents, I_F and I_R) based on the low-injection and high-injection models to obtain the model for all injection levels [61] For example, fitting I_F and I_R versus injection level gives the general expression for K in Fig 3.2(e) for all injection levels Once K is determined the general expressions for L, C_{11} (C_{22}) and R_{11} (R_{22}) can be deduced by fitting τ_E, τ_F and τ_R versus injection levels The resulting models for all injection levels have the same form as Fig 3 2 and Fig 3 3, though the expressions for the circuit elements differ from those applying for low and high injection

For the all-injection large-signal model, we denote the forward active transit time by TF reserving τ_F for low injection and high injection Similarly TDF replaces τ_{dF}, where the F refers to forward active operation; IF is a fitting parameter related to the forward current, etc. The circuit elements of this model are defined by

$$C_{11} = TF \cdot IF \left[\partial n_1(t)/v_1\right], \quad R_{11} = TDF/C_{11} \tag{3 24}$$

$$C_{22} = TR\ IR\ [\Delta n_2(t)/v_2], \quad R_{22} = TDR/C_{22} \tag{3 25}$$

$$R = (v_1 - v_2)/[1F\ \Delta n_1 - 1R\ \Delta n_2] \tag{3 26}$$

$$L = (v_1 - v_2)/[IF\ \Delta n_1/TDF - 1R\ \Delta n_2/TDR] \tag{3 27}$$

and for the small signal model

$$c_{11} = TF\ If\ [q\Delta N_1/kT], \quad r_{11} = TDF/c_{11} \tag{3 28}$$

$$c_{22} = TR\ Ir\ [q\Delta N_2/kT], \quad r_{22} = TDR/c_{22} \tag{3 29}$$

$$r = kT/(q1r\ \Delta N_2) \qquad L_{ss} = TDR/r \tag{3 30}$$

$$g_m = q(If\ \Delta N_1 - 1r\ \Delta N_2)/kT \tag{3 31}$$

The expressions for the fitting parameters, 1F, IR, If, Ir, TR, TF, TDF and TDR are listed in Appendix C.

We have assumed that the functional dependencies on current of time constants (TF, TR, TDF and TDR) of the large-signal model are the same as those of the small-signal model at all injection levels. This implies Q_B(base storage charge)/$I_C = dQ_B/dI_C$ [42]. This assumption introduces no error in low injection and high injection. For moderate injection, we retain this assumption to minimize the number of model parameters. To achieve better accuracy, we may follow the same fitting scheme to fit four more parameters for the small signal model.

Because of the reciprocity shown in (3-12), the forward delay time TDF is enough in principle to characterize the delay in the forward-active mode as well as in the reverse-active mode. In any subregion $\Delta x = (x_1 - x_2)$, however, we may have high injection at x_1 and low injection at x_2. Then reciprocity is invalid and TDF fails to describe the delay. Thus we need to fit an additional time constant TDR, which

is controlled by the injection level at x_2, to achieve better accuracy We can also replace $\Delta n_j/N_{Aj}$ (see Appendix C) which corresponds to the injection level at x_j, by

$$\int_{x_j - \Delta x_{j-1}/2}^{x_j + \Delta x_j/2} (\Delta n_j/N_{Aj})dx/(\Delta x_j/2 + \Delta x_{j-1}/2)$$

to reflect the injection level in subregion Δx_j Although we benefitted from the insight in [61], their fitting procedure ignored this possibility Therefore, their prediction of the reverse collector current and the reverse transit time differs from our prediction

The number of the subregions chosen in the models is mainly determined by doping profile and accuracy required In the simulation of heavily doped layers, the position dependence of diffusivity, lifetime and energy gap also need to be considered while partitioning base layers because positional averages of these parameters are used in each subregion

The models developed here are in the common base configuration To derive the common-emitter or the common-collector configuration of these models, one may exploit the indefinite admittance matrix [57] or choose the hybrid-π network representation in the realization of the two port equation A direct way to perform this transformation is to use the models shown in Fig 3-2(b) and Fig 3-3(b) As an example, we show a two-section small signal model in Fig 3-4 for the common-emitter configuration To implement the models into circuit simulators, such as SPICE we employ the method of User Defined Controlled Source [39] to accommodate nonlinear circuit elements

present in the models In Appendix C, we show three voltage controlled current sources for the implementation of the large-signal model

3 2 2 Inclusion of Plasma Induced Energy Gap Narrowing

The concept of apparent energy-gap narrowing ΔE_g is presently widely used [66] [67] Apparent energy gap narrowing is defined by the relation $pn = n_i^2 \exp(\Delta E_g/kT)$ which thus includes the effects of Fermi statistics present in the more physically correct relation, $pn = n_i^2 \exp(\Delta E_g'/kT)\, F_{1/2}[(qV_N - E_c)/kT] \exp[-(qV_N - E_c)/kT] F_{1/2}[(E_v - qV_p)/kT] \exp[(E_v - qV_p)/kT]$ where $\Delta E_g'$ is the true energy-gap narrowing measured between the conduction-band edge, E_c, and valence-band edge, E_v and where $F_{1/2}$ is the Fermi integral of order 1/2 In this chapter we will follow the prevailing practice of using the apparent energy gap narrowing In which the parameter ΔE_g includes the effect of Fermi statistics

Energy gap narrowing ΔE_g due to high concentrations Δn of excess carriers in lightly doped base layers was measured in [20] This plasma-induced band gap narrowing causes the electric field acting on holes to differ from that acting on electrons by $(1/q)\partial \Delta E_g/\partial x$ [68] Including this term in (3 5) and deriving the electron current under the assumption, $(p/n)(\mu_p/\mu_n)[j_N(x,t)/j_P(x,t)] \gg 1$, gives

$$j_N(x,t) = qD_n[\partial \Delta n/\partial x + (1/kT)\Delta n \partial \Delta E_g/\partial x] \qquad (3\ 32)$$

Equation (3 32) is a nonlinear equation because ΔE_g depends on Δn as determined in [20] [22]

$$\Delta E_g \text{ (plasma)} = a_0 (kT/q) \ln(\Delta n/n_1) = e_1 \qquad (3\ 33)$$

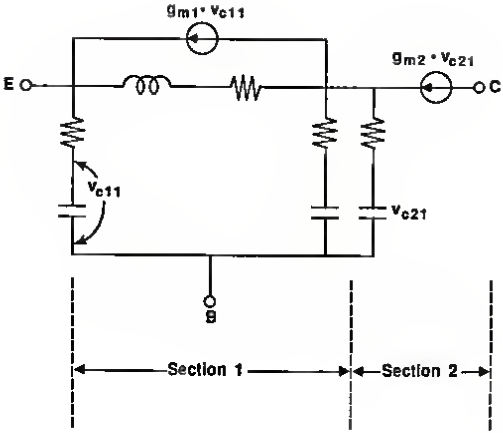

Fig 3.4 The two-section small-signal equivalent circuit model for a intrinsic base layer in the forward active mode.

which shows the dependence of ΔE_g(plasma) on the chemical potential $(kT/q)\ln(\Delta n/n_i)$. In (3.33), n_i is the intrinsic carrier concentration. Substituting (3.33) into (3.32) yields

$$J_N(x,t) = qD_n(2 - a_0/a_1)\partial\Delta n/\partial x = qD_n f_p \partial\Delta n/\partial x \qquad (3.34)$$

According to data measured in [20], a_0 is approximately 0.7 q and $a_1 \approx$ 265 mev for $\Delta n \leq 5\times10^{17}$ cm^{-3}, and $a_0 \approx q$ and $a_1 \approx 414$ mev for $\Delta n > 5\times10^{17}$ cm^{-3}. Thus, for $\Delta n \leq 5\times10^{17}$ cm^{-3}, f_p is about 1.3 instead of 2. That implies that the base transit time including ΔE_g in high injection will be about 1.5 times larger than that excluding ΔE_g in high injection. We can include this plasma effect in the models developed by adding f_p to the fitting parameters in Appendix C.

3.2.3 Inclusion of Significant Majority Hole Current (Low Current Gain)

We now relax the assumption, $(p/n)(\mu_p/\mu_n)[J_N(x,t)/J_p(x,t)] \gg 1$, made in Sections 3.2.1 and 3.2.2.

For transistors operating at high current levels, the minority electron current in the p type quasi neutral base layer increases less strongly with v_{BE} than does the majority current, because of extrinsic resistances or base pushout. Thus, even for forward active operation, the majority hole current could be comparable to the minority electron current at high injection levels. Furthermore, for transistors operating in the reverse-active or saturation modes, the majority hole current may even exceed the minority electron current. This implies that the current gain, β, could be smaller than unity.

From (3.2) and the inclusion of position-dependent energy-gap narrowing

$$E_n = (j_p + qD_p\partial p/\partial x)/q\mu_p p \qquad (1/q)\partial\Delta E_g/\partial x \tag{3.35}$$

Substituting (3.35) into (3.1) yields the expression for the minority electron current in high injection ($n \approx p$)

$$j_N = (\mu_n/\mu_p)j_p + f_p qD_n \partial n/\partial x \tag{3.36}$$

where f_p is defined in (3.34). Substituting (3.36) into (3.3) gives

$$\partial n/\partial t = (1/q)(\mu_n/\mu_p)\partial j_p/\partial x + f_p D_a \partial^2 n/\partial x^2 - n/\tau_H \tag{3.37}$$

where τ_H is the recombination lifetime in high injection. For simplicity and conciseness, we shall neglect recombination in the following derivation. Solving (3.4) and (3.37) in the base layer results in

$$n(x,s) = [s\sinh[\lambda_H(W-x)]\Delta n(0,s) + s\sinh(\lambda_H x)\Delta n(W,s)]/s\sinh(\lambda_H W) + p(x,s) \tag{3.38}$$

where $\lambda_H^2 = 2s/f_p D_a$ and D_A is the ambipolar diffusivity.

Substituting (3.38) into the Laplace Transformation of (3.4) and integrating the resulting equation from $x = 0$ to $x = W$ gives

$$j_p(0,s) = qs[(\cosh\lambda_H W - 1)/\lambda_H s\sinh\lambda_H W]\Delta n(0,s) \tag{3.39}$$

in the forward active operation and

$$j_p(W,s) = qs[(\cosh\lambda_H W - 1)/\lambda_H s\sinh\lambda_H W]\Delta n(W,s) \tag{3.40}$$

in the reverse-active operation. Substituting (3.38) - (3.40) into (3.36) results in a new two-port form

$$\begin{bmatrix} i_1(s) \\ i_2(s) \end{bmatrix} - \begin{bmatrix} A_{11}(s) & A_{12}(s) \\ A_{21}(s) & A_{22}(s) \end{bmatrix} \begin{bmatrix} \Delta n_1(s) \\ \Delta n_2(s) \end{bmatrix} \quad (3.41)$$

where

$$A_{11} = Aqf_p D_n \lambda_H \operatorname{csch}(\lambda_H W)[\cosh(\lambda_H W) - [D_n/(D_n + D_p)][\cosh(\lambda_H W) - 1]] = A_{22}$$

$$A_{12} = -(Aqf_p D_n)\lambda_H \operatorname{csch}(\lambda_H W) = A_{21}$$

Up to now, our discussion has focussed on including significant majority current (j_p) for high injection, and we have indicated the need to involve models for the quasi neutral emitter and the emitter base junction layers. Even for high-β transistors in which low injection prevails in the base layer, however, the forward-active response to extremely fast transient excitation may provoke the condition $j_p \approx j_N$ during a short time interval. This will occur only near the emitter edge ($x = 0$) of the space charge layer where it feeds the displacement current that charges the emitter junction layer capacitance (and changes the corresponding barrier height). To include this possibility, we follow the approach just described. Equation (3.35) remains valid for low injection where ΔE_g now reflects energy gap changes that result from space variations in chemical composition. But (3.36) is modified because in Eq. (3.6) on which it is based, the term, $(p/n)\langle \mu_p/\mu_n \rangle [j_N(x,t)/j_p(x,t)]$, may not be much greater than unity even though $p/n \gg 1$ in low injection. This violation will make (3.6) nonlinear. If this violation occurs, however, it will occur only near $x = 0$ and only for a short time interval. Inclusion of the emitter and base resistances and models for the emitter-base junction-layer capacitance [14] (as well as the model for the emitter layer), however,

will define $j_p(0,t)$ in the short time interval of interest when $j_p = j_N$, thus avoiding the nonlinearity. The analysis then proceeds straightforwardly to the low-injection replacements for (3.37) - (3.40) and the corresponding base layer model.

3.3 Assessments

3.3.1 Large-Signal Models

In Fig. 3.5(a), we plot the large-signal model prediction of the forward collector current versus the emitter/base junction voltage (V_{BE}) for different doping ratios K. In high injection ($V_{BE} > 0.8$ volts), the forward collector current has a slope proportional to $q/2kT$ and is independent of doping ratio K. In low injection ($V_{BE} < 0.5$ volts), the collector current has slope proportional to q/kT and depends on K. Our prediction differs from that of [61] because we do not assume that the base storage charge is independent of K in the simulation. In Fig. 3.5(b), we see the same trend for the reverse collector current plotted versus collector/base junction voltage (V_{BC}), except that the slope of reverse collector current for $K = 20\Omega$ at $V_{BC} = 0.55$ volts is not proportional to q/kT as predicted by [61]. This is because the injection level is still high ($n \approx p \gg N_A$) at $V_{BC} = 0.55$ volts.

In Fig. 3.6, we compare the model prediction of $I_C - V_{BE}$ against experimental data. The transistors measured have heavily doped collectors, which prevent base pushout in high injection. As shown, the model prediction agrees with experiment in low injection and moderate injection but disagrees in high injection. The discrepancy is probably

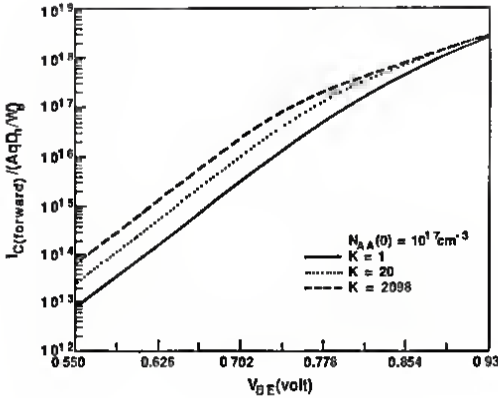

Fig 3.5 The model predictions of the collector current versus input voltage for exponentially doped base layers with different doping ratio, $K = N_A(0)/N_A(W_b)$.
(a) The forward collector current, (b) The reverse collector current

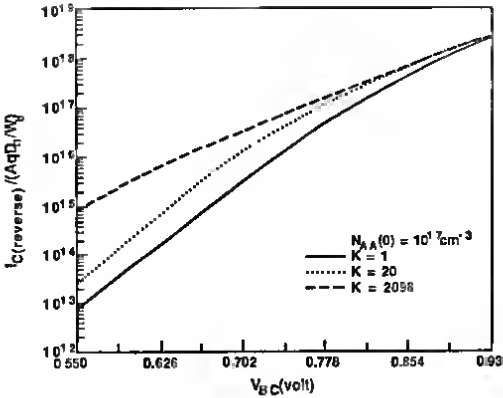

Fig 3.5(continued

due to the extrinsic resistances (R_E, R_C) and two-dimensional effects such as emitter crowding. Figure 3.7 compares the transient collector current predicted by the Gummel-Poon model and the models developed for a nearly step input voltage v_{BE}. The inductance version of the all injection non quasi static model shows intrinsic carrier propagation delay ($= \tau_d$ by Asher's definition) in the simulation while the Gummel-Poon models and the negative-capacitance model developed here follow the input voltage with no delay. The negative-capacitance model, which is similar to other recently developed models [4], [7], [12] and is less accurate than the inductance model, predicts the collector current has negative overshoot. This overshoot arises from large charging currents through the negative capacitance.

3.3.2 Small Signal Models

In Figs. 3.8(a) and 3.8(b) we plot the forward transit time versus V_{BE} and the reverse transit time versus V_{BC} respectively. In high injection, both the forward and the reverse transit time are independent of doping ratio, and they all merge at one half of the low injection values for a uniformly doped base. In low injection, the forward transit time decreases as doping ratio increases, while the reverse transit time tends to increase. Since the base layer, with K = 2.89, is still in high injection at $V_{BC} \approx 0.5$ volts, the effect of doping ratio to the reverse transit time is insignificant in Fig. 3.8(b). Figures 3.9(a) and 3.9(b) illustrate the model prediction of delay time versus input voltage. As shown, the dependence of delay time on doping ratios and on injection levels resembles the dependence

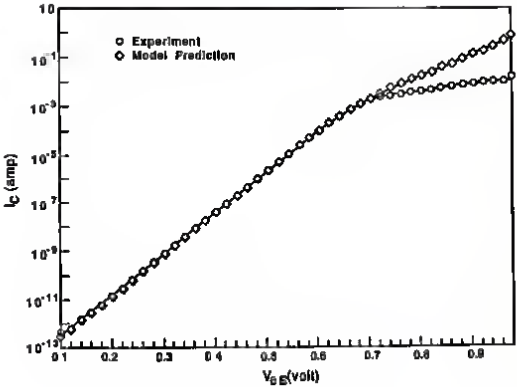

Fig 3.6 Comparison of the forward collector current versus V_{BE} between model prediction and experimental results

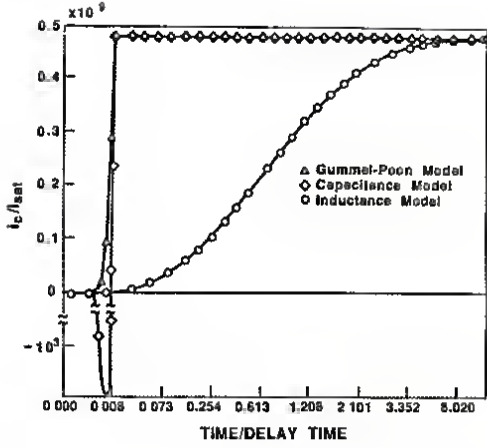

Fig 3.7 The collector current response to a large-signal step input voltage derived via the Gummel-Poon(GP) model, via the negative capacitance model and via the inductance model.

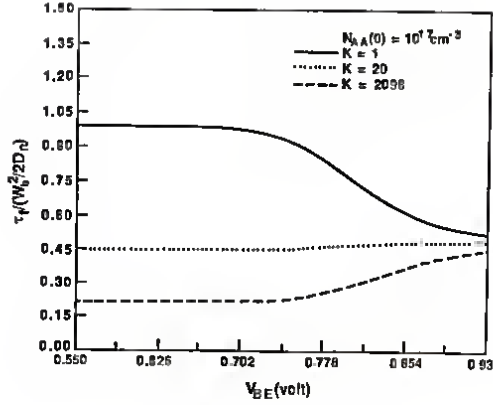

Fig 3.8 The model predictions of the transit time versus input voltage for exponentially doped base layers with different doping ratio
(a) The forward transit time; (b) The reverse transit time

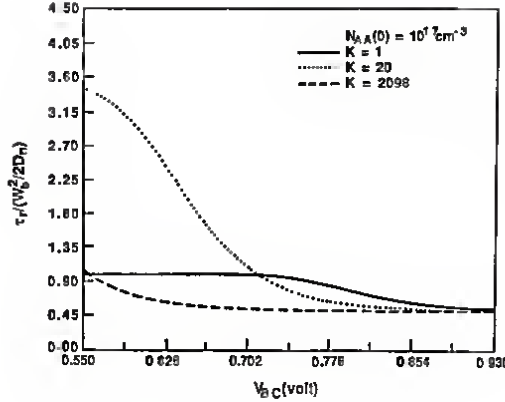

Fig 3.8- continued

of the transit time on doping ratios and injection levels in Fig 3 8. In comparing Figs 3 8(a) and 3 8(b) with Figs 3 9(a) and 3 9(b), we note that the reciprocity of the transit time or of the delay time is not generally valid. Reciprocity occurs only if (a) the doping profile is uniform and the entire base is either in high injection or low injection, or (b) the voltage applied is low enough that the entire base layer is in low injection [53], or (c) the voltage applied is large enough that the entire base layer is in high injection. Thus the curves in Figs 3 8 and 3 9 do not show reciprocity except the curve for a uniformly doped base ($K = 1$).

To show that the small-signal models in Fig 3 10 offer improvements, we compare against experiment the phase of h_{21} (short-circuit current gain) predicted by the Gummel-Poon model and by the new models developed here. We measured large transistors ($W_b = 14$ μm, $A = 35 \times 125$ μm^2 and $N_A = 4 \times 10^{15} \exp(0.115x)$ cm^{-3}) for which multi-dimensional effects are negligible and the extrinsic resistances and the junction capacitances are insignificant. The transistors were measured by standard s-parameter techniques. The range of frequencies is plotted in Fig 3 10. The DC operating point is defined by $I_C = 100$ μA and by $V_{BC} = -9.3$ volts. The new models show better agreement with the experiment than that shown by the Gummel-Poon model, especially for frequencies beyond the cut-off frequency f_T.

Figures 3 11(a) and 3 11(b) show the inaccuracy in base transit time and delay times caused by excluding the plasma induced energy-gap narrowing. Since the built-in electric field is reduced by this gap narrowing, both time constants are about 1.5 times larger than those

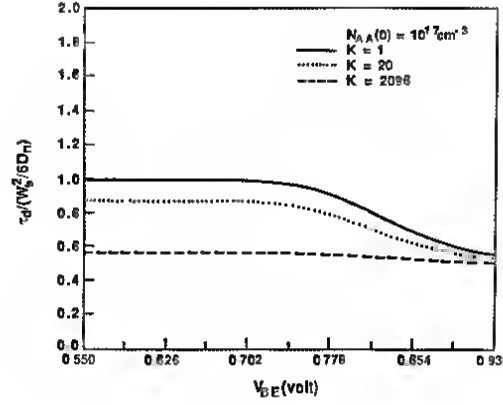

Fig 3 9 The model predictions of the delay time versus input voltages for exponentially doped base layers with different doping ratios
(a) The forward delay time, (b) The reverse delay time

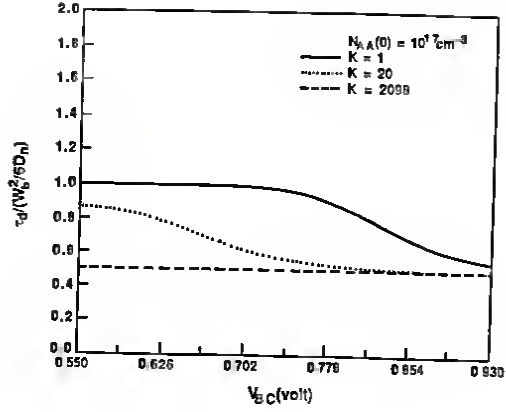

Fig 3.9--continued

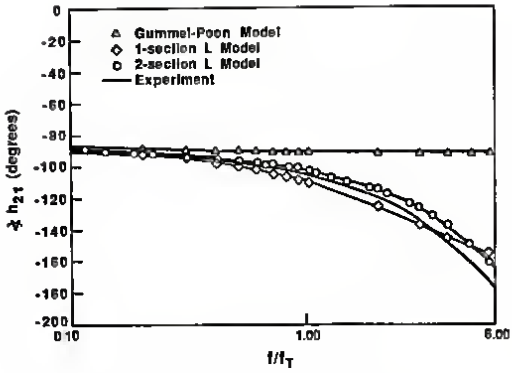

Fig. 3.10 Comparison of the relative phase of h_{21} predicted by the Gummel-Poon (GP) model by one section inductance model and by two section inductance model with experimental results

predicted if this gap narrowing is ignored. Similarly, Figs. 3.12(a) and 3.12(b) deal with the phase and the magnitude of h_{11} (the input impedance). The merging of the phase at low ($f/f_T < 10^{-3}$) or high ($f/f_T > 1$) frequencies occurs because the base diffusion capacitance has negligible influence. The frequency independent deviation of the magnitude at low and high frequencies arises because the energy gap narrowing decreases the base resistance. At moderate frequencies ($10^{-3} < f/f_T < 1$), both phase difference and magnitude deviate significantly because this narrowing increases the diffusion capacitance. Thus the electron-hole plasma slows the transient response and it adds to the phase shift of the input impedance and decreases its magnitude.

3.4 Conclusions

The one-dimensional non-quasi-static circuit models for bipolar junction transistors developed here apply for all injection levels. The large- and small-signal models include carrier propagation delay and, for the first time, the influence of a component of energy gap narrowing that arises at high collector currents from many-body interactions in the base. The models account for non-zero majority (hole) current, and hence for the low current gains, that could be present in the reverse-active or saturation modes of operation or generally for high injection.

The non-quasi-static large signal model developed shows propagation delay of the collector current larger than that predicted by previous models. The non-quasi-static small signal model predicts more phase shift of the short circuit current gain than does the (quasi-static)

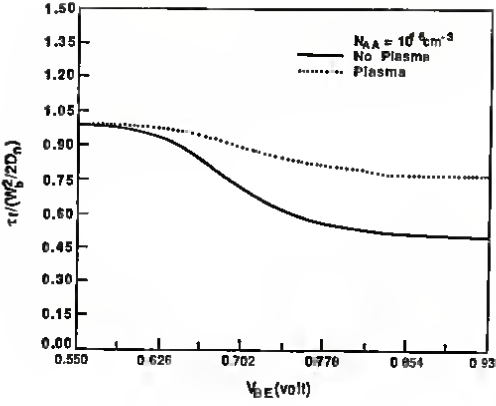

Fig 3 11 The effect of electron hole plasma to the base transit time (a) The forward base transit time, (b) The reverse base transit time

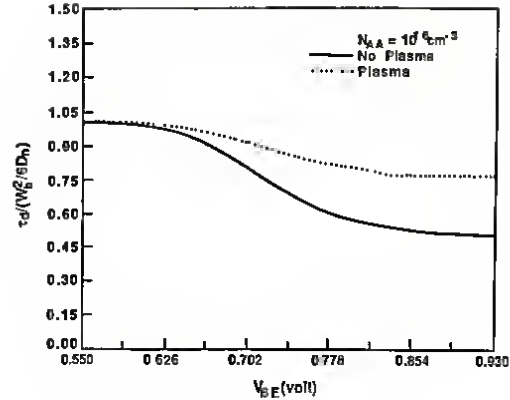

Fig 3 11--continued

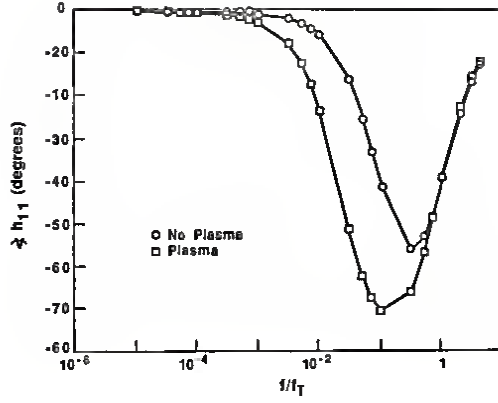

Fig 3.12 The effects of electron hole plasma to the input impedance h_{11} (a) The phase, (b) The magnitude

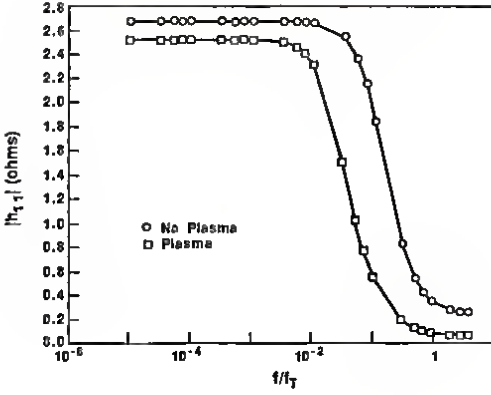

Fig. 3.12--continued

Gummel-Poon model, which experiment confirms. Plasma-induced energy-gap narrowing slows the base transit and delay times, and adds phase shift and reduces the magnitude of the input impedance. Extensions of these models to including base pushout and two-dimensional effects such as emitter crowding will be discussed in next chapters.

CHAPTER FOUR
HIGH INJECTION NON QUASI STATIC COMPACT MODELS FOR BIPOLAR JUNCTION TRANSISTORS HAVING LIGHTLY DOPED COLLECTORS

4.1 Introduction

Modern bipolar junction transistors have submicron base layers with doping concentration up to 10^{18} cm^{-3} to prevent punchthrough and collector doping as low as 10^{16} cm^{-3} to ensure reasonable breakdown voltage [69]. Scaling down the transistor geometry increases speed. But this also increases current density, which may result in high injection effects such as Webster effect [19], Kirk effect (base pushout) [24], energy gap narrowing due to carrier-carrier interaction [20]-[23], current crowding [16],[26] [27] and spreading [29]. High injection affects the performance of transistors [16],[19] [21]-[24] [26], [27],[29]. The use of a polysilicon technology enhances the device performance. But the resulting polysilicon emitter layer modifies the terminal performance [69]. Heavy doping effects in the emitter as well as base layers (such as Fermi-Dirac statistics, position-dependent diffusivity, lifetime and energy gap narrowing due to dopant-carrier interaction) need to be considered in determining the performance of transistors [14],[69].

The effects of heavy doping concentration and high current density on the performance of transistors have been discussed [14], [16], [19], [21]-[24],[26],[27] [29] [69]. The non quasi static effects, which take into account carrier propagation delay in quasi-neutral layers, become

important when base pushout occurs or when transistors have polysilicon emitter layers [14]. For compound semiconductor heterojunction bipolar transistors (HBT), the non-quasi static effects are even more important because the base resistance and the collector capacitance are substantially smaller than the values they have in silicon transistors [70].

In this chapter, we shall focus on integrating high injection and heavy doping effects into a non quasi-static lumped circuit model by using a systematic method presented before [14]. Non-quasi-static circuit models for heavily doped quasineutral emitter layers in low injection and for lightly doped quasineutral base layers in moderate and high injection have been developed in Chapters two and three and in [14] and [15] for $n^+/p/n^+$ (or $p^+/n/p^+$) transistors in which base pushout is negligible. However, a comprehensive simulation of modern transistors must include models for lightly doped collector layer in which base pushout occurs at moderate or high injection.

In moderately doped base layers ($N_A = 10^{18}$ cm^{-3}), ΔE_g (energy gap narrowing) $\approx$ 50 mV is predicted at low injection [71] and $\Delta E_g < 50$ mV is predicted at moderate injection [22]. Energy gap narrowing at low injection results from dopant-carrier interaction only. But at high injection the dopant-carrier interaction decreases because of the screening caused by excess carriers. Thus energy gap narrowing in the base decreases [22].

In lightly doped collector layers, the carrier concentration can be high enough to decrease the energy gap because of carrier-carrier

interaction or Debye screening. For Δn (excess carrier density) = 5×10^{17} cm^{-3}, ΔE_g = 40 mV [4].

In Section 4.2 we derive non quasi-static models including energy gap narrowing for heavily doped quasineutral base layers at low and high injection by applying the method presented in Chapter two and [14]. We then generalize the models to all injection levels by using the fitting scheme in Chapter three and in [15] and [61]. In Section 4.3, following a short description of the mechanisms occurring in the collector layer, we extend the non-quasi-static models to include the Kirk effect, or base pushout, in the collector layer. We show the model prediction of the transit and delay time at various input voltages in Section 4.4 and conclude this work in Section 4.5. In the derivation, we consider a one dimensional $n^{++}/p^{+}/n$ transistor shown in Fig. 4.1.

4.2 Models for Base Layers

4.2.1 Governing Equations for Model Derivation

As shown in Section 2.2, the one-dimensional carrier transport in quasi neutral layers of bipolar junction transistors is described by two current equations and two continuity equations:

$$j_N(x,t) = q\mu_n(x)n(x,t)E_n(x,t) + qD_n(x)(\partial n(x,t)/\partial x) \tag{4.1}$$

$$j_P(x,t) = q\mu_p(x)p(x,t)E_p(x,t) - qD_p(x)(\partial p(x,t)/\partial x) \tag{4.2}$$

$$\partial n(x,t)/\partial t = (1/q)(\partial j_N(x,t)/\partial x) - n(x,t)/\tau_n(x) \tag{4.3}$$

$$\partial p(x,t)/\partial t = -(1/q)(\partial j_P(x,t)/\partial x) - p(x,t)/\tau_p(x) \tag{4.4}$$

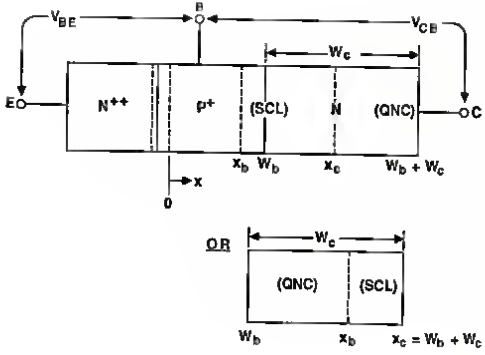

Fig 4.1 Schematic illustration of a one-dimensional $n^{++}/p^+/n$ bipolar junction transistor. Two possible situations, QNB/SCL(Space-Charge Layer)/QNC(Quasi-Neutral Collector)/contact and QNB/QNC/SCL/contact, are shown for the collector layer

The boundary conditions for any injection level are

$$\Delta n_j = (1/2)\{ [N_{Aj}^2 + 4n_{ie}^2(\exp(qV_{QFj}/kT)-1)]^{1/2} - N_{Aj} \} \quad j=1,2 \qquad (4.5)$$

Here, $V_{QFj}(x = x_j) = V_{Fj} - V_{Nj}$ is the difference between the hole and electron quasi-Fermi potentials, and n_{ie} is effective intrinsic doping concentration

$$n_{ie}^2 = n_{ie}^2 \exp(\Delta E_g/kT) \qquad (4.6)$$

where ΔE_g is apparent energy gap narrowing, which includes Fermi Dirac statistics. Note that ΔE_g and n_{ie} become functions of Δn when $\Delta n > 10^{17}$ cm^{-3} [20]

Based on eqs (4.1) - (4.5), we shall develop the governing equations for non quasi-static models at low and high injection in Sections 4.2.1.1 and 4.2.1.2

4.2.1.1 Governing equations for high injection models

For a moderately doped p-type quasi-neutral base layer under high injection ($\Delta p = \Delta n \gg N_A$), the electric field acting on holes $E_p = d(E_v/q)/dx$ differs from the electric field acting on electrons $E_n = d(E_c/q)/dx$, because of energy gap narrowing

$$E_n(x,t) = E_p(x,t) - (1/q)\partial\Delta E_g/\partial x \qquad (4.7)$$

where E_v and E_c are valence and conduction band edges respectively. Here, ΔE_g could result from dopant-carrier or carrier-carrier interaction or both [22]. From (4.2),

$$E_p(x,t) = (j_p + qD_p\partial p/\partial x)/q\mu_p p \qquad (4.8)$$

By substituting (4 7) and (4 8) into (4 1) we obtain the expression for electron current in high injection

$$j_N = qD_n[(\mu_n D_p/\mu_p D_n + 1)\partial\Delta n/\partial x \quad (\mu_n/D_n)(1/q)\Delta n\partial\Delta E_g/\partial x] + (\mu_n/\mu_p)j_p \tag{4 9}$$

The Einstein relations for a heavily doped p-type base layer in high injection are

$$D_n/\mu_n = kT/q \quad \text{and} \quad D_p/\mu_p = (kT/q)\, F_{1/2}(\eta_{FP})/F_{-1/2}(\eta_{FP}) \tag{4 10}$$

where $\eta_{FP} = (E_F - E_{PP})/kT$ and $F_{1/2}$ is Fermi-Dirac integral of order of 1/2 Substituting (4 10) into (4 9) yields

$$j_N(x\ t) = qD_n[(F + 1)\ \partial\Delta n/\partial x - (1/kT)\Delta n\ \partial\Delta E_g/\partial x] + (\mu_n/\mu_p)j_p \tag{4 11}$$

where F is defined as $F_{1/2}/F_{-1/2}$ which can be approximated by a polynomial function of doping concentration [72]

Equation (4 11) is nonlinear because of the term $\Delta n\partial\Delta E_g/\partial x$ But the dependence of ΔE_g on Δn and N_A can be determined by experiment [71] by an analytic approach [21] or by an numerical approach [22] Thus we can get analytic solution of (4 11) by fitting ΔE_g as function of $\ln(\Delta n + N_A)$ Assuming injection high enough that $\ln(\Delta n + N_A) \approx \ln(\Delta n)$, we may fit ΔE_g as a piecewise linear function of $\ln(\Delta n)$

$$\Delta E_g \approx a(kT/q)\ln(n/n_{i_a}) \quad b \approx a(kT/q)\ln(\Delta n/n_{i_a}) - b \tag{4 12}$$

in which a and b are determined by $\Delta E_g(n)$

Substituting (4 12) into (4 11) yields the governing equation for high injection

$$j_N = qD_n(F + 1 - a/q)\partial\Delta n/\partial x + (\mu_n/\mu_p)j_p = qD_n f_H \partial\Delta n/\partial x + (\mu_e/\mu_p)j_p \tag{4 13}$$

where $f_H = F + 1 - a/q$

Subsctituting (4 12) into (4 5) results in boundary conditions which explicitly show the dependence of Δn on V_{QF}

$$\Delta n_j = (n_{io}/\exp(b/kT))[\exp(qV_{QFj}/kT) - 1] \tag{4 14}$$

4 2 1 2 Governing equations for low-injection models

For low injection ($\Delta n \approx \Delta p \ll N_A$) by assuming nondegeneracy for the minority carriers we obtain the electric field acting on electrons

$$E_n(x,t) \approx E_n(x) \approx E_{no}(x) = (kT/q)d(\ln N_{Aeff})/dx \tag{4 15}$$

where E_{no} is the electric field acting on electrons in equilibrium and N_{Aeff} is the effective hole doping concentration defined as

$$N_{Aeff} = N_A \exp(-\Delta E_g/kT) \tag{4 16}$$

Subsctituting (4 15) into (4 1) yields

$$j_N(x,t) = qD_n(x)[\Delta n(x,t)d(\ln N_{Aeff})/dx + d\Delta n(x,t)/dx] \tag{4 17}$$

In low injection ΔE_g results from dopent-carrier interaction only Thus we fit ΔE_g as a piecewise linear function of $\ln(N_A)$ instead of $\ln(\Delta n)$

$$\Delta E_g \approx a'(kT/q)\ln(N_A/n_{io}) - b' \tag{4 18}$$

From (4 2) (4 7) and (4 15) (4 18) we obtain the governing equation for low injection models

$$j_N = qD_n(F/M + 1)\partial\Delta n/\partial x + (\mu_n/\mu_p M)j_P \approx qD_n f_L \partial\Delta n/\partial x + (\mu_n/\mu_p M)j_P \tag{4 19}$$

where $f_L = F/M + 1$ and $M = a'/(a - a')$

4 2 2 Models for High and Low Injection

Based on (4-13) and (4 19), we now derive analytical expressions for j_N at low and high injection in terms of Δn and j_P. Following the systematic method proposed in [14], we take the Laplace transformation of (4 2), (4 3), (4 4), (4 13) and (4 19) and obtain iterative expressions for j_N at x=0 by integrating (4 3), (4 4), (4 13) and (4 19) from 0 to x

$$j_N(0,s) = -q\frac{1}{\sum_{i=1}^{M} A_{2i-1}(W_b,s)}\{(1+\sum_{i=1}^{M} B_{2i}(W_b,s))\,\Delta n(0,s) \quad \Delta n(W_b,s)$$

$$+ (1/q)j_P(0,s)\sum_{i=1}^{M} C_{2i-1}(W_b,s)\} \qquad (4\ 20)$$

where

$$A_{2i-1}(x,s) = \int_0^x dx_1/D_n(x_1)f_P(x_1)\int_0^{x_1}\lambda^2(x_2,s)[1+\mu(x_2)]dx_2$$

$$\int_0^{x_{2i-2}} dx_{2i-1}/D_n(x_{2i-1})f_P(x_{2i-1})$$

$$B_{2i}(x,s) = \int_0^x dx_1/D_n(x_1)f_P(x_1)\int_0^{x_1}\lambda^2(x_2,s)[1+\mu(x_2)]dx_2$$

$$\int_0^{x_{2i-1}}\lambda^2(x_{2i},s)[1+\mu(x_{2i})]dx_{2i}$$

$$C_{2i-1}(x,s) = \int_0^x dx_1\mu(x_1)/D_N(x_1)f_P(x_1)\int_0^{x_1}\lambda^2(x_2,s)[1+\mu(x_2)]dx_2$$

$$\int_0^{x_{2i-2}} dx_{2i-1}\mu(x_{2i-1})/D_N(x_{2i-1})f_P(x_{2i-1})$$

in which, for high injection $f_P = f_H$, $\mu = \mu_n/\mu_p$ and

$\lambda^2(x,s) = s + 1/\tau_h(x)$ and $s = d/dt$.

for low injection $f_{\xi} = f_{L}$, $\mu = \mu_n/(\mu_p \cong 3)$ and

$$\lambda^2(x,s) = s + 1/\tau_n(x)$$

Here, τ_h and τ_n are recombination lifetime in high and low injection respectively. Since the base recombination lifetime is usually smaller than the base transit time, we shall neglect the recombination in the following derivation. From eqs (4.4) and (4.20), we obtain

$$j_p(0,s) = qAn(0,s)\{\int_0^{W_b}[1 + \Sigma E_{2i}(x,s)]dx - \int_0^{W_b}\Sigma A_{2i-1}(x,s)dx$$

$$\{1 + \Sigma E_{2i}(W_b,s)\}/\Sigma A_{2i-1}(W_b,s))/\{1/\lambda^2 + \int_0^{W_b}\Sigma C_{2i-1}(x,s)dx$$

$$\int_0^{W_b}\Sigma A_{2i-1}(x,s)dx\ [\Sigma C_{2i-1}(W_b,s)/\Sigma A_{2i-1}(W_b,s)]\} \qquad (4.21)$$

If we integrate (4.2), (4.3), (4.4), (4.13) and (4.19) from x to W_b instead of from 0 to x, we obtain $j_N(W_b,s)$ and $j_p(W_b,s)$. By defining A $j_N(0,s) = i_1(s)$, $A\,j_N(W_b,s) = -i_2(s)$; $v_1 = v_{QF}(x = 0)$, $v_2 = v_{QF}(x = W_b)$, $\Delta n_1 = \Delta n(x = 0)$ and $\Delta n_2 = \Delta n(x = W_b)$, we obtain the following two-port equation

$$\begin{bmatrix} i_1(s) \\ i_2(s) \end{bmatrix} = \begin{bmatrix} A_{11}(s) & A_{12}(s) \\ A_{21}(s) & A_{22}(s) \end{bmatrix} \begin{bmatrix} \Delta n_1(s) \\ \Delta n_2(s) \end{bmatrix} \qquad (4.22)$$

We now truncate the A parameters in (4.22) to the first order of s. This yields the large signal circuit model shown in Fig. 4.2, in which

$$i_{11}(s) = [A_{11}(s) + A_{12}(s)]\Delta n_1(s)$$

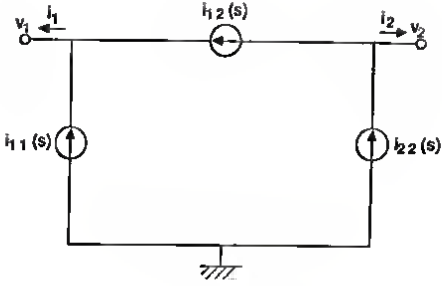

Fig 4 2 A network representation of the two port equation (including the majority hole current).

$$= I_{(h,l)}[\mathrm{sr}_{f(h,l)}/(1 + \mathrm{sr}_{d(h,l)})]\ \Delta n_1(s) \tag{4 23}$$

$$i_{22}(s) = [A_{22}(s) + A_{21}(s)]\Delta n_2(s)$$

$$= I_{(h,l)}[\mathrm{sr}_{r(h,l)}/(1 + \mathrm{sr}_{d(h,l)})]\ \Delta n_2(s) \tag{4 24}$$

$$i_{12}(s) = [\,A_{12}(s)]\ [\Delta n_1(s) \quad \Delta n_2(s)]$$

$$= I_{(h,l)}(1 + \mathrm{sr}_{d(h,l)})^{-1}\ [\Delta n_1(s) - \Delta n_2(s)] \tag{4 25}$$

$$I_{(h,l)} = Aq/\int_0^{W_b} \frac{1}{D_n f_p}\ dx \tag{4 26}$$

$$\tau_{f(h,l)} = \int_0^{W_b} \frac{1}{D_n f_p} \int_0^{x} (1 + \mu)\ dx_1 dx + \int_0^{W_b} \frac{\mu}{D_n f_p}\ dx \quad (W_b$$

$$\int_0^{W_b} \int_0^{x} \frac{1}{D_n f_p}\ dx_1 dx / \int_0^{W_b} \frac{1}{D_n f_p}\ dx) \tag{4 27}$$

$$\tau_{d(h,l)} = \int_0^{W_b} \frac{1}{D_n f_p} \int_0^{x} (1 + \mu) \int_0^{x_1} \frac{1}{D_n f_p}\ dx_2 dx_1 dx \Big/ \int_0^{W_b} \frac{1}{D_n f_p}\ dx \tag{4 28}$$

$$\tau_{r(h,l)} = \int_0^{W_b} \frac{1}{D_n f_p} \int_x^{W_b} (1 + \mu)\ dx_1 dx + \int_0^{W_b} \frac{\mu}{D_n f_p}\ dx \quad (W_b$$

$$\int_0^{W_b} \int_x^{W_b} \frac{1}{D_n f_p}\ dx_1 dx / \int_0^{W_b} \frac{1}{D_n f_p}\ dx) \tag{4 29}$$

in which subscript (h,l) denote the parameters for high and low injection respectively. Here τ_f is the forward base transit time, τ_r is the reverse base transit time, τ_d is the base delay time [55], [56]. If we neglect the effect of the Dember electric field, which results from difference between the diffusion coefficients for electrons and holes [73], $\mu = \mu_n/\mu_p = 1$.

By taking the inverse Laplace transformation of (4 23) - (4 25), we obtain the large signal circuit model shown in Fig. 4 3, where

$$C_{11} = I_{(h,I)}(r_{\varepsilon(h,I)})[\Delta n_1(t)/v_1], \quad R_{11} = r_{d(h,I)}/C_{11} \tag{4.30}$$

$$C_{22} = I_{(h,I)}(r_{r(h,I)})[\Delta n_2(t)/v_2], \quad R_{22} = r_{d(h,I)}/C_{22} \tag{4.31}$$

$$R = (v_1 + v_2)/[I_{(h,I)}(\Delta n_1 - \Delta n_2)], \quad L = r_{d(h,I)}R \tag{4.32}$$

We have sketched the derivation from analytical solutions, (4.23) - (4.25), to the circuit model, (4.30) - (4.32). Details of a similar derivation are in [14] and [15].

4.2.3 Models for All Level Injections

Based on the high- and low-injection models derived in Section 4.2.2, we now develop non quasi-static models for all level injections by utilizing the fitting scheme proposed in [15] and [61]. All-injection models have the same circuit configuration as high- and low-injection models except that the circuit elements contain fitting parameters. The circuit elements of all-injection model for large-signal excitation are as follows

$$C_{11} = TF \cdot IF\,[\Delta n_1(t)/v_1], \quad R_{11} = TDF/C_{11} \tag{4.33}$$

$$C_{22} = TR \cdot IR\,[\Delta n_2(t)/v_2] \quad R_{22} = TDR/C_{22} \tag{4.34}$$

$$R = (v_1 + v_2)/[IF \cdot \Delta n_1 \;\; IR \cdot \Delta n_2] \tag{4.35}$$

$$L = (v_1 + v_2)/[IF \cdot \Delta n_1 / TDF + IR \cdot \Delta n_2/TDR] \tag{4.36}$$

where the expressions for the fitting parameters, IF, IR, TR, TF, TDF and TDR are listed in Appendix D.

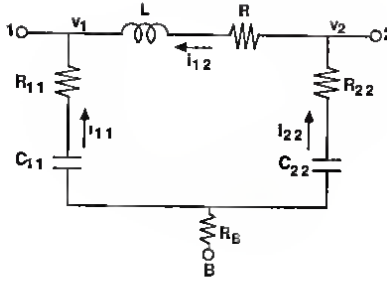

Fig. 4.3 The large signal quasi static model for the base layer (including the majority hole current).

For small-signal excitation, we assume $\exp(qv_j/kT) \approx \exp(qV_j/kT)(1 + q\hat{v}_j/kT)$. Follow the derivation of Section 4.2.2, and obtain the small signal model shown in Fig. 4.4, in which

$$c_{11} = TF\ If\ (q\Delta N_1/kT), \quad r_{11} = TDF/c_{11} \tag{4.37}$$

$$c_{22} = TR\ Ir\ (q\Delta N_2/kT), \quad r_{22} = TDR/c_{22} \tag{4.38}$$

$$r = kT/(qIt\ \Delta N_2), \quad L_{ss} = TDR/r \tag{4.39}$$

$$g_m = q(If\ \Delta N_1 - Ir\ \Delta N_2)/kT \tag{4.40}$$

where the expressions for the fitting parameters, if and ir are also listed in Appendix D.

4.2.4 Remarks

The physical meaning of the circuit elements — R_{11}, R_{22}, C_{11}, C_{22}, R and L — has been discussed in [14] and [15]. The majority hole current contributes substantially to the collector and emitter currents only when the current gain (β) is small, a condition that prevails, for example, for transistors operating in the reverse active, quasi saturation and saturation modes or at high injection.

Fitting parameters listed in Appendix D explicitly show the Webster effect in high injection. Adding the models for the quasi-neutral emitter and collector layers into Fig. 4.3 will yield a complete one dimensional large-signal model as shown in Fig. 4.5. The expressions for R_e, C_e and R_{ed}, which are associated with the injected hole current into the quasi neutral emitter layer, are presented in [14] and R_c, C_c and R_{cd}, which are associated with the injected hole current into the collector layer, are derived in Sec. 4.3.

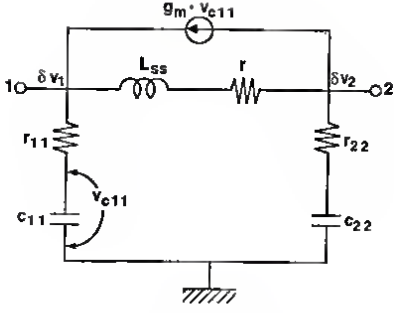

Fig 4 4 The small signal quasi-static model for the base layer (including the majority hole current)

The accuracy of the models developed depends on the accuracy of the approximations for the Fermi-Dirac integral, and on the empirical models used for mobility lifetime and, especially, energy-gap narrowing. Since the empirical models for energy gap narrowing in (4 12) and (4 18) cannot cover the whole application range (10^{17} cm^{-3} < N, An < 10^{20} cm^{-3}), we use different models for energy-gap narrowing in different ranges to achieve better accuracy. For example, according to data measured in [71], a' in (4 18) is approximately 0 61 q and b' ≈ 239 67 mev for An ≤ 10^{19} cm^{-3}, and a' ≈ 1 13 q and b' ≈ 503 86 mev for An > 10^{19} cm^{-3}. Similarly, a and b in (4 12) are determined for different An in [15].

The low-injection model developed in Section 4 2 2 differs from that in [14] because of the use of empirical model for energy-gap narrowing and the inclusion of the majority hole current in model derivation.

4 3 Models for Collector Layers

4 3 1 Overview

A lightly doped collector layer is widely used to assure high base/collector breakdown voltage and low base/collector junction capacitance. However, because the electron velocity cannot exceed the scatter-limited velocity, electrons will accumulate in the base/collector junction layer in greater numbers as the collector current is increased. These accumulated electrons will change the distribution of the electric field in the junction layer and will expand this space-charge layer (SCL) [24], [74], [75]. If we keep

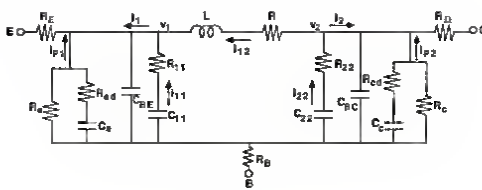

Fig. 4.5 The large signal non-quasi static model for a $n^{++}/p^{+}/n$ bipolar junction transistor (including the majority hole current) C_{BE} and C_{BC} are the space-charge capacitances in the base/emitter and base/collector junctions

increasing the collector current to the space-charge limited current level [76]. two mechanisms occur [77] 1) current-induced base layer stretching (base pushout) [24], [74], [78] and 2) lateral current spreading [77], [79]. On the other hand, the ohmic voltage drop across the quasi-neutral collector layer (QNL) tends to reduce the reverse voltage across the space-charge layer and which narrows the space charge layer and eventually causes quasi saturation [75], [80], [81]. The collector current I_C and applied voltage V_{CE} will determine the dominant tendency [63]. The expansion or contraction of the space-charge layer and base pushout, will effect the terminal performance of transistors in various ways such as lowering the cut off frequency f_T [24], [74], [77], decreasing current gain β [77] and causing quasi-saturation [82], [83]. Therefore, comprehensive and accurate models for these effects are essential for circuit simulation.

Analytical models including either one of the above effects or all of them have been reported [24], [74]-[84]. Based on this previous work and the base model developed in Section 4.2, we shall now extend this work by deriving a non-quasi static lumped circuit model for the collector layer. To avoid confusion caused by terminology, we categorize these effects into two groups: 1) the expansion and contraction modes which corresponds to QNB/SCL/QNC/contact and 2) the base pushout mode which corresponds to QNB/QNC/SCL/contact. We have shown previously the non-quasi-static model including these effects (except lateral current spreading) in Fig. 4.5, and we shall now determine the corresponding circuit elements by using a "regional approach", which de Graaff proposed in 1973 [63] and Liou used to

determine the capacitance model for space charge layer in the collector layer [65]

4 3.2 Model Derivation

The basic concept of regional approach is to make a detailed division of the (I_C, V_{CE}) plane into depletion (QNB/SCL/QNC/contact) and injection (QNB/QNL/SCL/contact) modes according to the collector doping concentration N_C and width (or thickness) W_C [63] A simplified (i_C, V_{CE}) plane is shown in Fig 4 6, where i_1 is the collector current that would flow if all carriers in the base/collector junction moved at the scatter-limited velocity and i_2 is the current below which the transistor is operating in the forward-active mode According to [75],

$$i_1 = qN_C v_s A_C \tag{4 41}$$

where A_C is the collector area and v_s is the saturation or scatter limited drift velocity (= 10^7 cm/s for Si at 300 °K), and

$$i_2 = qN_C \mu_n V_{BC} A_C / W_C \tag{4 42}$$

where V_{BC} is the base/collector applied voltage and where $V_{BE} = V_{BC} + V_{CE}$ or $V_{CE} = V_{CE}$ in the forward-active mode.

As shown in Fig 4 6 currents i_1 and i_2 divide the (I_C, V_{CE}) plane into six regions In Region i ($i_C \leq i_1 \leq i_2$), the large value of V_{CE} tends to expand space charge layer while In Region ii ($i_C \leq i_2 \leq i_1$), the small value of V_{CE} tends to contract it Thus Regions i and ii correspond to the collector layer in the QNB/SCL/QNC/contact mode In Region iii ($I_1 \leq i_C \leq I_2$), the collector is essentially fully depleted and space-charge-limited flow occurs [76], in Regions IV ($I_2 \leq i_C \leq$

I_1). $\forall$ ($l_2 \le l_1 \le l_C$) and $\forall$I ($l_1 \le l_2 \le l_C$) the transistor is in the saturation or quasi saturation modes. Thus we may roughly consider Regions III, IV, V, and VI to be in the QNB/QNC/SCL/contact mode. A more detailed division of the (I_C - V_{CE}) plane in [63] shows that small transition regions, in which the whole collector layer is occupied either by space-charge layer or by quasi-neutral layer, exist. But, because these transition regions are small [63] we neglect them in the present derivation.

In Sections 4.3.2.1 and 4.3.2.2, we shall apply the regional approach to decide the dominant mechanism in the collector layer for given I_C and V_{CE}, and then determine the corresponding circuit elements in Fig. 4.5. Since the same regional approach has been used to develop the capacitance model for the space-charge layer in the collector layer [55], we will deal with the circuit elements associated with the quasi-neutral layer only.

4.3.2.1 QNB/QNC/SCL/contact mode

In this subsection, we first develop a non quasi-static model for the collector layer in the reverse active or saturation modes ($V_{BC} \ge 0$). Then we will discuss the application of the model developed in the forward active mode (QNB/QNC/SCL/contact).

By following the systematic method presented in [14], we obtain the minority hole current I_{p2} injected into the collector layer in the reverse active or saturation modes:

$$i_{F2}(s) = I_{C0}[1 + s\tau_{ct}/(1 + s\tau_{cn})] \mathcal{L}\{\exp(qv_{BC}/kT) \quad 1\} \qquad (4.43)$$

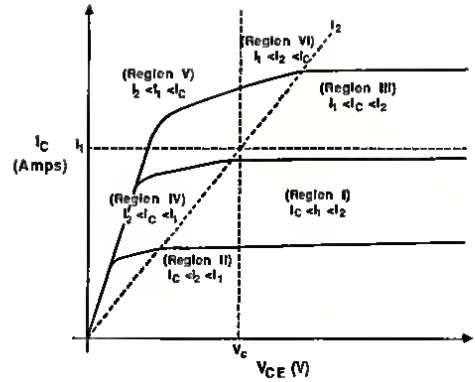

Fig 4.6 Illustration of the six operating regions in I_C versus V_{CE} characteristics

where I_{Co} is the collector saturation current τ_{cd} is the collector delay time, τ_{ct} is the collector transit time and $\mathcal{L}$ is the notation for Laplace transformation. Expressions for I_{Co}, τ_{cd} and τ_{ct} are listed in Appendix D. The circuit elements corresponding to (4.43) are shown in part of Fig. 4.5 in which

$$R_c = v_{BC}/[I_{Co}\exp(qV_{BC}/kT)] \tag{4.44}$$

$$C_c = \tau_{ct}/R_c \quad ; \quad R_{cd} = \tau_{cd}/C_c \tag{4.45}$$

$$R_\Omega = (W_c + W_b - x_c)/(q\mu_n N_c A_c) = W/(q\mu_n N_c A_c) \tag{4.46}$$

where x_c is the boundary between the space charge layer and the quasi neutral collector layer and W is the thickness of the quasi-neutral collector layer (Fig. 4.1). Note that x_b is the boundary between the space-charge layer and the quasi neutral base layer. Thus $x_c - x_b = X$ which is the thickness of the space-charge layer in the collector. By R_Ω we mean the ohmic resistance in the quasi-neutral collector layer.

Equation (4.43) is for low injection only. We may follow the method described in Section 4.2 to derive a model for all levels of injection. For a transistor having a heavily doped subcollector, (4.43) will become two-port matrix equations as (4.22). The small-signal version of (4.44) and (4.45) are

$$r_c = (kT/q)/[I_{Co}\exp(qV_{BC}/kT)], \quad c_c = \tau_{ct}/r_c, \quad r_{cd} = \tau_{cd}/c_c, \quad r_\Omega = R_\Omega \tag{4.47}$$

In Regions I and II by solving the Poisson's equation [85], we obtain the thickness X of SCL [75]

$$X = X_s\{1 - (I_C/I_2)/[1 - (I_C/I_1)]\}^{1/2} \tag{4.48}$$

where X_o is the thickness of SCL in equilibrium and can be obtained from the conventional depletion model. Note that $x_b \approx W_b$ because the base doping concentration is much higher than the collector doping concentration and thus $W_c + X \approx W$.

For the base/collector junction under reverse bias ($V_{BC} < 0$),

$$\Delta n_2(W_b) = \Delta n(x_b) \approx I_C/(qA_c v_d) \tag{4.49}$$

where v_d is the electron drift velocity. We may assume $v_d \approx v_s$ in (4.49) because of the high electric field at x_b [63], [85]. However we can use Ryder's model [86] for v_d to achieve better accuracy. Based on (4.49) and (4.5), we can determine v_2 ($= v_{QF}(x_b)$), which is the separation of quasi Fermi potentials at $x = x_b$. Note that v_2 differs from $V_{BC} - I_C R_\Omega$ because the quasi Fermi levels in the junction are not flat under reverse bias. Substituting the resulting Δn_2 and v_2 into (4.31) and (4.32) will yield the base model in this case.

To determine the corresponding collector model, we need to know $\Delta n(x_c)$ and $v_{QF}(x_c)$. For the base/collector junction under reverse bias, we may assume $\Delta n(x_c) \approx 0$. This implies that R_c approaches infinity and C_c approaches zero. Thus the collector model in Fig. 4.5 vanishes.

For the base/collector junction under forward bias ($V_{BC} > 0$), the quasi-Fermi level is nearly flat. Thus $\Delta n(x_b)$ and $\Delta n(x_c)$ as well as $v_{QF}(x_b)$ and $v_{QF}(x_c)$ are well defined and so are the corresponding base and collector models.

4.3.2.2 ONE/ONC/SCL/contact mode

When I_C exceeds some critical values, which we will specify in the following discussion, the excess electron density will be enough to

totally neutralize the depopulation charge in the junction and thus will release high electric field to the interface between epitaxial layer and substrate ($n^{++}/p^{+}/n/n^{++}$ structure) or ohmic contact ($n^{++}/p^{+}/n$ structure) [74]. In this case, base pushout occurs and the collector layer is in the QNE/QNC/SCL/contact mode, in which $x_e = W_b + W_e$ and $W = 0$. This implies that the collector model (R_{cc}, C_c and E_{cd} in Fig. 4.5) vanishes. To determine the base model, we must know Δn_2 and x_b.

In Region III, if $I_C < I_1 + I_2$ (V_C/V') = I_0, the collector layer is fully depleted, which implies $X = W_c$ and $W = 0$. Here, V_C corresponds to V_{CE} at which $I_1 = I_2$ (Fig. 4.6) and V' is the base/collector voltage at which the collector layer is fully depleted in the absence of I_C [75]

$$V' = qN_c W_c^2/2\epsilon \qquad (4.50)$$

where ϵ is the permittivity. If $I_C \geq I_0$, space-charge-limited flow occurs and, in a one-dimensional analysis, leads to base pushout [75]. In this case, $x_c = W_b + W_c$ and

$$x_b = W_b + W_c(1 - [(I_0 - I_1)/(I_C - I_1)]^{1/2}) = W_b + W_{clb} \qquad (4.51)$$

where W_{clb} denotes current induced base thickness. Since $I_C > I_1$, we may use (4.49) to find Δn_2.

In Region IV, the transistor is in quasi saturation or saturation mode, in which the assumption $v_d = v_e$ is invalid. Thus we use Ryder's model [86] for v_d and define a current I_3 corresponding to the onset of the non ohmic region in $v_d(E)$ [63], [85]

$$I_3 = A_c q \mu_n N_c E_2 \qquad (4.52)$$

in which $E_2 = 2.5 \times 10^3$ V/cm. Here, E_2 is the electric field at which the non ohmic region occurs in Ryder's model. For $i_C \leq I_3$, the space-charge layer vanishes [63] and $x_b = x_c = W_b + W_c$. In this case, $C_{BC} = 0$ [85]. $\Delta n(x_b) = 0$ for the ohmic contact. For $I_C > I_3$, base pushout occurs and [63]

$$x_b = W_b + W_c - \epsilon(1 + \theta)(f - E_2)/[qN_c(\Delta n_2/N_c - 1) + \theta(n'/N_c - 1)]$$

$$= W_b + W_{cib} \tag{4.53}$$

where

$$\Delta n_2 = N_c + (N_c/2B)(f/E_2 - 1)\{-1 + [1 + 4B(I_C/I_3 - 1)/(-f/E_2 - 1)]^{1/2}\} \tag{4.54}$$

$$n' = N_c, \quad \theta = 20 \text{ and } B = [\theta/(1 + \theta)](kT/q)(qN_c/\epsilon E_2^2) \tag{4.55}$$

$$f = I_C^2/(q\mu_n N_c I_3 A_c) \tag{4.56}$$

In Regions V and VI, the transistor also operates in the quasi-saturation or saturation modes but with I_C larger than I_1. Thus we may follow the same procedure as that in Region IV to obtain x_b and Δn_2 provided that the parameters used in (4.53)-(4.56) are changed as follows [63]

$$n' = I_C N_c/I_1, \quad \theta = 2.5, \text{ and } f = E_1 = -1.5 \times 10^4 \text{ V/cm} \tag{4.57}$$

where E_1 is the electric field at which the electron drift velocity start to saturate.

Based on Δn_2 and x_b, we can determine the base model corresponding to Regions III - VI by extending the integrations in (4.26) (4.29) from $[0, W_b]$ to $[0, W_b] + [W_b, x_b]$. In Regions III - VI, note that the collector model as well as R_Ω vanishes because $W = 0$.

4.4 Results

The non-quasi-static models developed in Sections 4.2 and 4.3 include high injection as well as heavy doping effects. Since the effects of heavy doping concentrations on the terminal performance of non quasi static models have been presented in [14], we show only the effects of high injection here. High injection mechanisms include Webster effect, Kirk effect and energy gap narrowing due to carrier-carrier interaction. We shall limit attention to the influence of these mechanisms on the transit and delay time, which are related to the cut-off frequency f_T. For background on the dc and quasi-static effects of high injections such as the falloff of the dc current gain β and the quasi saturation characteristics observed in the I_C versus V_{CE} plane, we refer the readers to the literature [24],[74],[75] and [63].

Figures 4.7 and 4.8 illustrate the forward transit time (Fig. 4.7) and delay time (Fig. 4.8) versus input voltage V_{BE} for different values of V_{CE}. The transistor simulated has $N_A = 8\times10^{15}$ cm^{-3}, N_c (collector doping concentration) = 1×10^{15} cm^{-3}, $W_b = 5.6\mu m$ and $W_c = 10\ \mu m$. In Figs. 4.7 and 4.8 the notation plasma, refers to the energy gap narrowing caused by the carrier-carrier interaction in a dense electron-hole plasma ($n = p > 10^{17}$ cm^{-3}).

As shown in both the figures, the transit and delay times with an electron-hole plasma present are larger than those without the electron hole plasma because the energy gap shrinkage provokes a higher current density and reduces the electric field [15]. The additional carriers resulting from the plasma-induced energy gap narrowing also neutralizes the dopant ion charges in the base/collector space-charge

layer, this causes base pushout to occur at a lower V_{BE} than that at which it would occur without the electron hole plasma present. Note that when base pushout occurs, the transit and delay times increase substantially.

When an electron hole plasma is present, base pushout occurs at almost the same V_{BE} even when the collector-base reverse bias is increased from 0 to 20 volts. However, a high reverse bias (V_{CB} = 20 V) causes both time constants to increase gradually after base pushout because the high electric field then present in the collector sweeps out more carriers and thus compensates for the effects of the electron-hole plasma.

As shown in Figs. 4.7 and 4.8, neglecting the electron-hole plasma leads to smaller transit and delay times and a higher onset voltage V_{BE} for base pushout. Also, for a higher V_{CB}, base pushout occurs at a higher V_{BE} because more depant-ion charges need to be neutralized. For the same reason, more carriers (larger values of V_{BE}) are required to neutralize the entire collector layer at a high value of V_{CB} than at a low value. At a low V_{CB}, slight increases of V_{BE} can produce enough excess carrier density to neutralize the entire collector layer. Thus the transit and delay times increase sharply in this case. Note that after the sharp increase, both time constants decrease because of the aiding electric field in high injection (Webster effect), which also reduces both time constants before base pushout occurs.

As illustrated, the electron-hole plasma tends to increase the transit and delay times while the aiding electric field in high injection (Webster effect) tends to reduce them. The electron hole

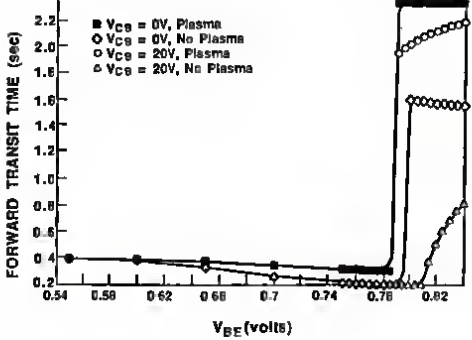

Fig 4 7 Model prediction of the forward transit time versus input voltage V_{BE} at different V_{CB}'s

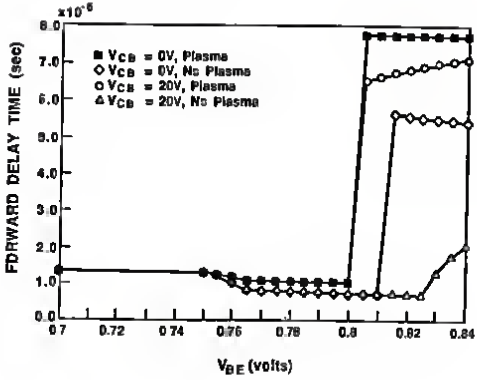

Fig. 4.8 Model prediction of the forward delay time versus input voltage V_{BE} at different V_{CB}'s.

plasma causes base pushout (Kirk effect) to occur at a lower V_{BE} while a large reverse bias on the base/collector junction increases the onset V_{BE} for base pushout

4.5 Conclusions

Comprehensive high-injection non-quasi-static models for a one-dimensional $n^{++}/p^{+}/n$ bipolar junction transistor were systematically derived. The large- and small-signal models developed take into account

1) high injection effects such as Webster effect, Kirk effect and energy gap narrowing due to carrier carrier interaction;
2) heavy doping effects such as Fermi-Dirac statistics, position dependent diffusivity, lifetime and energy-gap narrowing due to dopant-carrier interaction;
3) carrier propagation delay due to finite electron and hole velocities;
4) the majority hole current in the base layer, which becomes important when current gain (β) is small.

Despite the complicated mechanisms included, the models are compact enough to be implemented in conventional circuit simulators. For example, we may implement the models developed into SPICE2 by utilizing user defined Fortran subroutines, which are developed by various users to interact with SPICE, or by modifying the source code of SPICE. Since the models are compatible with the Gummel Poon model built into SPICE, implementation of the models is straightforward.

The development has focused on the intrinsic transistor. Extrinsic resistances and capacitances can be measured [87] and should be added to the models developed. We should an appropriate model for the base-emitter junction capacitance under forward voltage [47], and a standard model for junction breakdown.

CHAPTER FIVE
NON QUASI STATIC MODELS INCLUDING ALL INJECTION LEVELS AND DC, AC AND TRANSIENT EMITTER CROWDING IN TRANSISTORS

5.1 Introduction

For bipolar junction transistors operating at high current levels or at high frequencies, the flow of transverse current in the intrinsic base layer can appreciably modify the performance of the transistors [25]-[37]. The related, so-called emitter crowding, falls into two categories 1) dc crowding and 2) ac and transient crowding. Emitter crowding is one of the dominant mechanisms in transistor theory. Since 1958, it has occupied the attention of many authors. Yet previous treatments all have shortcomings, which we define and try to correct in this chapter.

DC emitter crowding results from transverse majority current in the intrinsic base layer. At high current levels, a sizable ohmic voltage drop occurs in the transverse direction and leads to a nonuniform minority current density distribution in the longitudinal direction. As a result, dc terminal currents (base, collector and emitter currents) will be less than is predicted by a one-dimensional model [1] that excludes crowding.

During transients or for small signal excitation, the majority base current charges both the emitter space charge layer and the quasineutral base layer through the resistance of the intrinsic base layer. The rate of charging involves three different time constants (a)

the dielectric relaxation time; (b) the time constant associated with the distributed resistance-capacitance charging of the emitter space-charge layer; and (c) the time constant associated with the distributed capacitance charging of the quasi-neutral base layer, which depends on the nonuniform minority carrier injection in both the transverse and longitudinal directions. As will become evident, the last time constant dominates in governing transient and ac emitter crowding. For transients, this time constant affects the delay seen at the device terminals. For ac excitation, it affects the phase shift and input and output impedances.

Pritchard [25] first incorporated the effect of ac emitter crowding into an expression for the base impedance, but neglected the effect of dc emitter crowding. Therefore his model only applies for bias currents so low that dc crowding is negligible. Hauser [26] solved a pertinent ordinary differential equation in the transverse direction and obtained analytical solutions for dc crowding. Severson [28] extended Hauser's model to include ac crowding. He also pointed out that a linear distributed model can account only for ac emitter crowding and cannot include the effects of dc crowding. Gosh [27] derived analytical solutions for dc and ac crowding and presented a nonuniform linear distributed model for transistor crowding. Schutt-Aine [32] applied the uniform version of Gosh's distributed model to develop a small-signal model for ion-implanted microwave transistors. Tong [34] examined the phenomenon of transient emitter crowding inside the intrinsic base layer by using a two-dimensional device simulator, FIELDAY [31]. Various other numerical methods to study emitter

crowding [29]-[30] have been developed. Based on Hauser's work, Lary et al. [35] developed formulations for the base resistance that includes dc crowding and ac crowding at low frequencies. Recently, Yuan and Liao [37] proposed a base resistance model, which takes into account dc crowding by partitioning the base layer into several subregions [33],[36]-[46].

All previous analytical treatments neglected that the current distribution in the longitudinal direction is nonuniform. They also failed to integrate the effects of dc, ac and transient crowding into a lumped circuit model. These shortcomings are overcome here.

Even though emitter crowding has been comprehensively treated by either the use of a distributed model or a device simulator such as PISCES or FIELDAY, an analytical approximation is useful for determining design principles and providing physical insight. Furthermore, analytical approximation can lead to lumped circuit models, which admits use of conventional network theory in the modeling process [88].

In Section 5.2, we derive analytical models for dc, ac and transient emitter crowding based on the assumptions made in Section 5.2.1. In Section 5.2.2, we adopt the systematic method presented in [14] to model crowding for low injection levels. In Section 5.2.3, we separate the two-dimensional continuity equations and follow the same systematic method to model high injection. Based on analytical solutions for low and high injection, we then determine onset conditions for emitter crowding in Section 5.2.4. In Section 5.2.5, we develop the large- and small-signal models for all injection levels by

adapting the fitting scheme in [15]. In Section 5.3, we illustrate how dc, ac and transient crowding affect the spatial distributions of the current and carrier densities in the intrinsic base layer. We also assess the validity of the models developed by comparing with experiment. Section 5.4 discusses possible extensions and modifications of the models.

The models developed take into account carrier propagation delay, all injection levels, arbitrary doping profiles, dc and ac emitter crowding and transient emitter crowding, yet are compact enough for use in circuit simulators such as SPICE. Because of their physical basis, the models have various degrees of accuracy and model complexity. This hierarchy enables a tradeoff between CPU time and accuracy in circuit simulation.

The analytical solutions obtained comprehensively describe the effects of emitter crowding in the quasineutral base.

5.2 Derivation of the Models

5.2.1 Basic Equations and Main Assumptions

Two-dimensional nonballistic carrier transport in quasi-neutral layers of bipolar junction transistors is described by two current equations and two continuity equations. The two-dimensional electron and hole current equations are

$$\bar{J}_N(x,y,t) = J_{Nx}(x,y,t)\,\bar{a}_x + J_{Ny}(x,y,t)\,\bar{a}_y \tag{5.1}$$

$$\bar{J}_P(x,y,t) = J_{Px}(x,y,t)\,\bar{a}_x + J_{Py}(x,y,t)\,\bar{a}_y \tag{5.2}$$

where

$$j_{Ny} = q n \mu_n E_{ny} + q D_n \partial n/\partial y \tag{5 3}$$

$$j_{Py} = q p \mu_p E_{py} - q D_p \partial p/\partial y \tag{5 4}$$

Replacing y in (5 3) and (5 4) with x will give the expressions for j_{Nx} and j_{Px} The two dimensional electron and hole continuity equations are

$$\partial n(x,y,t)/\partial t = (1/q)\nabla \cdot \vec{j}_N(x,y,t) \quad n(x,y,t)/\tau_n(x,y,t) \tag{5 5}$$

$$\partial p(x,y,t)/\partial t = -(1/q)\nabla \cdot \vec{j}_P(x,y,t) - p(x,y,t)/\tau_p(x,y,t) \tag{5 6}$$

For concreteness, we limit attention to an ideal double stripe n+/p/n vertical transistor as shown in Fig 5 1 In the figure, x denotes the longitudinal direction and y represents the transverse direction Because eqs (5 1)-(5 6) are nonlinear and coupled numerical methods such as the Gummel method and the Newton method are required to obtain general solutions [40] In order to get closed-form solutions, which are essential to deriving analytical models we make the following assumptions based on physical and practical considerations

1 The separations of the electron and hole quasi Fermi levels at (0,0) and (W_b,0) are equal to the terminal voltages v_{BE} and v_{BC}, respectively, less any voltage drops in the extrinsic resistances

2 $j_{Nx} \gg j_{Px}$ in low injection for a forward active transistor (the common emitter current gain $\beta = 100$ or greater for this assumption to be valid)

3 $j_{Py} \gg j_{Ny}$ because the electric field in the y direction aids the hole current and retards the electron current

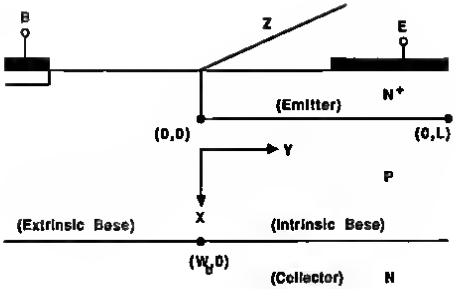

Fig 5.1 The structure of an n/p/n vertical bipolar junction transistor. We define the transverse direction as y axis and the longitudinal direction as x axis. Origin is at the join of the intrinsic and extrinsic base layers and the emitter layer

4. The hole and electron mobilities are constant ($\neq f(x,y,t)$) in the base, and the energy gap narrowing is negligible.
5. The base layer has an exponential doping profile.
6. The energy gap narrowing resulting from the electron hole plasma[20]-[22] at high current density is negligible.
7. Base pushout is negligible.

Assumptions 2 through 7 reduce the complexity of the models but are not essential, and their removal is discussed below.

Assumption 2 might be invalid for transistors operating in the reverse active or saturation modes. To avoid this problem we can include j_{Px} in the derivation by using the method discussed in [15]. Assumption 3 is generally true in the intrinsic base layer of most transistors [29]. We used the device simulator, FISCES, to verify this assumption at different positions x for various bias conditions. Fig. 5.2 is a selected result of our simulations that confirm assumption 3. In Sections 5.2.2 and 5.2.3, we briefly discuss extensions of the models that include arbitrarily and heavily doped base layers and plasma-induced energy gap narrowing [20]-[22]. We also demonstrate a possible method to include the effect of base pushout. Detailed descriptions of these extensions will appear in Section 5.4.

5.2.2 Low Injection

To derive the two port equation for low injection ($\Delta n < N_A$) we first consider the currents in the y direction. According to assumption 3 we assume that $j_{Ny} \approx 0$. This enables us to determine E_{Ny} in (5.3)

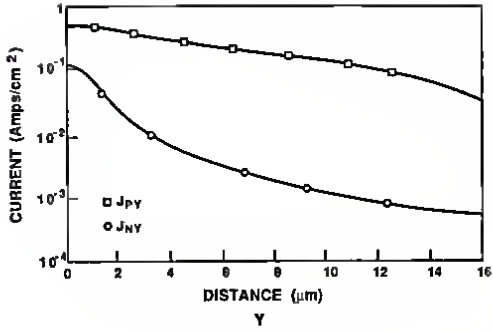

Fig 5 2 PISCES simulation of $J_{Py}(0,y)$ and $J_{Ny}(0,y)$ in y direction for $V_{BE} = 0.7$ volts.

Since $E_{Ny} = E_{Py}$ for a lightly doped base layer, we obtain j_{Py} by substituting E_{Py} into (5.4)

$$j_{Py} = qD_p p_o \partial(\ln\Delta p)/\partial y \qquad (5.7)$$

Taking the Laplace transform of (5.7) and integrating the resulting equation with respect to y from 0 to y at $x = x'$ gives

$$\mathcal{L}\left(\ln\left[\frac{\Delta p(x',y,t)}{\Delta p(x',0,t)}\right]\right) = \mathcal{L}\left(\int_0^y j_{Py}/qD_p p_o dy\right) \qquad (5.8)$$

Inverse Laplace transformation of (5.8) leads to one of the governing equations

$$\Delta p(x',y,t) = \Delta p(x',0,t)\exp\left[-\int_0^y j_{Py}(x',y,t)dy/qD_p p_o\right] \qquad (5.9)$$

The other governing equation results from integrating (5.6) with respect to y from 0 to y at $x = x'$

$$j_{Py}(x',y,t) - j_{Py}(x',0,t) = q\,\lambda(s)\int_0^y \Delta p(x',y,t)dy \qquad (5.10)$$

where $\lambda(s) = s + 1/\tau_p$ and $s = d/dt$.

An iterative analytical solution of (5.9) and (5.10) can be derived based on the procedure discussed in [14]

$$\Delta p(x',y,t) = \Delta p(x',0,t)\exp\left[(1/qD_p p_o)\int_0^y [j_{Py}(x',0,t) - q\,\lambda(s)\right.$$

$$\int_0^y \Delta p(x',0,t)\exp\left[-(1/qD_p p_o)\int_0^y (j_{Py}(x',0,t) - q\,\lambda(s)\right.$$

$$\left.\int_0^y \Delta p(x',0,t)\exp\{ \right. \qquad (5.11)$$

where the dots indicate repetition following the pattern established earlier in the equation. If $j_{PY}(x', 0, t)y/(qD_pP_o) \ll 1$, a condition that prevails for the modern transistors, (5.11) becomes

$$\Delta p(x', y, t) = \Delta p(x', 0, t) \exp\{-(1/qD_pP_o)j_{Py}(x', 0, t)\, y\}$$

$$= \Delta p(x', 0, t)\,\{1 - (1/qD_pP_o)j_{Py}(x', 0, t)\, y\} \qquad (5.12)$$

Integrating (5.6) from $y = 0$ to $y = L$ instead of y and employing the boundary condition $j_{Py}(x', L, t) = 0$ which results from symmetry of the double stripe base, yields

$$j_{Py}(x', 0, t) = q\,\lambda(o) \int_0^L \Delta p(x', y, t)\,dy \qquad (5.13)$$

Substituting (5.13) into (5.12) gives

$$\Delta p(x', y, t) = \Delta p(x', 0, t)\,\{1 - 1/[L/2 + D_pP_o(x)/\lambda\Delta p(x', 0, t)L]\, y\} \qquad (5.14)$$

If $L/2 \ll D_pP_o(x)/\lambda\, \Delta p(x', 0, t)L$, we can reduce (5.14) to

$$\Delta p(x', y, t) = \Delta p(x', 0, t)[1 - m(x', t)y] \qquad (5.15)$$

where $m(x', t) = \lambda\, \Delta p(x', 0, t)L/D_pP_o$. Equation (5.15) illustrates the y dependence of the excess hole concentration.

To determine the x dependence of Δp, we solve the electron current and continuity equations in the x direction at $y = 0$ by following the systematic method discussed in [15]. This procedure results in

$$\Delta p(x, 0, t) = \exp(\ln K\, x/2W_b)/(\sinh \lambda_n W_b)\,\{\sinh \lambda_n(x - W_b)\, \Delta p(0, 0, t)$$

$$+ \sinh \lambda_n x\, \Delta p(W_b, 0, t)/\sqrt{K}\,\} \qquad (5.16)$$

where $\lambda_n^2 = (\ln K/2W_b)^2 + (1 + s\tau_n)/L_n^2$ and K is the doping ratio

Substituting (5.16) into (5.15) will complete the derivation of $\Delta p(x,y,t)$. Note that (5.16) is derived for a lightly doped base with an exponential profile.

Consider now a heavily doped base with an arbitrary profile. We can derive $\Delta p(x,0,t)$ by using the method discussed in [14]. Since the doping profile in the y direction is uniform, (5.15) is still valid. Thus, substituting $\Delta p(x,0,t)$ into (5.15) will lead to an expression for $\Delta p(x,y,t)$. Based on $\Delta p(x,y,t)$, we can derive the two-dimensional minority electron and majority hole currents and the electric field.

To develop a non-quasi-static description that includes emitter crowding in low injection, we first derive the minority electron current in the intrinsic base layer. According to [15],

$$j_{Nx} = qD_n\{-\eta\Delta n + \partial\Delta n/\partial x\} \tag{5.17}$$

where $\eta = 1/kT/W_b$. Substituting (5.15) and (5.16) into (5.17) yields

$$j_{Nx}(x,y,t) = qD_n[\exp(\eta x/2 - \eta y)/\sinh\lambda_n W_b]$$
$$\{[\eta\sinh\lambda_n(x\ W_b)\ (1/2 + 3\eta y/2) - (1\ \eta y)\lambda_n\cosh\lambda_n(x\ W_b)]\Delta n_1 +$$
$$[\ \eta\sinh\lambda_n x\ (1/2 + 3\eta y/2) + (1-\eta y)\lambda_n\cosh\lambda_n x]\Delta n_2/\sqrt{K}\} \tag{5.18}$$

where $\Delta n_1 = \Delta n(0,0,t) = f(v_{BE})$ and $\Delta n_2 = \Delta n(W_b,0,t) = f(v_{BC})$. Integrating (5.18) with respect to y from 0 to L at $x = 0$ and $x = W_b$ gives the minority currents flowing through the emitter/base junction (i_1) and the collector/base junction (i_2) respectively. The expressions for these two currents can be put in the form of the following two-port equation, which is the basis for deriving the non quasi-static model

$$\begin{bmatrix} i_1 \\ i_2 \end{bmatrix} = \begin{bmatrix} A_{11} & A_{12} \\ A_{21} & A_{22} \end{bmatrix} \begin{bmatrix} \Delta n_1 \\ \Delta n_2 \end{bmatrix} \tag{5.19}$$

where

$$A_{11} = (AqD_n)[\lambda_n \coth(\lambda_n W_b)\exp(-m_1 L) + (1nK/2W_b)\exp(-3m_1 L/2)]$$

$$A_{22} = (AqD_n)[\lambda_n \coth(\lambda_n W_b)\exp(-m_2 L) - (1nK/2W_b)\exp(-3m_2 L/2)]$$

$$A_{12} = -(AqD_n)\lambda_n \operatorname{csch}(\lambda_n W_b)\exp(-m_1 L)/\sqrt{K}$$

$$A_{21} = -(AqD_n)\lambda_n \operatorname{csch}(\lambda_n W_b)\exp(-m_2 L)\sqrt{K}$$

in which $m_1 = m(x=0, t)$ and $m_2 = m(x=W_b, t)$

Truncation of (5.19) for a uniformly doped base with negligible recombination (which corresponds to $K = 1$ and $\lambda_n^2 = \infty/D_n$) yields

$$A_{11} = \frac{AqD_n}{W_b}\left[\frac{1 + s[\tau_{dy}(\Delta n_1/N_{A1}) + \tau_{tx}]}{1 + s[(7/3)\tau_{ty}(\Delta n_1/N_{A1}) + \tau_{dx}]}\right] \tag{5.20}$$

$$A_{22} = \frac{AqD_n}{W_b}\left[\frac{1 + s[\tau_{dy}(\Delta n_2/N_{A2}) + \tau_{tx}]}{1 + s[(7/3)\tau_{ty}(\Delta n_2/N_{A2}) + \tau_{dx}]}\right] \tag{5.21}$$

$$A_{12} = -\frac{AqD_n}{W_b}\left[\frac{1 + s\tau_{dy}(\Delta n_1/N_{A1})}{1 + s[(7/3)\tau_{ty}(\Delta n_1/N_{A1}) + \tau_{dx}]}\right] \tag{5.22}$$

$$A_{21} = -\frac{AqD_n}{W_b}\left[\frac{1 + s\tau_{dy}(\Delta n_2/N_{A2})}{1 + s[(7/3)\tau_{ty}(\Delta n_2/N_{A2}) + \tau_{dx}]}\right] \tag{5.23}$$

where $\tau_{ty} = L^2/2D_p$, $\tau_{dy} = L^2/6D_p$, $\tau_{tx} = W_b^2/2D_n$ & $\tau_{dx} = W_b^2/6D_n$ and $N_{A1} = N_A(0, 0)$, $N_{A2} = N_A(W_b, 0)$

Because $\Delta n \ll N_A$ in low injection, the contributions of τ_{dy} and τ_{ty} in (5.20) - (5.23) are negligible. This implies that emitter crowding is insignificant for transistors operating in low injection. However, we

used the two port equation in low injection to develop models for all levels of injection In Section 5 2 5, we shall develop circuit models corresponding to (5 19)

5 2 3 High Injection

Although emitter crowding is insignificant for low injection it can occur prominently if high injection prevails Emitter crowding derives from a voltage difference developed in the transverse or y direction From these observations, we conclude that for transistors operating in high injection ($\Delta n \approx \Delta p > N_A$), the electric field E_y in the y direction which aids the hole current and retards the electron current exceeds E_y in low injection This assures validity of the assumption $j_{Py} > j_{Ny}$ In high injection or in the reverse active or saturation modes however, the assumption of $\beta \gg 1$ could be violated Therefore, in deriving the two-port equation for high injection, we cannot assume $j_{Px} \approx 0$ as we did before

From $j_{Py} > j_{Ny}$ or $j_{NY} \approx 0$, we obtain E_y and

$$j_{Py} = -2qD_p \partial p/\partial y \tag{5 24}$$

From the standard expression for j_{Px}, we solve for E_x and obtain

$$j_{Nx} = (\mu_n/\mu_p) j_{Px} + 2qD_n \partial n/\partial x \tag{5 25}$$

In deriving (5 24) and (5 25), we have assumed no plasma-induced energy gap narrowing present [20] [22] Thus the electric field acting on holes equals that acting on electrons An extended high-injection model that includes plasma-induced energy-gap narrowing has been derived in [15] Based on the models presented in [15], $2D_n$ in (5 24)

and $2D_p$ in (5 25) should be replaced with $1\ 3\ D_n$ and $1\ 3\ D_p$ if a high density electron-hole plasma is present

Taking the Laplace transforms of (5 24) and (5 25) and substituting the resulting equations into Laplace transformations of (5 5) and (5 6) gives two linear, partial differential equations in variables j_{Px} and $\Delta n = \Delta p$ Eliminating j_{Px} from these two equations results in the following governing equation for high injection

$$\lambda_h^2 \Delta n = \partial^2 \Delta n/\partial x^2 + \partial^2 \Delta n/\partial y^2 \tag{5 26}$$

where $\lambda_h^2 = (1 + s\tau_h)/(D_A \tau_h)$, D_A is the ambipolar diffusivity and τ_h is the recombination lifetime in high injection

Application of the product method to (5 26) leads to

$$\Delta n(x\ y,s) = F(x\ s)\ Q(y,s) \tag{5 27}$$

Substituting (5 27) into (5 26) yields

$$(\lambda_h^2 - \nu)\ F = \partial^2 F/\partial x^2 = \lambda_{hx}^2\ F \tag{5 28}$$

$$(\lambda_h^2 + \nu)\ Q = \partial^2 Q/\partial y^2 = \lambda_{hy}^2\ Q \tag{5 29}$$

where ν is a constant with respect to x and y We now assume that ν is independent of s, an assumption that one can show introduces negligible error in the solutions that follow This implies that ν depends on de emitter crowding only Using the boundary condition $j_{Py}(x\ L,s) = 0$ we obtain $\Delta n(x\ y,s)$ from the above equations

$$\Delta n = \frac{\cosh[\lambda_{hy}(L-y)]}{\cosh(\lambda_{hy} L)\sinh(\lambda_{hx} W_b)}\ (\sinh[\lambda_{hx}(W_b - x)]\Delta n_1 + \sinh(\lambda_{hx} x)\Delta n_2] \tag{5 30}$$

Substituting (5 30) into (5 25) yields

$$j_{Nx} = 2qD_n \frac{\cosh[\lambda_{hy}(L-y)]}{\cosh(\lambda_{hy}L)\sinh(\lambda_{hx}W)} \lambda_{hx}\{-\cosh[\lambda_{hx}(W_b-x)]\Delta n_1 + \cosh(\lambda_{hx}x)\Delta n_2\} + \frac{\mu_n}{\mu_p} j_{Px} \qquad (5.31)$$

Substituting (5 30) and (5.24) into (5.6) results in

$$j_{Px} = j_{Px}(0,y,e) - q(e + 1/\tau_h) \frac{\mu_p \cosh[\lambda_{hy}(L-y)]}{\mu_n \lambda_{hx} \cosh(\lambda_{hy}L)\sinh(\lambda_{hx}W_b)} \{[\cosh[\lambda_{hx}(W_b-x)] \cosh(\lambda_{hx}W_b)]\Delta n_1 + [\cosh(\lambda_{hx}x)-1]\Delta n_2\} \qquad (5\ 32)$$

To determine the dc value of ν in the forward active mode, we neglect net recombination in the emitter junction space charge layer, which implies that $j_{Px}(0\ L) = j_E(-x_{scr}\ L)$, where $j_E(-x_{scr}\ L)$ is the minority hole current density injected into the emitter layer. Thus

$$\sqrt{\nu_f}\cosh\sqrt{\nu_f}L \frac{1 - \cos\sqrt{\nu_f}W_b}{\sin\sqrt{\nu_f}W_b} = \frac{J_{Eo}\Delta n_1}{2qD_p n_1^2} \qquad (5\ 33)$$

where J_{Eo} is the saturation current density in the emitter layer and the subscript, f, designates forward-active operation. By using the Newton-Raphson method we can numerically determine ν_f in (5 33). For $\sqrt{\nu_f}W_b \ll 1$ and $\sqrt{\nu_f}L \ll 1$, inequalities that are valid in low and moderate injection, we can obtain an analytical expression for ν_f by truncating cosh, cos and sin in (5 33) to the first order in $\sqrt{\nu_f}W_b$ and $\sqrt{\nu_f}L$. Fig 5 3 compares the resulting ν_f with accurate values obtained by the Newton-Raphson method. As shown in Fig 5 3, good agreement exists in low and moderate injection, which corresponds to $V_{BE} < 0.85$ volts for

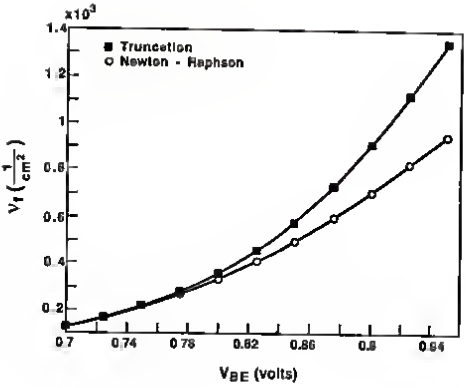

Fig. 5.3 Comparison of truncated v_T and v_T obtained by the Newton-Raphson method versus input voltage V_{BE}

the particular transistor studied. Similarly, we can use the assumption $j_{Px}(W_b,L) = j_C(W_b+x_{scr},L)$ to determine the value of ν_r (ν in the reverse-active mode).

To obtain the two-port equation for high injection we apply the integration scheme in Section 5.2.2 to (5.31). We ignore $(\mu_n/\mu_p)j_{Px}$ in (5.31), which introduces negligible error if $\beta > 10$. After truncation, the matrix elements of the resulting two-port equation (see equation 5.19) are

$$A_{11} = \frac{2AqD_n}{W_b}\,\frac{(1+\nu_f L^2/6)(1+\nu_f W_b^2/2)}{(1+\nu_f L^2/2)(1+\nu_f W_b^2/6)}$$

$$\frac{1+s[\tau'_{dy}/(1+\nu_f L^2/6)+\tau_{tx}/(1+\nu_f W_b^2/6)]}{1+s[\tau'_{ty}/(1+\nu_f L^2/2)+\tau'_{dx}/(1+\nu_f W_b^2/6)]} \qquad (5.34)$$

$$A_{12} = -\frac{2AqD_n}{W_b}\,\frac{(1+\nu_r L^2/6)}{(1+\nu_r L^2/2)(1+\nu_r W_b^2/6)}$$

$$\frac{1+s\tau'_{dy}/(1+\nu_r L^2/6)}{1+s[\tau'_{ty}/(1+\nu_r L^2/2)+\tau'_{dx}/(1+\nu_r W_b^2/6)]} \qquad (5.35)$$

$$A_{22} = A_{11}(\nu_f \longrightarrow \nu_r) \qquad (5.36)$$

$$A_{21} = A_{12}(\nu_r \longrightarrow \nu_f) \qquad (5.37)$$

where $\nu_f \longrightarrow \nu_r$ means ν_f replaced with ν_r

In (5.34) (5.35), $\tau'_{ty} = L^2/4D_p$, $\tau'_{dy} = L^2/12D_p$, $\tau'_{tx} = W_b^2/4D_n$, $\tau'_{dx} = W_b^2/12D_n$.

If $\beta > 10$ is not true, or if we wish to use the above analysis to describe the reverse-active operation, we can include j_{Px} in (5.31), which will change the expressions for the A parameters in (5.34) (5.37)

and introduce two more voltage controlled current sources These two additional current sources are related to the minority hole currents injected into the emitter layer and into the collector layer [15]

5 2 4 Onset of Emitter Crowding

Based on the analytical solutions obtained in Sections 5 2 2 and 5 2 3 we can determine the onset current or voltage for emitter crowding Although we shall deal only with dc emitter crowding in this section a similar treatment applies to ac and transient crowding

Integrating (5 19) and (5 31) from $y = 0$ to $y = L$ at $x = W_b$ will give the expressions for the forward collector currents at low and high injection respectively We define the onset of dc emitter crowding by the relation, I_C (onset) = I_C (low injection) = I_C (high injection), which, for example, for uniformly doped base and emitter layers, yields

$$i_C(\text{onset}) = (2qZLD_n W_e N_D)/(2L^2/3 \quad W_b^2/3) \tag{5 38}$$

The onset electron density at (0,0) in Fig 5 1 is

$$\Delta n_1(\text{onset}) = (qD_p W_b n_i^2)/[J_{Eo}(2L^2/3 - W_b^2/3)] \tag{5 39}$$

Equations (5 38) and (5 39) are based on first-order truncations of sinh cosh sin and cos in eqs (5 19) and (5 31) We can derive the onset emitter-base voltage for emitter crowding at (0,0) from (5 39) by using the standard relation between density and voltage

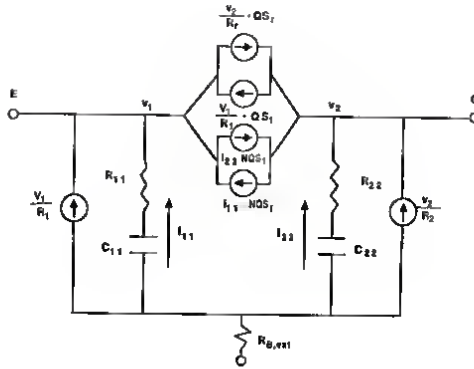

Fig 5.4 The large-signal version of the two-dimensional non-quasi-static circuit model for the quasi-neutral base layer. The small-signal version has the same circuit configuration as the large-signal version but the expressions for circuit elements differ.

5 2 5 All-Injection Models

In this section we develop all injection models by utilizing the two-port equations obtained in Sections 5 2 2 and 5 2 3 The two port equation of (5 19) corresponds to a π network representation Taking the second Cauer form [89] of the resulting π network representation leads to a large-signal all-injection model including emitter crowding in Fig 5 4 Details of the procedure employed to obtain the circuit models from the two-port equation are in [14] In Fig 5 4, the circuit elements associated with the forward active mode are

$$R_1 = \frac{(1 + \nu_f L^2/2)(1 - \nu_f W_b^2/6)}{(\nu_f W_b^2/2)(1 + \nu_f L^2/6)} \quad R_f \quad , \; R_f = (v_1/\Delta n_1)/1F \tag{5 40}$$

$$C_{11} = (1/R_f)[[(-\nu_f W_b^2/2)TDYF + (1 + \nu_f L^2/6)TTXF](1 + \nu_f L^2/2)(1 - \nu_f W_b^2/6) + (1 + \nu_f L^2/6)(\nu_f W_b^2/2)[(1 - \nu_f W_b^2/6)TTYF + (1 + \nu_f L^2/2)TDXF]]/ [(1 + \nu_f L^2/2)^2 (1 - \nu_f W_b^2/6)^2] \tag{5 41}$$

$$R_{11} = [1/C_{11}(\nu_f)][TTYF/(1 + \nu_f L^2/2) + TDXF/(1 - \nu_f W_b^2/6)] \tag{5 42}$$

$$QS_f = (1 + \nu_f L^2/6)/[(1 + \nu_f L^2/2)(1 - \nu_f W_b^2/6)] \tag{5 43}$$

$$NQS_f = (TDYF - (1 + \nu_f L^2/6)[TTYF/(1 + \nu_f L^2/2) + TDXF/(1 - \nu_f W_b^2/6)])/ [[(-\nu_f W_b^2/2)TDYF + (\nu_f L^2/6 + 1)TTXF] + (\nu_f W_b^2/2)(1 + \nu_f L^2/6) [TTYF/(1 + \nu_f L^2/2) + TDXF/(1 - \nu_f W_b^2/6)]] \tag{5 44}$$

and the circuit elements associated with the reverse active model are

$$R_2 = R_1(\nu_f \longrightarrow \nu_r)[R_r/R_f] \quad R_r = (v_2/\Delta n_2)/1R \tag{5 45}$$

$$C_{22} = C_{11}(\nu_f \longrightarrow \nu_r \text{ TTXF} \longrightarrow \text{TTXR, TDXF} \longrightarrow \text{TDXR, TTYF} \longrightarrow \text{TTYR,}$$

$$\text{TDYF} \longrightarrow \text{TDYR})[R_f/R_r] \tag{5.46}$$

$$R_{22} = R_{11}(\nu_f \longrightarrow \nu_r, \text{TDXF} \longrightarrow \text{TDXR, TTYF} \longrightarrow \text{TTYR})C_{11}/C_{22} \tag{5.47}$$

$$QS_r = QS_f(\nu_f \longrightarrow \nu_r) \tag{5.48}$$

$$NQS_r = NQS_f(\nu_f \longrightarrow \nu_r, \text{TDXF} \longrightarrow \text{TDXR, TTXF} \longrightarrow \text{TTXR, TTYF} \longrightarrow \text{TTYR,}$$

$$\text{TDYF} \longrightarrow \text{TDYR}) \tag{5.49}$$

where $\nu_f \longrightarrow \nu_r$ means ν_f replaced with ν_r, etc.

In eqs. (5.40)-(5.49), TDYF and TDYR are the time constants associated with delay in y direction for the forward active and reverse-active modes. TDXF and TDXR denote the delay time in the x direction for the forward-active and reverse-active modes. TTXF and TTXR denote the transit time in x direction for the forward active and reverse-active modes. TTYF and TTYR denote the transit time in the y direction for the forward active and reverse-active modes. IF and IR are related to the forward and reverse collector currents for dc excitation. The expressions for these fitting parameters (IF, IR, TTXF, TTXR, TDXF, TDXR, TTYF, TTYR, TDYF and TDYR) are listed in Appendix E. In Appendix E, we only show the fitting parameters for exponentially doped base layers. We will show the fitting parameters for arbitrarily and heavily doped base layers in a future planned paper. Since doping profiles in the transverse direction are uniform, we may assume that the expressions for TDYF, TDYR, TTYF and TTYR in Appendix E still apply to arbitrarily and heavily doped base layers. Detailed descriptions of the fitting scheme that leads to the parameters listed in Appendix E appear in [15], [61].

The small-signal version of the two-dimensional circuit model developed has the same form as the large signal version in Fig 5 4 The only differences are the expressions for the circuit elements If we assume that the transit time and the delay time for large-signal excitation are equal to those for small signal excitation [42] in the x direction as well as in y direction, we can obtain the expressions for the circuit elements of the small-signal model by replacing $v_1(v_2)$ IF and IR in (5 40)-(5.43) with kT/q, I_f and I_r The expressions for the fitting parameters I_f and I_r, are also in Appendix E

If we compare the two-dimensional (2-D) non quasi-static circuit model in Fig 5 4 with the one dimensional (1 D) non quasi-static circuit model in Chapters Two and Three, two additional voltage-controlled current sources v_1/R_1 and v_2/R_2, which represent the effect of dc crowding appear in the 2 D model All circuit elements in the 2 D model differ from those in the 1 D model due to the effects of current crowding Detailed descriptions of the physical meaning of the circuit elements in Fig 5.4 (except R_1 and R_2) and the method for model implementation are in Chapters Two and Three and [14] and [15]

The resulting (2-D) circuit model also includes possible collector crowding for a transistor operating in the reverse-active or saturation mode Since the doping profiles in emitter and collector layers differ current crowding at the base/emitter and base/collector junctions is non-reciprocal Therefore in the 2-D model we treat the forward-active and the reverse active modes individually and split the current between nodes E and C in Fig 5 4 into four current sources instead of the two present in the 1 D model They are 1) forward quasi-static

current (v_1 QS_f/R_f), 2) reverse quasi-static current (v_2 QS_r/R_r), 3) forward non quasi static current (1_{11} NQS_f) and 4) reverse non-quasi-static current (1_{22} NQS_r).

5.3 Assessments

In this section, we assess the models developed for three kinds of excitations, namely dc, ac and transient. We first demonstrate the effect of emitter crowding on the carrier and current distributions inside the intrinsic base layer. This demonstration is based on the analytical solutions obtained in the model derivation. We then show the terminal performance of the models and compare the model predictions with experiments. The transistors simulated or measured in Figs. 5.3-5.5, 5.9 and 5.11-5.16 have dimensions W_b = 1.4 μm, L = 17.5 μm, A = 35 x 125 μm^2 and doping profile $N_A = 4 \times 10^{15} \exp(-0.115x)$ cm^{-3}.

5.3.1 DC Crowding

Based on the analytical solutions for the forward-active mode, we plot the longitudinal minority electron current density, $J_{NX}(0,y)$, versus y/L in Fig. 5.5 and the transverse majority hole current density, $J_{PY}(x,0)$, versus x/W_b in Fig. 5.6. These figures show that these current densities crowd toward the emitter edges as the emitter-base voltage increases. As shown in both figures, current crowding becomes significant at high injection levels (V_{EE} > 0.85 volt). Fig. 5.5 shows that $J_{NX}(0,y)$ peaks at the emitter edge (y = 0). Fig. 5.6 shows that $J_{PY}(x,0)$ peaks at the emitter/base junction (x = 0). Fig. 5.7 through 5.9 show $J_{PX}(0,y)/J_{E0}$, n(0,y) and n(x,0)/J_{E0} is the

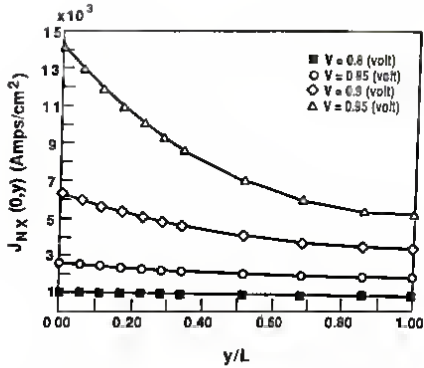

Fig. 5.5 Analytical solutions for the longitudinal component of the electron current density in the transverse direction of the intrinsic base layer at V_{EE} = 0.8, 0.85, 0.9 and 0.95 volt

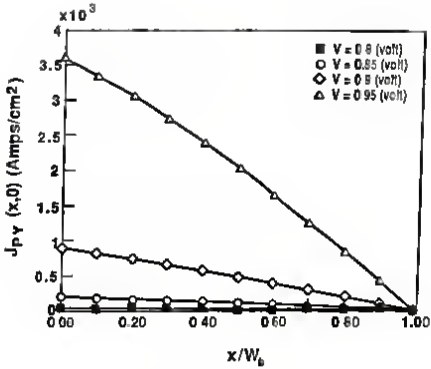

Fig 5.6 Analytical solutions for the transverse component of the hole current density in the longitudinal direction of the intrinsic base layer at V_{BE} = 0.8, 0.85, 0.9 and 0.95 volt

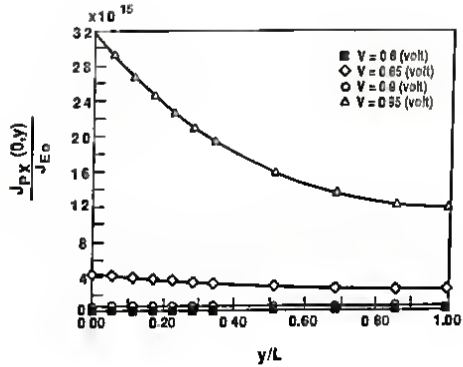

Fig 5 7 Analytical solutions for the longitudinal component of the normalized majority hole current density in the transverse direction of the intrinsic base layer at V_{BE} = 0 8, 0 85, 0 9 and 0 95 volt. J_{E0} is the saturation current in the emitter/base junction

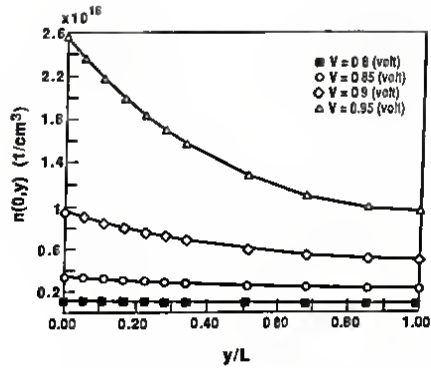

Fig. 5.8 Analytical solutions for the distribution of the excess electron density in the transverse direction of the intrinsic base layer at V_{BE} = 0.8, 0.85, 0.9 and 0.95 volt

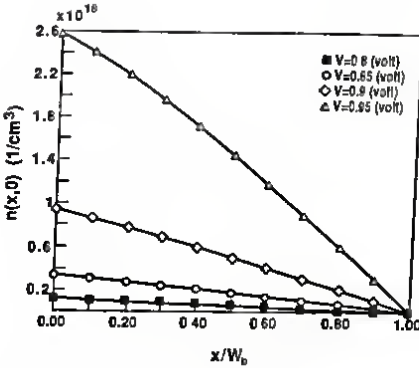

Fig. 5.9 Analytical solutions for the distribution of the excess electron density in the longitudinal direction of the intrinsic base layer at V_{BE} = 0.8, 0.85, 0.9 and 0.95 volt

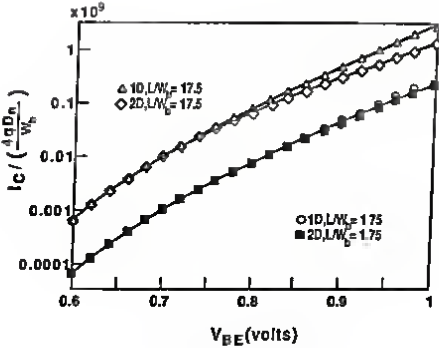

Fig. 5.10 The one-dimensional and two-dimensional model predictions of the collector current versus input voltage for transistors with $L/W_b = 1.75$ and 17.5. In comparison we assume that the base doping concentrations for both cases are the same ($N_A = 10^{16}$ cm^{-3}).

saturation current in the emitter/base junction. In Figs. 5.8 and 5.9, the curvatures of n_i, which correspond to the direction of the electric fields, are determined by the sign of ν_E in eqs. (5.28) and (5.29).

To see how de emitter crowding affects terminal currents, we plot in Fig. 5.10 the collector current versus the input voltage for different emitter lengths (L) and base thickness (W_b) ratios. As shown for $L/W_b = 1.75$, the prediction of the one dimensional model agrees with that of the two-dimensional model. Thus de emitter crowding is not significant for these transistors with $L/W_b = 1.75$. For $L/W_b = 17.5$, however, a condition which is typical of most advanced transistors, the prediction of the two-dimensional model deviates dramatically from that of the one dimensional model in the high injection range ($V_{BE} > 0.85$ volt) because significant de emitter crowding occurs. As illustrated, the collector current predicted by the two dimensional model is smaller than that predicted by the one-dimensional model for $L/W_b = 17.5$. Since the deviation between the model predictions quantitatively indicates the effect of the current-dependent intrinsic base resistance on the collector current, we can extract the value of intrinsic base resistance from Fig. 5.10.

As mentioned by Gosh [27], Severson [28] and Schutt-Aine [32], a lumped representation of the base resistance will inaccurately model the high frequency or fast transient response because of the distributed nature of the base resistance. Instead of a lumped base resistance, we implicitly include the effects of the intrinsic base resistance in the circuit elements between nodes B and E in Fig. 5.4. We use, however, a lumped circuit element for the extrinsic base

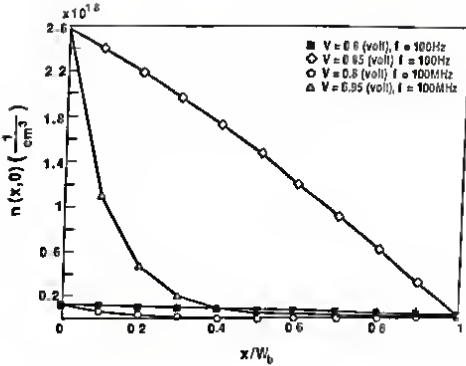

Fig. 5.11 Analytical solutions for the electron density in the longitudinal direction of the intrinsic base layer at V_{EE} = 0.8 and 0.95 volt and at frequency = 100 and 100 MHz

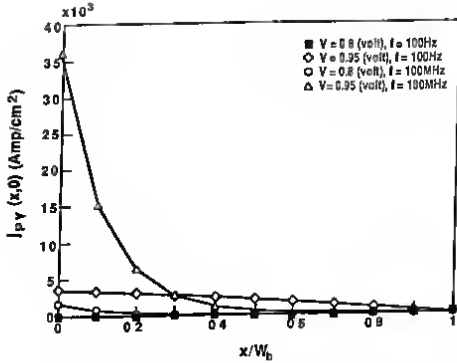

Fig 5.12 Analytical solutions for the transverse component of the hole current density in the longitudinal direction of the intrinsic base layer at V_{EE} = 0 8 and 0 95 volt and at frequency = 100 Hz and 100 MHz

resistance. The voltage across the extrinsic base resistance represents the ohmic drop between the voltage applied to the base contact and the voltage at (0,0), which is a voltage acting on the intrinsic base layer.

5.3.2 AC Crowding

To show how ac crowding affects the distribution of the carrier and current density in the intrinsic base layer, we plot $n(x,0)$ versus x/W_b in Fig. 5.11, $j_{PY}(x,0)$ versus x/W_b in Fig. 5.12 and $j_{PX}(0,y)/J_{E0}$ versus y/L in Fig. 5.13 for different biases and different frequencies. As shown in Figs. 5.11, 5.12 and 5.13, the ac crowding becomes more significant at high frequency ($f = 100$ MHz) and high injection ($V = 0.95$ volt) than at low frequency ($f = 100$ Hz) and low injection ($V < 0.8$ volt). Similar results occur for $n(0,y)$ versus y/L and $j_{NX}(0,y)$ versus y/L. Figures 5.11, 5.12 and 5.13 illustrate the strong effect of dc bias which Fritchard [25] neglected. Since the current density depends on the derivative of the excess carrier density, the overshoot of $j_{PY}(0,0)$ at $f = 100$ MHz in Fig. 5.12 is due to the crowding of the electron density, n, at $x = 0$ and $y = 0$.

Figure 5.14 describes the phase of the input impedance h_{11} predicted by the one-dimensional and two-dimensional models at different biases. At low frequencies ($f < 0.1$ MHz) the one dimensional and two-dimensional models predict the same phase shift even at high injection level ($V = 0.95$ volt) because the diffusion and junction capacitances then negligibly affect the phase of h_{11}. At high frequencies, the one-dimensional and two-dimensional model predictions

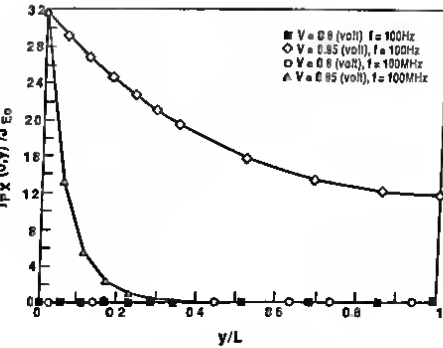

Fig 5.13 Analytical solutions for the longitudinal component of the normalized majority hole current density in the transverse direction of the intrinsic base layer at V_{BE} = 0.8 and 0.95 volt and at frequency = 100 Hz and 100 MHz. J_{ε_0} is the saturation current in the emitter/base junction

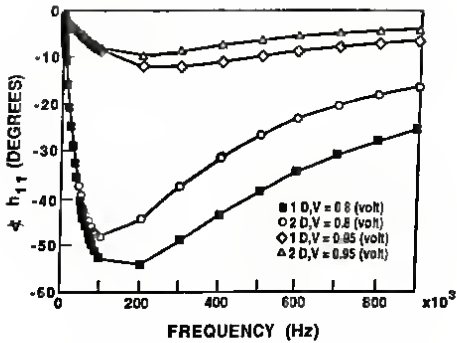

Fig. 5.14 The one dimensional and two dimensional model predictions of the phase of the input impedance h_{11} at $V_{GS} = 0.8$ and 0.95 volt.

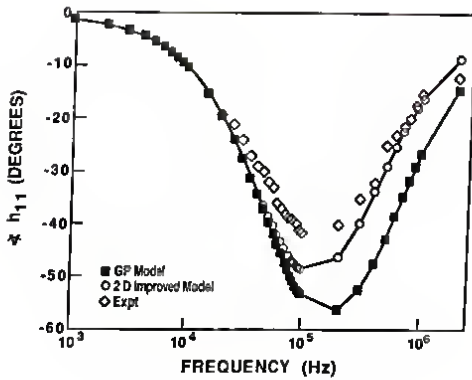

Fig. 5.15 Comparison of the phase of h_{11} predicted by the Gummel-Poon (GP) model and by the two dimensional non quasi-static model with experimental results measured at V_{BE} = 0.85 volt.

disagree more at high bias levels (V = 0 95 volt) than at low bias levels (V = 0 8 volt) because significant dc current crowding occurs in high injection The magnitude of the input impedance h_{11} shows similar trends

To evaluate the validity of the two-dimensional model for small-signal excitation, we compare the phase of h_{11} against experiments and the model predictions in Fig 5 15 We measure the transistor at V = 0 85 volt using an HP 4194A (Impedance/Gain-Phase Analyzer) The extrinsic base resistance in this case is about 7 ohms The transistor measured has a heavily doped collector layer which prevents base pushout in high injection As illustrated the experiment agrees with the predictions of the one-dimensional Gummel-Poon (GP) model and the two dimensional model at low frequencies At high frequency, the two dimensional model shows better accuracy than does the one dimensional Gummel-Poon model We see similar results in comparing the model prediction of the magnitude of h_{11} against experiment Since the transistor measured has L/W_b = 1 75, the improvement of the two-dimensional model is insignificant in Fig 5 15, but is expected to be sizable for transistors with a higher L/W_b ratio The discrepancy between the experiment and the two-dimensional model prediction in Fig 5 15 occurs probably because we neglected base width modulation and used a one dimensional space charge layer capacitance (see Sec 5 4)

5 3 3 Transient Crowding

In Fig 5 16 we plot $j_{NX}(0,y,t)$ the longitudinal component of the injected minority electron currents under the emitter layer, in the

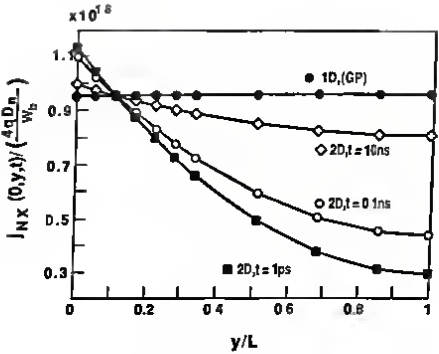

Fig 5.16 The distribution of the longitudinal component of the electron current density in transverse direction of the intrinsic base layer predicted by the Gummel-Poon (GP) model and by the two dimensional non-quasi-static model at t = 1 ps, 0.1 ns and 10ns for a step input voltage.

transverse direction for step input voltage to show the effects of transient current crowding. In the very beginning ($t = 1$ ps) $j_{NX}(0,y,t)$ peaks sharply at the emitter edge. Then, as time passes, it spreads through the whole intrinsic base layer and reaches steady state ($t = 10$ ns), which reflects dc crowding. For comparison, we also plot in Fig. 5.16 the prediction of the Gummel-Poon model, which shows no transient current crowding. The transient current crowding illustrated in Fig. 5.16 is consistent with the prediction of the FIELDAY [31].

5.4 Modifications and Extensions

5.4.1 Modifications

The models derived in Section 5.2 apply to an intrinsic quasi-neutral base layer with a rectangular boundary as shown in Fig. 5.1. When significant base width modulation or base pushout occurs, however, the boundary of the intrinsic quasi-neutral layer is not rectangular.

For instance, the voltage drop along the junctions caused by current crowding in the transverse direction will result in an x-dependent emitter edge of the quasi-neutral base layer, the shape of which can be determined by the following iterative approach. First, assume that the emitter edge is x-independent, as an initial guess. Second, use Eq. (5.30) or its low injection counterpart Eq. (5.15) to determine Δn at discrete values of y along this edge. Third, use the standard relation to determine the quasi-Fermi potential separation V at each of these discrete values of y. Fourth, use an all-injection space-charge-layer capacitance model to determine x corresponding to each discrete value of y. This specifies the first iteration functional

dependence $x^{(1)}(y)$ of the emitter edge of the quasi-neutral base, which sets the starting condition for the second iteration. The process is repeated until the sequence $\{x(y)\}$ converges.

The same iterative method applies to determining the two-dimensional extended base thickness when base pushout occurs. Instead of using the separation of the quasi-Fermi potentials, we use the longitudinal minority current density along $x = W_b$, which is obtained from Eqs. (5.18) and (5.31), as the initial guess in iteration. Based on this initial guess of current and on analytic models for base pushout [82], [86], [90], we can determine $W_b^{(1)}(y)$, the first-iteration base thickness. From $W_b^{(1)}(y)$ we obtain $J_{NX}^{(1)}(y)$. An iterative procedure is then employed until the sequence $\{W_b(y)\}$ converges to $W_b(y)$, which is the base thickness in the presence of pushout.

5.4.2 Extensions

To derive a complete two dimensional model, we need to include the current spreading which occurs in the extrinsic base layer and in the collector layer, and the sidewall injection between the emitter layer and the extrinsic base layer. In principle, we can still use the method described in Section 5.2 to derive the model for the current spreading except that the assumption, $J_{NY} \ll J_{PY}$, is true only in the intrinsic base layer. Instead, we assume that $J_{PX} \ll J_{NX}$ in the extrinsic base layer and the collector layer to derive the model for current spreading. PISCES simulations indicate that this assumption is adequate for the device geometries examined. In addition, because of sidewall

injection, we need to modify the boundary condition when we derive the current-spreading model for the extrinsic base layer.

5.5 Conclusions

We have derived two-dimensional analytical lumped circuit models for bipolar junction transistors. The models developed take into account carrier propagation delay, all injection levels, dc and ac emitter crowding and transient emitter crowding. We developed the models based on the analytical solutions obtained from solving two-dimensional time-dependent continuity equations. These analytical solutions enable us to characterize the phenomena of dc, ac and transient current crowding inside the intrinsic base layer, and they provide information for parameter extraction such as the intrinsic base resistance. In addition, based on these analytical solutions, we can express the total charge stored in the quasi neutral layers in analytic form as a function of terminal current and voltage. Thus we can derive a non-quasi-static two-dimensional charge-controlled circuit model. The resulting large- and small-signal circuit models are based on a truncation scheme which leads to a hierarchy of the models with various accuracies. As an example to illustrate that the two-dimensional models offer better accuracy than the Gummel-Poon model, we compared model predictions of input impedance h_{11} versus frequency with experiment.

The treatment here assumed silicon bipolar transistors. But the results also apply to heterojunction bipolar transistors excited by very high frequency signals.

CHAPTER SIX
CONCLUSION AND EXTENSIONS

6.1 Conclusion

Non-quasi-static lumped circuit models for bipolar junction transistors were derived for use in circuit simulators. The model derivation was based on a systematic method developed in Chapter Two. The method resulted in analytical solutions for current and carrier densities and produced both large- and small-signal non-quasi-static models.

The models include in compact, lumped circuits the following aspects of transistor physics:

1) carrier propagation delay due to the finite electron and hole velocity;
2) position-dependent diffusivity, mobility and lifetime;
3) Fermi-Dirac statistics and general Einstein relation for degenerate material;
4) energy gap narrowing due to dopant-carrier (heavy doping) and carrier-carrier (high injection) interactions;
5) Webster effect, which is the sliding effect of the electric field in the quasi-neutral base at high injection;
6) thickness modulation of the quasi-neutral layers due to contraction or expansion of the space-charge layers under different biases.

7) conductivity modulation in the quasi neutral layers at different injection levels,

8) Kirk effect which is base pushout occurring at high injection,

9) non-negligible majority current in the quasi-neutral base layer when current gain (β) is small,

10) dc ac and transient emitter crowding due to the transverse current in the quasi neutral base layer

The models describe high frequency, high speed or high power bipolar junction transistors operating in the forward- and reverse-active modes as well as in the saturation and quasi saturation modes.

The models provide physical insight and information for parameter extraction. The analytical approach leads to the development of a model hierarchy, which enables a tradeoff between model accuracy and complexity. Because the models are compatible with the Gummel-Poon model built in the SPICE, the implementation of the models is feasible either by using user defined controlled source or by directly modifying the source codes of the SPICE.

The measurements done by computer simulation and by experiment indicate that the models developed have advantages over the conventional Gummel Poon model and other conventional models in the simulation of frequency and transient responses. The model accuracy depends strongly on the accuracy of the input parameters such as device makeup (geometry and doping profile). The accuracy of the physical models for mobility, diffusivity and lifetime also affects the model accuracy.

6.2 Extensions

In this section, we indicate several mechanisms which we neglected in the previous model derivation, and discuss possible extensions of the models to include these mechanisms

6.2.1 Avalanche Breakdown

To prevent base pushout, which degrades the transistor performance at high injection, one can increase the collector doping concentration As a result, the electric field in the base/collector junction increases and thus the base/collector breakdown voltage decreases Models for avalanche breakdown have been published [91],[92] Most of them are based on a local "lucky electron" model [93]-[95], which assume that the number of possible ionization per primary carrier transit is very large This assumption implies the validity of using "continuous" devices physics [96]-[98] However, in many modern small devices, the number of possible impact ionizations per primary transit is very small Thus continuum physics breaks down and a theory based on a finite number of discrete ionization processes must be used to develop associated models [99]

6.2.2 Collector and Base Current Spreading

According to [29] and [79], more than 30% of the collector current may flow in the extrinsic base and collector layers of small transistors Thus inclusion of the spreading current in the extrinsic base and collector layers will improve model accuracy In principle, we

can apply the method described in Chapter Five to model current spreading. Details of this extension is in Section Four of Chapter Five.

§ 2.3 Current Crowding in the Emitter Layer and Contact

In Chapter Five, we considered the current crowding in the transverse and longitudinal directions of the quasi-neutral base. By neglecting the generation and recombination current inside the base/emitter junction, we may extend our two-dimensional models to include current crowding at the edge of the quasi-neutral emitter and the base/emitter space charge layers. Because of the current crowding at the edge, the distribution of the injected minority current along the transverse direction in the whole emitter layer is nonuniform. This implies that the current is nonuniformly distributed in the transverse direction at the emitter (ohmic) contact or at the interfacial layer between the emitter and polysilicon layers. We have to consider these nonuniformities in determining emitter and contact resistances. We may apply the method used in Chapter Five to include these effects.

§ 2.4 Models for Heterojunction Bipolar Transistors (HBT)

As mentioned in Section One of Chapter Four, non-quasi-static effects in the intrinsic quasi-neutral layers of heterojunction bipolar transistors are even more important than they are in homojunction transistors because the base resistance and the collector capacitance are substantially reduced. As reported [70], the emitter and base transit time constants become dominant factors in determining the

frequency response of heterojunction bipolar transistors. Since the delay time is comparable with the transit time in both emitter and base layers, we may expect significant non-quasi-static effects in heterojunction bipolar transistors.

We may extend the method presented in Chapter Two to derive non quasi-static models for heterojunction bipolar transistors. Because of band edge discontinuities are presumed to exist in III-V compound materials whose composition is position dependent, thermionic emission-tunneling and diffusion-drift mechanisms occur in the emitter/base junction. Furthermore velocity overshoot occurs in the collector/base junction. These mechanisms modify the boundary conditions in the quasi-neutral base layers, and we need an augmented current expression [100] to include the effects of velocity overshoot.

APPENDIX A
PROOF OF RECIPROCITY IN THE QUASI NEUTRAL BASE LAYER

To prove $A_{12} = A_{21}$ in (2 11), we first prove that r_{12} in (2 18) is equal to r_{21} in (2 19) Defining $f_1 = 1/D_n n_o$ and $f_2 = n_o$ yields

$$r_{12} = \int_0^{W_b} f_1(x) \int_0^{x} f_2(x_1) \int_0^{x_1} f_1(x_2)\, dx_2 dx_1 dx \Big/ \int_0^{W_b} f_1(x) dx \qquad (A\ 1)$$

$$r_{21} = \int_0^{W_b} f_1(x) \int_x^{W_b} f_2(x_1) \int_{x_1}^{W_b} f_1(x_2)\, dx_2 dx_1 dx \Big/ \int_0^{W_b} f_1(x) dx \qquad (A\ 2)$$

Defining $F_1(x_1) = \int f_1(x_2)\, dx_2$ and substituting this into (A 1) and (A 2) we can remove the inner integral in both equations Removing all the integrals in both equations by successively applying this method we find that r_{21} is equal to r_{12} The high-order terms in A_{12} or A_{21} can be shown equal by the same procedure

APPENDIX B

LIST OF THE PARAMETERS FOR THE MODELS DERIVED IN CHAPTER TWO

In the large signal model for the base layer

$$i_{jj}(t) = \exp(-t/\tau_{12})[(1/\tau_{12}) \int_0^t \exp(t'/\tau_{12})[d(C_{jj}v_j)/dt]dt' + i_{jj}(0)] \quad (B\ 1)$$

$$i_{12}(t) = \exp(-t/\tau_{12})[(1/\tau_{12}) \int_0^t \exp(t'/\tau_{12})\, i_{QS}(t')dt' + i_{12}(0)] \quad (B\ 2)$$

In the large signal model for emitter layer

$$i_{PNQS}(t) = \exp(-t/\tau_{ed})[(1/\tau_{ed}) \int_0^t \exp(t'/\tau_{ed})[d(C_e v_{BE})/dt]dt' + i_{PNQS}(0)] \quad (B\ 3)$$

The expressions for the parameters used in the model for emitter layer.

$$l_{Ee} = qAa_0/b_0 \quad (B\ 4)$$

$$\tau_{et} = \theta_1/\theta_0 \quad h_1/b_0 \quad (B\ 5)$$

$$\tau_{ed} = b_1/b_0 \quad (B\ 6)$$

$$\theta_0 = \int_0^{W_e} p_0(x)[1 + B_2^*(x)]dx/\tau_p(x) + S_p p_0(W_e)[1 + B_2^*(W_e)] \quad (B\ 7)$$

$$a_1 = \int_0^{W_e} p_0(x)[1 + B_2^*(x) + B(x)/\tau_p(x)]dx + S_p p_0(W_e)B(W_e) \quad (B\ 8)$$

$$b_0 = 1 + \int_0^{W_e} p_0(x)\, A_1(x)dx/r_p(x) + S_p p_0(W_e)A_1(W_e) \qquad (\text{Ж } 9)$$

$$b_1 = \int_0^{W_e} p_0(x)A_1(x)dx \qquad (\text{Ж } 10)$$

$$A_1(x) = \int_0^{x} dx/p_0(x)D_p(x) \qquad (\text{Ж } 11)$$

$$M_2^1(x) = \int_0^{x} dx_1/D_p(x_1)p_e(x_1) \int_0^{x_1} p_e(x_2)/r_p(x_2)dx_2 \qquad (\text{Ж } 12)$$

$$M(x) = \int_0^{x} dx_1/D_p(x_1)p_e(x_1) \int_0^{x_1} p_e(x_2)dx_2 \qquad (\text{Ж } 13)$$

APPENDIX C

LIST OF THE PARAMETERS FOR THE MODELS DERIVED IN CHAPTER THREE

$$f_1 = (K-1)/K\ln K \qquad (C\ 1)$$

$$\tau_E = (\Delta x^2/2D)(2/\ln K)[1 + (1 \quad K)/(K\ln K)] = (\Delta x^2/2D)\ f_2 \qquad (C\ 2)$$

$$\tau_d = (\Delta x^2/6D)(6/\ln K)[(K + 1)/(K \quad 1) \quad 2/\ln K)] = (\Delta x^2/6D)\ f_3 \qquad (C\ 3)$$

$$\tau_r = (\Delta x^2/2D)(\ 2/\ln K)[1 + (1 \quad K)/\ln K] = (\Delta x^2/2D)\ f_4 \qquad (C\ 4)$$

For uniform doping profile or for high injection, f_1 f_2, f_3 and f_4 become unity

By using $\Delta n_j/N_{Aj} = u_j$ as the indication of injection level at x_j we fit the associated parameters as follows

$$IF = (A_q D_n/\Delta x)\{[(1+f_1) + u_1]/[(1+f_1)\ f_1 + 0\ 5u_1]\} \qquad (C\ 5)$$

$$IR = (A_q D_n/\Delta x)(0\ 5)\{[2/\sqrt{K} + u_2]/[\sqrt{K}\ f_1 + 0\ 25u_2]\} \qquad (C\ 6)$$

$$TF = (\Delta x^2/2D_n)\{[(1+f_1) + u_1]/[(1+f_1)/f_2 + 2u_1]\} \qquad (C\ 7)$$

$$TR = (\Delta x^2/2D_n)\{[f_4/(f_1\ \sqrt{K}) + 0\ 5u_2]/[1/f_1\ \sqrt{K} + u_2]\} \qquad (C\ 8)$$

$$TDF = (\Delta x^2/6D_n)\{[(1+f_1) + 0\ 5u_1]/[(1+f_1)/f_3 + u_1]\} \qquad (C\ 9)$$

$$TDR = (\Delta x^2/6D_n)\{[(1+f_1) + 0\ 5u_2]/[(1+f_1)/f_3 + u_2]\} \qquad (C\ 10)$$

$$If = (AqD_n/\Delta x)\{[(1+f_1) + u_1]/[(1+f_1)\ f_1 + u_1]\} \qquad (C\ 11)$$

$$Ir = (AqD_n/\Delta x)(0.5)([2/\sqrt{K} + u_2]/[\sqrt{K}\ f_1 + 0.5u_2]) \qquad (C\ 12)$$

When the above parameters are used in the small signal model, Δn_j in n_j have to be replaced by ΔN_j.

By solving (3.16) and (3.17) and using the time constants for all injection levels, we obtain $i_{11}(t)$, $i_{22}(t)$ and $i_{12}(t)$ in the large-signal model for the circuit application

$$i_{11}(t) = \exp(-t/TDF)[(1/TDF)\int_0^t \exp(t'/TDF)[d(TF\ IF\ \Delta n_1)/dt']dt' + i_{11}(0)] \qquad (C\ 13)$$

$$i_{22}(t) = \exp(-t/TDR)[(1/TDR)\int_0^t \exp(t'/TDR)[d(TR\ IR\ \Delta n_2)/dt']dt' + i_{22}(0)] \qquad (C\ 14)$$

$$i_{12}(t) = \exp(-t/TDF)[(1/TDF)\int_0^t \exp(t'/TDF)IF\ \Delta n_1 dt' + i_1(0)] -$$
$$\exp(-t/TDR)[(1/TDR)\int_0^t \exp(t'/TDR)IR\ \Delta n_2 dt' + i_2(0)] \qquad (C\ 15)$$

APPENDIX D
LIST OF THE PARAMETERS FOR THE MODELS DERIVED IN CHAPTER FOUR

The fitting parameters in Section 4.2.3 are listed below

$$IF = [(1+f_1) + u_1]/[(1+f_1)f_1 + u_1/I_h] \tag{D.1}$$

$$IR = (1/I_h)\{[I_h/\sqrt{K} + u_2]/[\sqrt{K}\, f_1 + (1/I_h)^2 u_2]\} \tag{D.2}$$

$$TF = [(1+f_1) + u_1]/[(1+f_1)/r_{fl} + u_2/r_{fh}] \tag{D.3}$$

$$TR = [r_{rl}/(f_1\sqrt{K}) + r_{rh}u_2]/[1/f_1\sqrt{K} + u_2] \tag{D.4}$$

$$TDF = [(1+f_1) + r_{dh}u_1]/[(1+f_1)/r_{dl} + u_1] \tag{D.5}$$

$$TDR = [(1+f_1) + r_{dh}u_2]/[(1+f_1)/r_{dl} + u_2] \tag{D.6}$$

$$If = [(1+f_1) + u_1]/[(1+f_1)f_1 + 2u_1/I_h] \tag{D.7}$$

$$Ir = (1/I_h)\{[I_h/\sqrt{K} + u_2]/[\sqrt{K}\, f_1 + 2u_2/I_h^2]\} \tag{D.8}$$

where $f_1 = 1/I_1 = \int_0^{W_b} dx/(D_n f_1)/A_q$;

$$K = (n_{e2}/n_{e1}) = (N_{A1}/N_{A2})\exp[(\Delta E_{g2} - \Delta E_{g1})/kT],$$

and u's are the indications of injection level. For example, $u_j = \Delta n_j/N_{Aj}$, which is the indication of injection level at x_j in the base layer. While the above parameters are used in the small-signal model Δn_j in u_j have to be replaced by ΔN_j.

The expressions for the parameters used in the model for collector layer;

$$I_{Ca} = qA_c a_0/b_0 \tag{D 9}$$

$$r_{et} = a_1/a_0 - b_1/b_0 \tag{D 10}$$

$$r_{ef} = b_1/b_0 \tag{D 11}$$

$$a_0 = (p_0/r_p)[W + W^3/(6D_p r_p)] + S_{pc}p_0[1 + W^2/(2D_p r_p)] \tag{D 12}$$

$$a_1 = p_0[W + W^3/(3D_p r_p)] + S_{pc}p_0 W^2/D_p \tag{D 13}$$

$$b_0 = 1 + W^2/(2D_p r_p) + S_{pc}W/D_p \tag{D 14}$$

$$b_1 = W^2/(2D_p) \tag{D 15}$$

where W is the thickness of the quasi-neutral collector layer (= W_e + W_b - x_c) and S_{pc} is the surface recombination velocity for holes at the collector contact

APPENDIX E

LIST OF THE PARAMETERS FOR THE MODELS DERIVED IN CHAPTER FIVE

By using $An_j/N_{Aj} = u_j$ as the indication of injection level at x_j, we fit the parameters in Section 5 2 5 for an exponentially doped base layer as follows:

$$IF = (AqD_n/W_b)([(1+f_1) + u_1]/[(1+f_1)\ f_1 + 0\ 5u_1]) \quad (E\ 1)$$

$$IR = (AqD_n/W_b)(0\ 5)([2/\sqrt{K} + u_2]/[\sqrt{K}\ f_1 + 0\ 25u_2]) \quad (E\ 2)$$

$$TTXF = (W_b^2/2D_n)([(1+f_1) + u_1]/[(1+f_1)/f_2 + 2u_1]) \quad (E\ 3)$$

$$TTXR = (W_b^2/2D_n)([f_4/(f_1\sqrt{K}) + 0\ 5u_2]/[1/f_1\sqrt{K} + u_2]) \quad (E\ 4)$$

$$TDXF = (W_b^2/6D_n)([(1+f_1) + 0\ 5u_1]/[(1+f_1)/f_3 + u_1]) \quad (E\ 5)$$

$$TDXR = (W_b^2/6D_n)([(1+f_1) + 0\ 5u_2]/[(1+f_1)/f_3 + u_2]) \quad (E\ 6)$$

$$TTYF = (L^2/2D_p)((7/3)u_1/[1+2(7/3)u_1/(D_p/D_n+1)]) \quad (E\ 7)$$

$$TTYR = (L^2/2D_p)((7/3)u_2/[1+2(7/3)u_2/(D_p/D_n+1)]) \quad (E\ 8)$$

$$TDYF = (L^2/6D_p)(u_1/[1+2u_1/(D_p/D_n+1)]) \quad (E\ 9)$$

$$TDYR = (L^2/6D_p)(u_2/[1+2u_2/(D_p/D_n+1)]) \quad (E\ 10)$$

$$If = (AqD_n/W_b)([(1+f_1) + u_1]/[(1+f_1)\ f_1 + u_1]) \quad (E\ 11)$$

$$Ir = (AqD_n/W_b)(0\ 5)([2/\sqrt{K} + u_2]/[\sqrt{K}\ f_1 + 0\ 5u_2]) \quad (E\ 12)$$

where f_1, f_2, f_3 and f_4 are defined in Appendix C For uniform doping

profile or for high injection, f_1, f_2 f_3 and f_4 become unity When the parameters in (E 1)-(E 12) are used in the small signal model Δn_j in u_j have to be replaced by ΔN_j

REFERENCES

[1] H K Gummel and H C Poon, "An integral charge control model of bipolar transistors," Bell Syst Tech J., vol. 49, pp. 827-852, May 1970

[2] T W Jung, Use of transients in quasi neutral regions for characterizing solar cells, diodes, and transistors, University of Florida, Ph D dissertation, May 1986

[3] F A Lindholm, M K Chan, S S Wu and T W Jung, "Models including carrier propagation for bipolar circuit simulation," SRC Topical Conference, Gainesville, Florida, April 1986.

[4] J. G. Fossum and S. Veeraraghavan, "A fabrication based modelling of bipolar transistors for non quasi static circuit simulation," IEEE Electron Device Letters, vol. EDL-7, pp. 652-654, Dec. 1986

[5] F A Lindholm, S S Wu, M K Chan, J J Liou and T W Jung, "Modeling of carrier propagation delay and forward voltage space-charge-region capacitance in bipolar transistors", SRC Topical Conference, Gainesville, Florida, May 1987

[6] M K Chan, F A Lindholm and T W Jung, "Non-quasi static small-signal models for semiconductor junction diodes with extensions for transistors," Solid-State Electronics, vol. 30, pp. 883-885, 1987

[7] H Klose and A W Wieder, "The transient integral charge control relation — A novel formulation of the currents in a bipolar transistor," IEEE Trans. Electron Devices, vol. ED-34, pp. 1090-1099, May 1987

[8] S S Wu, M K Chan, F A Lindholm and T W Jung, "Carrier-propagation delay (CPD) models for bipolar circuit simulation," Custom IC Conference, Portland, Oregon, May 1987

[9] F A Lindholm, M K Chan, S S Wu, J J Liou and T W Jung, "Improvements of the Gummel-Poon Integral Charge Control Model and Illustrations of Relevance in SPICE2 Circuit Simulation," IEEE Bipolar Circuits and Technology Meeting, Minneapolis, Minnesota, Sept. 1987.

[10] J A Saltchik, A Chatterjee and F Yang, "An accurate bipolar model for large signal transient and dc applications," In IEDM

Tech Dig , pp 244-247, 1987

[11] M K Chen, F A Lindholm and S S Wu "Comparison and extension of recent one-dimensional bipolar transistor models " IEEE Trans Electron Devices, vol ED-35, pp 1D96-1D6, July 1988

[12] G A Hurkx, "A new approach to A C characterization of bipolar transistors," Solid-State Electronics vol 31 pp 1269-1275 Aug 1988

[13] S S Wu and F A Lindholm "Physical Equivalent Circuit Models for Large and Small signal Bipolar Transistor Simulation " SRC TECHCON'88, Dallas, Texas Oct 1988

[14] S S Wu and F A Lindholm "One-dimensional non-quasi-static models for arbitrarily and heavily doped quasineutral layers in bipolar transistors," IEEE Trans Electron Devices vol ED-36, pp 737-747 April, 1989

[15] S S Wu and F A Lindholm "One Dimensional All-Injection Non-Quasi-Static Models for Arbitrarily Doped Quasi-Neutral Layers in Bipolar Junction Transistors Including Plasma Induced Energy Gap Narrowing," to be published in IEEE Trans Electron Devices Aug 1989

[16] S S Wu and F A Lindholm "Non quasi-static models including all injection levels and dc, ac and transient emitter crowding in transistors," submitted for publication Aug 1989

[17] S S Wu and F A Lindholm, "High-Injection non-quasi-static compact models for bipolar junction transistors having lightly doped collectors," submitted for publication Aug 1989

[18] L W Nagel, SPICE2 A computer program to simulate semiconductor circuits, University of California Ph D dissertation, May 1975

[19] W M Webster, "On the variation of junction-transistor current-amplification factor with emitter current," Proc IRE vol 42, pp 914-920 1954

[20] A Neugroschel, J S Wang and F A Lindholm " Evidence for excess carrier storage in electron-hole plasma in silicon transistors " IEEE Electron Devices Letters, vol EDL-6, pp 253-255 May 1985

[21] P T Landsberg, A Neugroschel, F A Lindholm and C T Sah, "A model for band gap shrinkage in semiconductors with application to silicon," Phys Stat Sol (b) vol 130, pp 255-266, 1985

[22] J R Lowney, "The effect of high injection on the density of states in silicon " in Proc Bipolar Circuit and Technology Meeting, pp 188-190, Minneapolis Minnesota Sept 1988

[23] F A Lindholm and S S Wu "Energy-gap and electron-affinity contractions and their importance in bipolar device simulators," in Proc. Bipolar Circuit and Technology Meeting, pp 191-194, Minneapolis, Minnesota, Sept 1988

[24] C. T. Kirk, Jr., "A theory of transistor cutoff frequency (f_T) falloff at high current densities," IRE Trans. Electron Devices, vol. ED-9, pp. 164-174, March 1962

[25] R. L. Pritchard, "Two-dimensional current flow in junction transistors at high frequencies," Proc. IRE, vol. 46, pp. 1152-1160, June 1958

[26] J. R. Hauser, "The effects of distributed base potential on emitter-current injection density and effective base resistance for stripe transistor geometries," IEEE Trans. Electron Devices, vol. ED-11, pp. 238-242, 1964.

[27] H. N. Ghosh, "A distributed model of the junction transistor and its application in the prediction of the emitter-base pulse response of the device," IEEE Trans. Electron Devices, vol. ED-12, p. 513-531, Oct. 1965

[28] F. Severeon, "The effects of A.C. and D.C. current crowding on the input impedance of planar transistors," Technical Report, Tektronix Labs., Beaverton, Oregon, June 1973

[29] J. W. Slotboom, "Computer Aided Two Dimensional Analysis of Bipolar Transistors," IEEE Trans. Electron Devices, vol. ED-20, pp. 669-679, Aug. 1973

[30] O. Menck, H. H. Heimeier and W. L. Engl, "High injection in a two-dimensional transistor," IEEE Trans. Electron Devices, vol. ED-21, pp. 403-409, July 1974.

[31] E. M. Buturla, P. E. Cottrell, B. M. Grossman, K. A. Salsburg, "Finite-element analysis of semiconductor devices: The FIELDAY program," IBM J. Res. Develop., vol. 25, pp. 218-231, 1981

[32] J. E. Schutt-Aine, "Determination of a small-signal model for ion implanted microwave transistors," IEEE Trans. Electron Devices, vol. ED-30, pp. 750-758, July 1983

[33] F. Y. Chang and L. F. Wagner, "The generation of three-dimensional bipolar transistor models for circuit analysis," IBM J. Res. Develop., vol. 29, pp. 252-262, May 1985

[34] D. D. Tang, "Switch-on transient of shallow-profile bipolar transistors," IEEE Trans. Electron Devices, vol. ED-32, pp. 2224-2226, Nov. 1985

[35] J. R. Lary and R. L. Anderson, "Effective base resistance of bipolar transistors," IEEE Trans. Electron Devices, vol. ED-32, pp. 2503-2505, Nov. 1985.

[36] J. Lue and S. Graham, "A quasi 3-D base resistance R_{B1} simulator for non-walled emitter transistors," in Proc. IEEE Bipolar Circuits Technol. Meeting, pp. 13-17, Minneapolis, Minnesota, July 1987.

[37] J. S. Yuan, J. J. Liou and W. R. Eisenstadt, "A physics-based current dependent base resistance model for advanced bipolar transistors," IEEE Trans. Electron Devices, vol. ED-35, pp. 1055-1062, July 1988.

[38] C. T. Sah, "The equivalent circuit model in solid-state electronics-III: conduction and displacement currents," Solid-State Electronics, vol. 13, pp. 1547-1575, Dec. 1970.

[39] SLICE Manual Rev. 5.01, Harris Semiconductor Corp., Melbourne, Florida, July 1986.

[40] M. R. Pinto, Conor S. Rafferty, Hal R. Yeager and R. W. Dutton, PISCES IIB, Supplementary Report, Stanford Electronics Laboratories, Stanford, California, 1985.

[41] H. Kroemer, "Two integral relations pertaining to the electron transport through a bipolar transistor with a nonuniform energy gap in the base region," Solid State Electronics, vol. 28, pp. 1101-1103, 1985.

[42] I. E. Getreu, Modelling the Bipolar Transistor, New York: Elsevier, 1978.

[43] S. W. Lee and E. J. Prendergast, "Analytical relations for determining the base transit times and forward-biased junction capacitances of bipolar transistors," Solid-State Electronics, vol. 28, pp. 767-773, Aug. 1985.

[44] D. J. Hamilton, F. A. Lindholm and J. A. Narud, "Large signal models for junction transistors," International Solid-State Circuit Conference, pp. 56-57, Philadelphia, Pennsylvania, Feb. 1963.

[45] M. R. Chen, Methods for developing and measuring circuit models for bipolar diodes and transistors, University of Florida, Ph.D. dissertation, Aug. 1989.

[46] E. Y. Hwang, V. de la Torre, H. Nadworny, E. Herald, S. Garrison and P. J. Zdebel, "Numerical mixed-level simulation for bipolar devices and circuit optimization," SRC Topical Research Conference, Gainesville, Florida, May 1987.

[47] J. J. Liou, F. A. Lindholm and J. S. Park, "Forward-voltage capacitance and thickness of p-n junction space charge regions," IEEE Trans. Electron Devices, vol. 34, pp. 1571-1579, July 1987.

[48] C. T. Chuang, D. D. Tang, G. P. Li and E. Hackbarth, "On the punchthrough characteristics of advanced self-aligned bipolar transistors," IEEE Trans. Electron Devices, vol. ED-34, pp. 1519-1524, July 1987.

[49] K. Kikuchi, S. Kameyama, M. Kajiyama, M. Nishio and T. Kamada, "A high speed bipolar LSI process using self-aligned double diffusion polysilicon technology," in IEDM Tech. Dig., pp. 420-423, 1986.

[50] N. Takemura, T. Kamiya, S. Ohi, M. Sugiyama, T. Teshiro and M. Nakamae, "Submicron epitaxial layer and RTA technology for extremely high speed bipolar transistors," in IEDM Tech. Dig., pp. 424-427, 1986.

[51] S. E. Swirhun, Y. H. Kwark and R. M. Swanson, "Measurement of electron lifetime, electron mobility and band gap narrowing in heavily doped p-type silicon," in IEDM Tech. Dig., pp. 24-26, 1986.

[52] D. K. Lynn, C. S. Meyer and D. J. Hamilton, Analysis and Design of Integrated Circuits, Chap. 4, New York: McGraw-Hill, 1967.

[53] K. Mlsiskos and F. A. Lindholm, "Generalized reciprocity theorem for semiconductor devices," Journal of Applied Physics, vol. 58(12), pp. 15-16, Dec. 1985.

[54] Y. H. Kwark and R. M. Swanson, "A generalized proof of the reciprocity theorem," IEEE Trans. Electron Devices, vol. ED-33, pp. 865-866, June 1986.

[55] W. C. Elmore, "The transient response of damped linear networks with particular regard to wide band amplifiers," Journal of Applied Physics, vol. 19, pp. 55-63, Jan. 1948.

[56] K. G. Asher, "The method of estimating delay in switching circuits and the figure of merit of a switching transistor," IEEE Trans. Electron Devices, vol. ED-11, pp. 497-506, Nov. 1964.

[57] J. L. Arreola and F. A. Lindholm, "A nonlinear indefinite admittance matrix for modeling electronic devices," IEEE Trans. Electron Devices, vol. ED-24, pp. 765-767, June 1977.

[58] J. S. Park, A. Neugroschel and F. A. Lindholm, "Systematic analytical solutions for minority carrier transport in semiconductors with position-dependent composition, with application to heavily doped silicon," IEEE Trans. Electron Devices, vol. ED-33, pp. 240-249, Feb. 1986.

[59] G. E. Paul and C. L. Searle, Electronic Principles: Physics Models and Circuits, New York: John Wiley & Son, Inc., 1969.

[60] F. J. Zdebel, R. J. Falda, S-Y. Hwang, V. d l. Torre and A. Wagner, "MOSAIC III---A high performance bipolar technology with advanced self-aligned devices," in Proc. Bipolar Circuits and Technology Meeting, Minneapolis, Minnesota, Sept. 1987.

[61] H. C. de Graeff and W. J. Kleestermen, "New formulation of the current and charge relations in bipolar transistor modeling for CACD purposes," IEEE Trans. Electron Devices, vol. ED-32, pp. 2415-2421, Nov. 1985.

[62] R. D. Middlebrook, "Conditions at a p-n junction in the presence of collected current," Solid-State Electronics, vol. 6, p. 555, 1963.

[63] H. C. de Graeff, "Collector models for bipolar transistors," Solid-State Electronics, vol. 16, pp. 587-600, 1973.

[64] P. C. H. Chen and C. T. Sah, "Computer aided study of steady-state carrier lifetimes under arbitrary injection conditions," Solid State Electronics, vol. 22, pp. 921-926, 1979.

[65] D. K. Lynn, C. S. Meyer and D. J. Hamilton, Analysis and Design of Integrated Circuits, Chap. 4, New York: McGraw-Hill, 1967.

[66] H. J. DeMan, "The influence of heavy doping on the emitter efficiency of a bipolar transistor," IEEE Trans. Electron Devices, vol. ED-18, pp. 833-835, 1971.

[67] J. W. Slotboom and H. C. De Graeff, "Measurement of bandgap narrowing in Si bipolar transistors," Solid State Electron., vol. 19, pp. 857-862, 1976.

[68] H. Kroemer, "Quasi-electric and quasi-magnetic field in nonuniform semiconductor," RCA Review, vol. 28, pp. 332-342, 1957.

[69] S. Y. Yung, The modeling and design optimization of polysilicon emitter transistors, including experimental verification, Ph.D. dissertation, Univ. of Florida, 1987.

[70] H. Kroemer, "Heterostructure bipolar transistors and integrated circuits," Proc. IEEE, vol. 70, pp. 13-25, Jan. 1982.

[71] J. Wagner and J. A. del Alamo, "Band gap narrowing in heavily doped silicon: a comparison of optical and electrical data," J. Appl. Phys., vol. 63(2), pp. 425-427, Jan. 1988.

[72] J. S. Blakemore, "Approximations for Fermi-Dirac integrals, especially the function $F_{1/2}(\eta)$ used to describe electron density in a semiconductor," Solid-State Electronics, vol. 25, pp. 1067

1076, 1982.

[73] J. F. McKelvey, Solid State and Semiconductor Physics, Chap. 10, New York: Harper & Row, 1971.

[74] H. C. Poon, H. K. Gummel and D. L. Scharfetter, "High injection in epitaxial transistors," IEEE Trans. Electron Devices, vol. ED-16, pp. 455-457, Jun. 1969.

[75] D. L. Bowler and F. A. Lindholm, "High current regimes in transistor collector regions," IEEE Trans. Electron Devices, vol. ED-20, pp. 257-263, March 1973.

[76] F. A. Lindholm, "Device characterization for computer analysis of large circuits," IEEE Trans. Nucl. Sci., vol. NS-18, pp. 206-211, Dec. 1971.

[77] R. J. Whittier and D. A. Tremere, "Current gain and cutoff frequency falloff at high currents," IEEE Trans. Electron Devices, vol. ED-16, pp. 39-57, Jan. 1969.

[78] G. Rey, F. Dupuy and J. F. Bolhe, "A unified approach to the base widening mechanisms in bipolar transistors," Solid State Electronics, vol. 18, pp. 863-866, 1975.

[79] A. van der Ziel and D. Agouridis, "The cutoff frequency falloff in UHF transistors at high currents," Proc. IEEE(Lett.), vol. 54, pp. 411-412, March 1966.

[80] J. R. A. Beale and J. A. G. Slatter, "The equivalent circuit of a transistor with a lightly-doped collector operating in saturation," Solid State Electron., vol. 11, pp. 241-252, 1968.

[81] L. E. Clark, "Characteristics of two-region saturation phenomena," IEEE Trans. Electron Devices, vol. ED-16, pp. 113-116, Jan. 1969.

[82] G. M. Kull, L. W. Nagel, S. W. Lee, P. Lloyd, E. J. Prendergast and H. Dirks, "A unified circuit model for bipolar transistors including quasi-saturation effects," IEEE Trans. Electron Devices, vol. ED-32, pp. 1103-1113, June 1985.

[83] H. Jaeng and J. G. Fossum, "Physical modeling of high-current transients for bipolar transistor circuit simulation," IEEE Trans. Electron Devices, vol. ED-34, pp. 898-905, April 1987.

[84] S. L. Crump and R. M. Warner, Jr., "An analytical model for the epitaxial bipolar transistor," Solid-State Electronics, vol. 20, pp. 753-771, 1977.

[85] J. J. Liou, "Base-collector junction capacitance of bipolar transistors operating at high current densities," IEEE Trans.

Electron Devices, vol ED-34, pp 2304-2308, Nov 1987.

[86] E. J. Ryder, "Mobility of holes and electrons in high electric fields," Phys. Rev. 90, p. 766, 1953.

[87] J. S. Park and A. Neugroschel, "Parameter extraction for bipolar transistors," IEEE Trans. Electron Devices, vol. ED-36, pp. 88-95, Jan. 1989.

[88] N. H. Fletcher, "Some aspects of the design of power transistors," Proc. IRE, vol. 43, pp. 551-559, May 1955.

[89] M. S. Ghausi and J. J. Kelly, Introduction to Distributed-Parameter Networks—With Application to Integrated Circuits. New York: Holt, Rinehart and Winston, Inc., 1968.

[90] J. J. Liou, F. A. Lindholm and B. S. Wu, "Analytical Cutoff Frequency Model for Heterojunction Bipolar Transistors Including High Current Effects," submitted for publication, Feb. 1989.

[91] W. J. Kleinsterman and H. C. de Graaff, "Avalanche multiplication in a compact bipolar transistor model for circuit simulation," in Proc. Bipolar Circuit and Technology Meeting, pp. 103-108, Minneapolis, Minnesota, Sept. 1988.

[92] H. Jaeng and J. G. Fossum, "Modeling impact ionization in advanced bipolar transistors for device/circuit simulation," in Proc. Bipolar Circuit and Technology Meeting, pp. 107-110, Minneapolis, Minnesota, Sept. 1988.

[93] A. G. Chynoweth, "Ionization rates for electron and holes in silicon," Phys. Rev. vol. 109, pp. 1537-1540, 1958.

[94] W. Shockley, "Problems related to p-n junctions in silicon," Solid-State Electron., vol. 2, pp. 35-67, 1961.

[95] C. Hu, S. C. Tam, F.-C. Hsu, P.-K. Ko, T.-Y. Chan and K. W. Terrill, "Hot-electron-induced MOSFET degradation - model, monitor, and improvement," IEEE Trans. Electron Devices, vol. ED-32, pp. 375-385, Feb. 1985.

[96] R. J. McIntyre, "Multiplication Noise in Uniform Avalanche Photodiodes: Theory," IEEE Trans. Electron Devices, vol. 13, p. 703, 1971.

[97] S. D. Personick, "New Results on Avalanche Multiplication Statistics with Applications to Optical Detection," Bell Syst. Tech. J., vol. 50, p. 3075, 1971.

[98] A. S. Tager, "Current Fluctuations in a Semiconductor (Dielectric) under the Conditions of Impact Ionization and Avalanche Breakdown," Sov. Phys. Solid State, vol. 6, p. 1919,

1965.

[99] K. M. van Vliet, A. Friedmann and L. M. Rucker, "Theory of Carrier Multiplication and Noise in Avalanche Devices—Part II: Two-Carrier Processes," IEEE Trans. Electron Devices, vol. ED-26, pp. 752-764, May 1979.

[100] K. K. Thornber, "Current equations for velocity overshoot," IEEE Trans. Electron Device Letters, vol. EDL-3, pp. 69-71, March 1982.

BIOGRAPHICAL SKETCH

Being Song Wu was born in Tainan, Taiwan, Republic of China, on June 1, 1960. He received the B.S. degree in electrical engineering from National Taiwan University, Taiwan, in 1982 and the M.S. degree in electrical engineering from the University of Florida, Gainesville, in 1985.

From 1982-1984 he served in the Air Force of the Republic of China as an electronics officer. Since August 1985 he has been working toward the Ph.D. degree in electrical engineering at the University of Florida, Gainesville.

His research interests include semiconductor device physics, technology, and measurement with a present emphasis on circuit simulation and modeling.

He is a member of Phi Kappa Phi and Eta Kappa Nu.

I certify that I have read this study and that in my opinion it conforms to acceptable standards of scholarly presentation and is fully adequate, in scope and quality, as a dissertation for the degree of Doctor of Philosophy

Fredrik A. Lindholm, Chairman
Professor of Electrical Engineering

I certify that I have read this study and that in my opinion it conforms to acceptable standards of scholarly presentation and is fully adequate, in scope and quality, as a dissertation for the degree of Doctor of Philosophy.

Chih Tang Sah
Graduate Research Professor of
Electrical Engineering

I certify that I have read this study and that in my opinion it conforms to acceptable standards of scholarly presentation and is fully adequate, in scope and quality, as a dissertation for the degree of Doctor of Philosophy.

Arnost Neugroschel
Professor of Electrical Engineering

I certify that I have read this study and that in my opinion it conforms to acceptable standards of scholarly presentation and is fully adequate, in scope and quality, as a dissertation for the degree of Doctor of Philosophy

Sheng S. Li
Professor of Electrical Engineering

I certify that I have read this study and that in my opinion it conforms to acceptable standards of scholarly presentation and is fully adequate, in scope and quality, as a dissertation for the degree of Doctor of Philosophy

Chen C. Hsu
Professor of Aerospace Engineering,
Mechanics, and Engineering Science

This dissertation was submitted to the Graduate Faculty of the College of Engineering and to the Graduate School and was accepted as partial fulfillment of the requirements for the degree of Doctor of Philosophy

August 1989

Dean, College of Engineering

Dean, Graduate School